Determining the efficiency of *in situ* iron remediation (ISIR) technology using ozonation in the Atlantis primary aquifer, Western Cape, South Africa

Mushirah Rehman

A thesis submitted in fulfilment of the requirements for the

Degree

Master of Science

In

Environmental and Water Science

Department of Earth Science, Faculty of Natural Sciences, University of the Western Cape

Supervisor: Dr Sumaya Israel

Co-Supervisor: Dr Thokozani Kanyerere

December 2021

Declaration

I, Mushirah Rehman, hereby declare that *Determining the efficiency of in situ iron remediation (ISIR) technology using ozonation in the Atlantis primary aquifer, Western Cape, South Africa* is my own work, that it has not previously been submitted for any degree or examination in any other university, and that all the sources cited or quoted have been indicated and acknowledged by a complete reference list.

Full names: Mushirah Rehman

Date: 1st December 2021

Signature:

Dedication

I would like to dedicate this thesis to my mother Mrs Muneera Rehman, father Mr Fuaad Rehman, and sister Madeegha Rehman for their selfless acts towards my future.

Abstract

In situ iron remediation (ISIR) applications has become a popular technique for reducing iron and manganese concentrations in boreholes that impose aesthetic and potable issues to groundwater quality and water supply schemes. Production borehole yields are reduced by screens clogged with iron and manganese precipitates, which jeopardizes groundwater extraction volumes and affect the supply of groundwater from supply schemes. Repeated iron- and manganese-related borehole clogging in primary and fractured rock aquifers is a well-known phenomenon in South Africa's potable groundwater supply schemes. Preliminary work completed at the study site aimed to investigate the feasibility of the ISIR technique in the prevention of iron- and manganese-related borehole clogging in a South African primary aquifer. In having fulfilled the research, more information was collected to deal with the long-term prevention of iron-related problems in South African groundwater supply schemes. However, a knowledge gap exists concerning treatment efficiencies of ISIR using ozonation in primary aquifer settings in South Africa. *In situ* iron remediation using ozone (O_3) is a treatment method applied to clogged production boreholes by introducing ozonated water into an aquifer setting through borehole injections.

This thesis aimed to provide an assessment of the potential for the efficient use of ozonation as an ISIR technology in a primary aquifer to reduce occurrences of borehole clogging which could maximize production borehole abstraction for water supplies to industrial, agricultural and surrounding towns in the Western Cape. The first objective was to assess the effects of clogging on production boreholes. The second was to understand the spatial and temporal response of hydrochemical parameters to O_3. The last objective was to quantify the efficiency of ISIR using ozonation. This would establish procedural suitability for site-specific conditions of the primary aquifer.

The effects of clogging on borehole yield was assessed by measuring the change in specific capacity (Sc) of production borehole. To evaluate the performance of the production borehole and quantify baseline hydraulic characteristics of the Atlantis aquifer under a controlled discharge rate, a step-drawdown test was used before O_3 injection. The test involves increasing the discharge rate from a low constant rate through a series of equal duration pumping intervals of higher constant rates through a series of equal duration pumping intervals of higher constant rates. Results show that the specific capacity average decreased by less than 5 m^3/day/m between 2013 and 2019. However due to a combination of inaccurate historical data and

inconsistent flow rates during this study that affected specific capacity during the step-drawdown test before ozonation, the change in specific capacity could not be quantified. Based on these findings it was recommended that more frequent and accurate step-drawdown tests be performed with consistent abstraction flow rates per step, step duration, and measurement intervals to gain more conclusive evidence on the effects of clogging on production boreholes.

To understand the spatial and temporal response of hydrochemical parameters to O_3, data collected from manual sampling and the telemetry system between October 2019 and March 2020 was performed. Using a WTW Multi 3420 SET G water quality multi-parameter device, manual field measurements of pH, dissolved oxygen (DO), electrical conductivity (EC), and temperature) were recorded. Favourable measurements related to iron oxidation and precipitation were achieved as a result of O_3 injection. This was observed by the results of pH levels that ranged between 5.5 and 8.2, and DO concentrations between 14 and 20 mg/L. Electrical conductivity values increased by roughly 30 µS/cm at the start of O_3 injection, when compared to baseline EC values. The overall mean temperature of 19.18 °C during O_3 injection remained consistent throughout the O_3 injection period, indicating the subsurface response to iron oxidation. An automated GeoTel data collection system (telemetry) for 24/7 continuous data was used to measure field parameters of DO, water levels, temperature, injection flow rate, and EC. Manual measurements of DO, temperature, EC and pH are highly comparable in majority of the monitoring boreholes when compared to the results recorded by the telemetry system. This indicates evidence of data accuracy and reliability. Variable hydrochemical analysis during the application of ISIR technology at inconsistent O_3 injection rates were favourable enough to indicate reducing iron and manganese (in some instances) concentrations. Based on these findings, the study concluded that these variable injection rates of O_3 significantly influences spatial and temporal groundwater hydrochemical data favourable to iron and manganese concentrations.

The efficiency of ISIR using ozonation was quantified by interpreting the results obtained from monitored and telemetry data. Although the initial intention was to use the removal efficiency equation, the substitution of the volumetric ratio of the abstracted volume of groundwater with reduced iron (Vgw) and the volume of injected volume (Vinj) was not possible, as these values were not recorded effectively during monitoring purposes of this study. However, the study was able to determine that the injection of O_3 *in situ* reduced iron and manganese concentrations in the subsurface even during inconsistent O_3 injection rates (1.7, 1.0, 0.5, 0.43, 0.1, and < 0.1 L/s). It was recommended that a prolonged duration of the study be re-introduced

at the study site to collect suitable parameters to derive the removal efficiency of ISIR using ozonation. By using the removal efficiency equation, more conclusive evidence to quantify the the nature and extent of removal efficiency will be able to be determined.

Keywords: *In situ* iron remediation (ISIR); ozonation; borehole clogging; iron; manganese; hydrochemical.

Acknowledgements

I would like to express my profound appreciation to the following individuals and organisations:

Dr Sumaya Israel, my supervisor, for your generous time, advice, and knowledge as a great mentor and role-model in my career in hydrogeology. I am truly privileged to have been able to learn from the best.

To the supervisory team from the University of the Western Cape Dr Kevin Pietersen, Dr Thokozani Kanyerere and writing coach Mr Dewald Schoeman for their appreciated support, assistance and guidance during the course of the study.

To National Research Fund (NRF) for their financial assistance, without which any of this research would be possible.

To collaborative partners from the Council for Geoscience (CGS) and Department of Water and Sanitation (City of Cape Town) for their assistance and access to data.

I would also like to thank Mrs Lebo Nhleko, Dr Meris Mills, Dr Gideon Tredoux, Miss Albie Steyn, Mr Cecil Donnelly, and Mr Bradley Abrahams for their advice, assistance and support during the course of the study.

I would also like to thank my mother Mrs Muneera Rehman, father Mr Fuaad Rehman, sister Madeegha Rehman for their moral support, laughter, and motivation even though you all had no idea what my thesis was all about. I appreciate the time spent and lost together during the write up of this dissertation.

In the Name of Allāh, the Most Gracious, the Most Merciful

Above all I would like to thank the Almighty Allah (SWT), through whom all things are possible.

Table of Contents

List of Figures

List of Tables

Chapter 1: Introduction

1. Background of the study

In situ iron remediation (ISIR) is a treatment method applied to clogged production boreholes by introducing oxidant-rich water into an aquifer setting through borehole injection (Robey, 2014). The purpose of ISIR technologies is to promote oxidation and precipitation of iron and manganese in the aquifer, to prevent clogging of borehole infrastructure such as pumps, screens and piping. By precipitating iron and manganese precipitates out of production boreholes, and along aquifer domains, the occurrence of borehole clogging is reduced and production borehole abstraction efficiencies is maximised (Robey, 2014). Associated benefits of ISIR treatment applications include:

- Treatment simplicity and affordability;
- Energy efficiency and low water resource consumption;
- Easy adaptation to variable project magnitudes;
- Prevention of aggressive chemical additives;
- Minimal exposure to effluent or waste generation; and its
- Rapid approach in dealing with micronutrient removal in boreholes (Robey, 2014)

With many benefits to ISIR, there has been interest in implementation in South Africa to address increased borehole clogging occurrences demonstrated in Atlantis and Koo Valley (Tredoux *et al.*, 2004; Robey, 2014). A variety of ISIR technologies have been implemented internationally and locally. Figure 1.1 identifies the town of Atlantis in the Western Cape, South Africa.

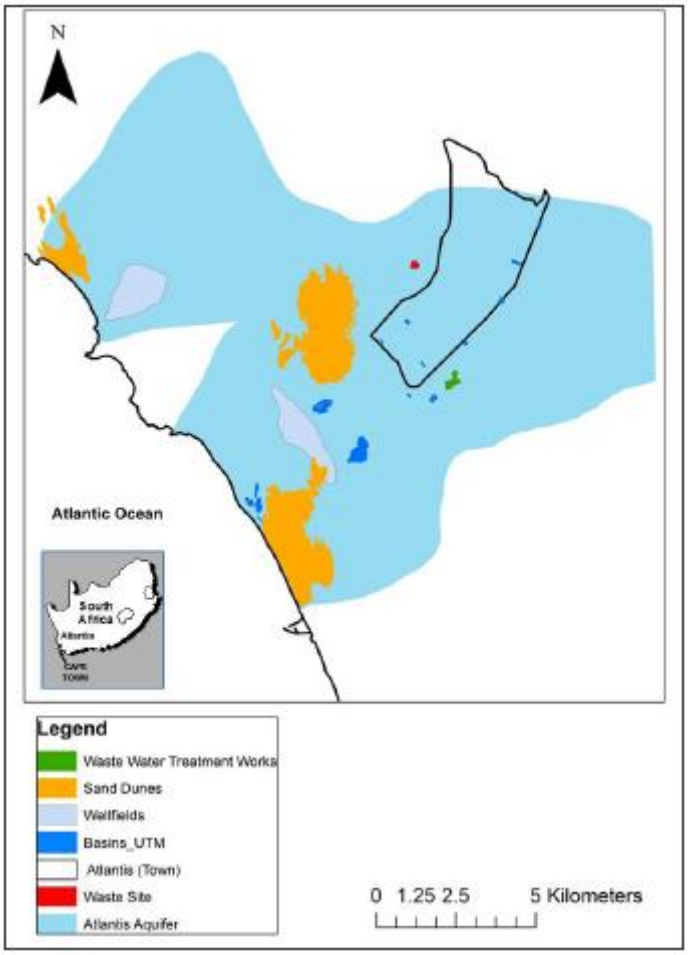

Figure 1.1: Locality map of Atlantis, Western Cape, South Africa (Bugan et al., 2012).

1.1 Groundwater abstraction and remediation techniques

The lowering of water tables and increased borehole abstraction yields can enhance the clogging of some boreholes (Robey, 2014; Gorelick and Zheng, 2015; Jovanovic *et al.*, 2017). These activities introduce oxygen to iron-rich groundwater which initiates the chemical reaction responsible for oxidizing soluble ferrous iron (Fe^{2+}) into insoluble ferric iron (Fe^{3+}). Production boreholes that are affected cannot maintain consistent abstraction volumes, which ultimately compromises pumping abilities due to borehole or aquifer clogging (Smith, 2006; van Halem *et al.*, 2010; Ebermann *et al.*, 2012; Robey, 2014).

Borehole remediation techniques can be biological, chemical, and physical treatments applied to boreholes to improve borehole productivity. The treatment techniques are to counter the effects of oxyhydroxide precipitate and sedimentation accumulation in the borehole and/or aquifer that induces clogging (Robey *et al.*, 2014). *In situ* borehole remediation treatments

involves the injection of oxidant-saturated water directly into the aquifer through boreholes, whereas *ex situ* treatments are applied after groundwater extraction above ground. The selection of borehole rehabilitation techniques are:

- Declining borehole abstraction yields;
- Increasing water levels;
- Hydrogeological characteristics;
- Borehole construction; and
- Deteriorating groundwater quality (Bugan *et al.*, 2016)

Borehole treatments to reduce iron and manganese concentrations in groundwater using *ex situ* (Ellis *et al.*, 2000; Sallanko *et al.*, 2007; El Araby *et al.*, 2009), and *in situ* removal techniques have been implemented successfully both internationally and locally (Hallberg and Martinell, 1976; Appelo *et al.*, 1999; Mettler *et al.*, 2001; Tredoux *et al.*, 2004; Robey, 2014). Iron and manganese are common elements found in water and share similar biogeochemical properties in solution (Environment, 2008). The presence of naturally occurring dissolved iron and manganese in groundwater can cause problems with groundwater supplies, including aesthetic and potable issues (Silveria, 1988; Robey, 2014).

Aesthetic quality issues for domestic users, technical difficulties in public potable water supply systems, and complaints from industrial users have been reported due to iron and manganese concentrations in groundwater (Silveria, 1988; Robey, 2014). Many rural and urban areas exclusively depend on groundwater, this reiterates the extent of South Africa's limited water security and provides an incentive to supply iron- and manganese-free potable groundwater in a sustainable manner (Xu and Usher, 2006). Sustainable groundwater systems should be governed by the effectiveness of groundwater extraction through pre-determined and well established pumping regimes (Gorelick and Zheng, 2015). This study determines the sustainability of ISIR technology by injecting ozonated water in the subsurface to reduce or prevent, and control clogging occurrences of production boreholes in the Atlantis primary aquifer, Western Cape, South Africa.

1.2 Research problem

Iron-related borehole clogging in primary and fractured rock aquifers is a well-known phenomenon in South Africa's potable groundwater supply schemes (Robey, 2014). Borehole

yields began declining in Atlantis in 1997 when production boreholes yielding 15 litres per second (L/s) declined unexpectedly to 2 L/s (DWAF, 2009). These declining yields raised concerns when considering long-term borehole clogging prevention implementations and decision making to groundwater supply schemes in South Africa. Groundwater quality fluctuations introduce a range of complications to safe consumption and water usage (Jolly, 2002). Both iron and manganese impose aesthetic and potable issues on groundwater quality and water supply schemes (Robey, 2014). Production borehole yields are affected due to clogging of screens with iron and manganese precipitate resulting in reduced borehole abstraction yields (Robey, 2014). Attempts to chemically rehabilitate boreholes in South Africa with low borehole yields as a result of borehole clogging has previously adopted aggressive chemical treatments. The Blended Chemical Heat Treatment (BCHT) and Electrochemically Activated Water (EAW) technology are aggressive chemical treatments which changes pH levels in the aquifer and are only effective if managed successfully (Bishop, 2006; Smith, 2006).

Previous work completed by Robey (2014) investigated the feasibility of ISIR to prevent iron- and manganese-related issues, such as water quality and supply, in the Atlantis primary aquifer. Robey (2014) objectives were set out to determine site characterisation and preliminary evaluation of the study area to investigate the feasibility of the ISIR application. Furthermore, to design and construct an ISIR prototype and methodology at the study site, and to assess the effectiveness of iron and manganese removal by ISIR treatment. Robey (2014) designed and constructed an ISIR prototype which was used for the feasibility study and test four effective methodologies. The small-scale and short-term field investigation applied by Robey (2014) indicated that iron and manganese removal was achievable using the ISIR treatment method and using O_3, which was most effective than aeration investigations and comparable to using oxygen gas. Recommendations suggested that an investigation of a longer-term effectiveness of ISIR treatment using O_3 at the study site be applied. It was also recommended that multimeter probes for continuous measurement of pH, electrical conductivity (EC), and dissolved oxygen (DO) in the injected water, production borehole and monitoring boreholes at screen depth be monitored to understand the zone of influence and assist in optimising the systems design.

South African research has identified remediation of borehole clogging, but knowledge is required to determine preventative measures in controlling the source of borehole clogging. With no further studies investigating the long term treatment efficiencies of ISIR using

ozonation in primary aquifer settings in South Africa, developing an understanding of hydrogeological characteristics is of critical importance to establish long-term treatment suitability and the efficiency thereof (Mettler *et al.*, 2001; Jolly, 2002). This research emphasizes concerns developed over the years related to groundwater supply schemes susceptibility to failure. These concerns are water quality fluctuations, production borehole capacity failures, and declining water levels that affect potable water distributions for domestic and industrial purposes (Jolly, 2002). Iron-related borehole clogging is identified in Figure 1.2.

Figure 1.2: Iron-related borehole clogging experienced at the Atlantis Aquifer in the distribution pipeline (left) and flow meter at borehole (BH) 34022 in 1999 (Robey, 2014).

1.3 Research question and thesis statement

How efficient is the application of *in-situ* remediation technology using ozonation on production boreholes?

Developed from a previous study which was to investigate the feasibility of the ISIR technique in the prevention of iron- and manganese-related problems (i.e. water quality and supply) in a South African primary aquifer. This study demonstrated on a full production scale that iron and manganese borehole-related clogging problems experienced in South Africa can be prevented by means of ISIR technology using ozonation. In addition, this study included the addition of new injection boreholes compared to the previous, and adapted a different injection regime

during *in situ* O_3 injection. The proposed argument of this study is that the successful implementation of ISIR technology using O_3 would force iron oxidation within the primary aquifer to reduce production borehole clogging, thereby promoting sustainable borehole abstraction yields.

1.4 Study aim and objectives

This study aims to explain the use of ozonation as an ISIR technology in a primary aquifer to reduce borehole clogging occurrences and maximize production borehole abstraction efficiencies for water supplies in the Western Cape.

The study has the following 3 objectives:

1. To assess the effects of clogging on production boreholes using a combination of current and historical data to describe spatial and temporal yield variations in production and monitoring boreholes.
2. To analyse hydrochemical parameters' spatial and temporal responses to ozonation by, the collection of data before, during and after ozonation and delineating the relationships between groundwater quality datasets and quantitative field measurements by manual sampling and the telemetry system.
3. To quantify the efficiency of ISIR using ozonation, by the interpretation of iron and manganese concentration data gathered during ozonation from the telemetry system and manual sampling data.

1.5 Significance of the study

The study aims to achieve an optimum practical solution to improve and maintain the long-term management of production boreholes by reducing or preventing the occurrence of borehole clogging. The study incorporates data on available ISIR technologies, hydrochemical parameters in groundwater and determines the efficiency of O_3 treatment. This information can be utilized for educational and forthcoming research purposes within the extended research area. Information retrieved may also be used as an optimum approach in groundwater resource management schemes.

This study adopts less environmental impacts in comparison to some other treatment methods. The study uses O_3 which acknowledges unharmful environmental deposits and/or residues,

which is suitable during the precipitation of iron and manganese within the aquifer during the treatment technique (El Araby *et al.*, 2009). Its non-toxic abilities are presented most effectively when dissolved in water, making O_3 a suitable oxidant for ISIR treatment (Robey *et al.*, 2014). Its *in situ* use in this study, rather than *ex situ*, is emphasized by the ability of iron and manganese to oxidize faster when exposed to oxygen above ground. The use of an *in situ* technique will be adapted to allow maximum efficiency of the treatment procedure using O_3 injection to reduce, prevent and manage borehole clogging.

1.6 Scope and nature of the study

This research scope assesses the effects of using ISIR to reduce clogging in production boreholes in South Africa. Using the concept adopted from the Vyredox methodology (Braester and Martinell, 1988), ozonated water was injected *in situ* at constant injection regimes which effectively increased dissolved oxygen (DO) levels in the subsurface, affecting iron and manganese concentrations. By analysing hydrochemical parameters, a spatial and temporal response to ozonation will be assessed to assist in quantifying the efficiency of *in situ* ozonation. Incorporating these elements, an understanding and proposed method in preventing borehole clogging efficiently will be achieved.

The current study adopts a quantitative experimental and desktop design in achieving the three objectives outlined. For this study, field-work comprised of collecting hydrochemical data to develop a spatial and temporal response to the implemented system, thereby achieving the second objective using a quantitative experimental design approach. The desktop design approach for this study consists of collecting available data identifying the effects of clogging occurrences on production boreholes and quantifying efficiency in the application of ISIR to achieve objectives one and three respectively.

1.7 Research framework

Figure 1.3 shows the research framework of the study. The study is aimed at understanding remediation techniques to assist in preventing the occurrence of production borehole clogging which facilitates reduced borehole abstraction yields. Developing an understanding will assist in determining the efficiency of ISIR technology using ozonation in the Atlantis primary aquifer. To achieve the main objective, three specific objectives were established. The first

objective focussed on assessing the effects of clogging on production boreholes. The second objective focussed on analysing hydrochemical parameters spatial and temporal responses to ozonation. Lastly, the third objective focussed on quantifying the efficiency of ISIR using ozonation as the preferred remediation method. By achieving these objectives, the efficiency of using ISIR using ozonation at production boreholes would be established. The successfully implementation of ISIR using ozonation would ultimately prevent or reduce production borehole clogging, thereby promoting sustainable borehole abstraction yields.

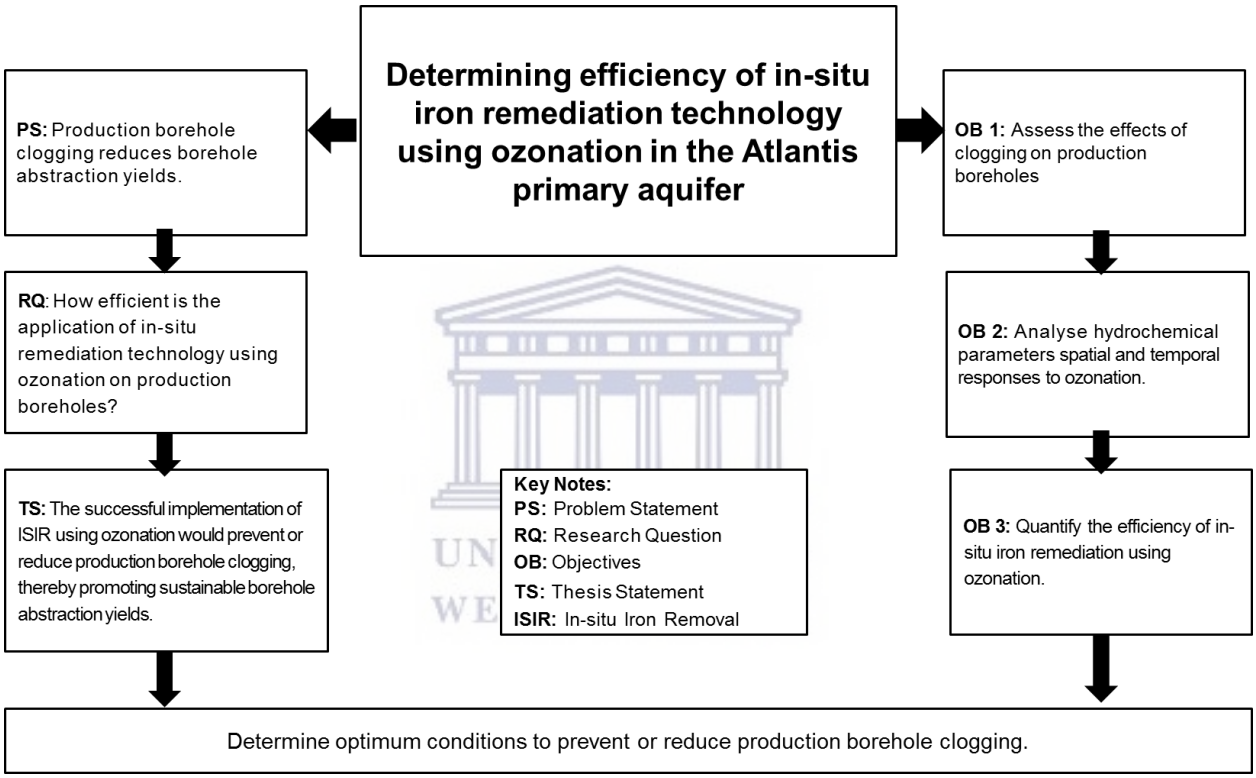

Figure 1.3: Research framework of the study

1.8 Study area description and justification

Situated north of Cape Town's metropolitan area, Atlantis is an industrial town well-known for manufacturing textiles (Murray and Harris, 2010). The study site (33°37'38.0"S 18°26'28.6"E) is the Atlantis Primary Aquifer, located along the semi-arid to arid west coast of South Africa where there is limited surface water. Atlantis primary aquifer is sloped and overlies Malmesbury Group bedrock, reaching an area coverage of 130 km^2 extending eastward from the Atlantic Ocean up until the town of Atlantis (Tredoux *et al.*, 2009; Tredoux *et al.*, 2011; Jovanovic *et al.*, 2017). The Malmesbury Group consists of phyllitic shale and greywacke, and

is overlain by unconsolidated Cenozoic sediments (Tredoux *et al.*, 2009; Jovanovic *et al.*, 2017). Sand thickness varies across the total area, ranging between 25 – 60 m, and saturation thickness reaches a maximum of 35 m (Tredoux *et al.*, 2009; Bugan *et al.*, 2016).

Atlantis relies on a mixture of groundwater from the Atlantis aquifer and surface water. The aquifer receives natural recharge from seasonal rains and managed artificial recharge from stormwater and treated wastewater. These combined sources filter into the sandy aquifer, abstracted through boreholes and then treated before potable distribution to the municipality. Site selection was based on the presence of advanced production borehole clogging occurrences that contribute to unsustainable borehole abstraction yields, threatening the town of Atlantis and neighbouring town's water supplies. By performing this research, an improved understanding of possible sites likely to experience borehole clogging, remediation strategies of production boreholes and iron oxide precipitation genesis will be derived. Furthermore, it aims to assist in the development of a feasibility case study assessing long term ISIR in the primary aquifer.

1.9 Thesis outline

The thesis is divided into 8 chapters: Chapter 1 provides the general overview of the study, outlining the research problem description, research question, and thesis statement, study aim, and objectives, the significance of the study, scope and nature of the study, a framework of the study and an overall outline of the thesis. Chapter 2 presents a review of literature with regards to iron and manganese chemistry, iron and manganese remediation technologies in groundwater, and ISIR technologies in South Africa and beyond. Chapter 3 provides a descriptive understanding of the research design and a detailed description of the study area. Chapter 4 provides a brief introduction and description of the methodology, followed by each of the three objectives results in Chapters 5, 6, and, 7. Chapter 8 provides conclusions and recommendations to the findings suggested in this study.

Chapter 2: Literature review

2. Introduction

This chapter describes iron and manganese in terms of its sources in groundwater, chemistry and effects on water supplies. It highlights the mechanics of borehole clogging and describes site characteristics and associated factors affecting iron and manganese treatment and removal from groundwater. A criterion for study area suitability for *in situ* iron remediation (ISIR) treatment using the Vyredox treatment is explained. ISIR techniques and efficiency rates are described, and international and local ISIR case studies are identified. With groundwater contributing to approximately 15% of South Africa's water supply, a third of this has been used for potable domestic water supply across South Africa (Engelbrecht, 1998; Robey, 2014).

2.1 Sources/origin of iron and manganese in groundwater

Both iron and manganese are common metallic elements that bare similar biogeochemical properties in solution (Ahmad, 2012; Robey, 2014). They generally co-exist naturally in anoxic environments, such as in deep boreholes (Ahmad, 2012).

2.1.1. Sources of iron in groundwater

Iron is a common element naturally found in water sources, rock formations, and iron sinks crucial to the livelihood of all living organisms (Environment, 2008). Iron can be found in three oxidation states elemental iron (Fe^0), ferrous iron (Fe^{2+}), and ferric iron (Fe^{3+}) (Smith, 2006; Ityel, 2011). Its presence in groundwater is influenced by precipitation and natural weathering of iron-bearing minerals that introduce dissolved iron content into solution with iron content between 0.5 and 5% (Environment, 2008). These iron minerals include amphiboles, biotite, pyroxenes, olivine, iron sulphides, oxides, carbonates, iron clay minerals, and sedimentary rocks (Simonson *et al.*, 2003; Smith, 2006; Ityel, 2011; Ahmad, 2012). In the event of weathering of most rocks, clay minerals are formed. Iron present in mafic rocks oxidizes and thereafter precipitates to a mineral of iron hydroxides, and oxides (Smith, 2006). Although naturally occurring iron concentrations rarely exceed 10 mg/L, it is generally the most abundant dissolved trace metal in groundwater (Ityel, 2011).

Anthropogenic factors such as mining activities, landfill leachate, effluent and borehole infrastructure corrosion, and organic acid accumulations in recharge water are additional sources contributing to iron concentrations in groundwater (Smith, 2006; Environment, 2008). Anthropogenic occurring iron concentrations has been documented to reach up to 10 mg/L or more in Florida (Wang *et al.*, 2011), and up to more than 30 mg/L in leachate-polluted aquifers close to landfills (Albrechtsen and Chrsitensen, 1994). These natural and anthropogenic processes promote the occurrence of iron in groundwater due to percolation through formations that dissolve and subsequently gather in aquifers (Ityel, 2011).

2.1.2 Sources of manganese in groundwater

In areas of manganese-rich soils and minerals, such as manganite, rhodonite, and manganese carbonates, natural weathering dissolves this metallic element in groundwater (Environment, 2008; Ahmad, 2012). Similar to iron, anthropogenic factors play a role in common sources of manganese in groundwater (Environment, 2008). Geology, soil, and subsoil contribute to manganese concentrations found in groundwater (Ahmad, 2012). Although iron concentrations generally exceed manganese concentrations, manganese is more soluble in natural waters (Braester and Martinell, 1988).

2.2 Iron and manganese chemistry

2.2.1 Iron

In water, iron exists in either of the two states:

- Soluble divalent Fe^{2+}
- Insoluble trivalent Fe^{3+}

The chemical reaction responsible for converting Fe^{2+} into Fe^{3+} in the presence of oxygen is simply understood by Teunissen (2007) through Figure 2.1 of the oxidation process:

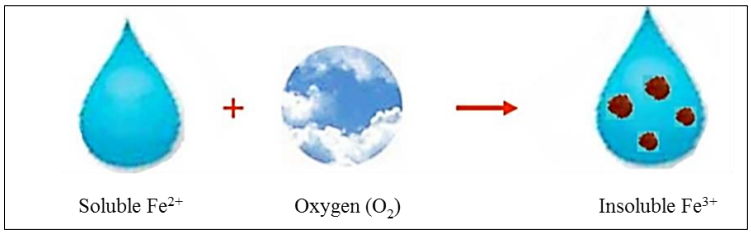

Figure 2.1: Oxidation process of soluble iron (Fe^{2+}) to precipitated insoluble iron (Fe^{3+}) in the presence of oxygen (Teunissen, 2007)

$$Fe^{2+} \rightleftharpoons Fe^{3+} + e^{-} \quad \text{(Equation 1)}$$

$$Fe^{3+} + 3OH^{-} \rightleftharpoons Fe(OH)_3 \quad \text{(Equation 2)}$$

$$Fe^{2+} + 3H_2O \rightleftharpoons Fe(OH)_3 + 3H^{+} + e^{-} \quad \text{(Equation 3)}$$

Equation 1 represents the first half-reaction, whereby divalent Fe^{2+} is oxidized to trivalent Fe^{3+} (Silveria, 1988; Walter, 1997). In the presence of high dissolved oxygen (DO) concentrations, the trivalent state can react with hydroxyl groups to precipitate into solid form (Equation 2). Equation 3 represents the primary sequence of the oxidation-reduction (redox) reaction forming iron-related clogging in a groundwater system (Walter, 1997; Ahmad, 2012). Although ferric hydroxide [Fe $(OH)_3$] is the most dominant form of solid iron in natural aquatic systems, precipitated iron can also occur as iron sulphate ($FeSO_4$) or ferrous carbonate ($FeCO_3$). Mineral and chemical data can determine whether ferric hydroxide is a primary inorganic factor and generally including the presence of manganese and carbonate to initiate well production clogging (Walter, 1997; Misstear *et al.*, 2006).

Pourbaix diagrams plots redox potential (referred to as pE or Eh) vs pH (Figure 2.2 and 2.3). It indicates the stability zone of water and the solubility phases of iron (Silveria, 1988). The equilibrium between iron species are represented by horizontal lines (Figure 2.2) and demonstrates redox reactions as the potentials are independent of pH with no protons involved in the chemical reactions between Fe^{2+} and Fe^{3+} (Clark, 1988). These regions experiences conditions under which the oxidation of iron to a soluble product will form corrosion. These stable phases are the solutions of Fe^{2+} and Fe^{3+}. The equilibrium between soluble Fe^{3+} and insoluble $Fe(OH)_3$ is demonstrated by the vertical line, independent of the redox potential and considered as an acid-base reaction (Figure 2.2) (Silveria, 1988). The sloped lines in the

pourbaix diagram refers to chemical reactions in which protons and electrons are transferred, indicating that corresponding potentials are a function of pH (Figure 2.2). In the water stability region, indicated between the two parallel sloped lines (Figure 2.2), iron is present in its most stable forms either in solution (soluble) or as an oxide (insoluble) depending on certain variables such as the concentration of each species.

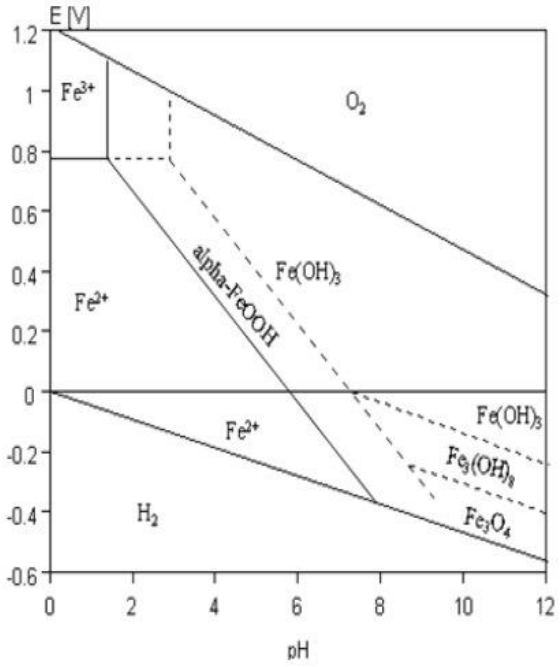

Figure 2.2: Pourbaix diagram of iron in natural water environments representing redox potential (V) and pH (Robey, 2014)

2.2.2 Manganese

The most common forms of manganese in water exist as soluble divalent manganese (Mn^{2+}) and insoluble manganese (Mn^{4+}). Its chemical behaviour and occurrence are similar to iron (Silveria, 1988). The exchange of electrons, converting one state of manganese to another is expressed in Equation 4:

$$Mn^{2+} + 2H_2O \rightleftharpoons MnO_2 + 4H^+ + 2e^- \quad \text{(Equation 4)}$$

Manganese dioxide (MnO_2) is the solid-state of manganese under natural aquatic porous conditions (Silveria, 1988).

With similar concepts derived from the pourbaix diagram explained in 2.2.1, the pourbaix diagram of manganese indicates the stability zone of water and the solubility phases of

manganese (Silveria, 1988). The equilibrium between the manganese specie Mn^{2+} and water (H_2O) is demonstrated by the horizontal line (Figure 2.3). This equilibrium indicates redox reactions that are independent of pH with no protons involved in the chemical reactions between Mn^{2+} and H_2O. The water stability region, indicated between the two parallel sloped lines (Figure 2.3) indicates the region where manganese is in its most stable forms either in solution as Mn^{2+} or as an oxide as MnO_2, depending on certain variables such as the concentration of each species.

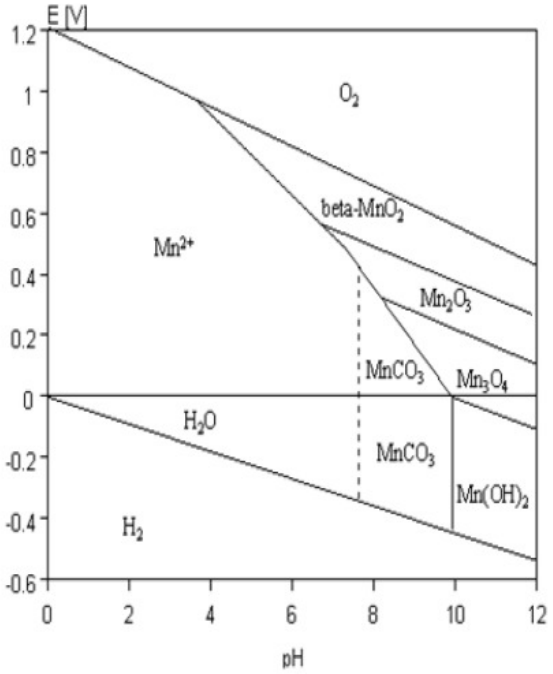

Figure 2.3: Pourbaix diagram of manganese in natural water environments representing redox potential (V) and pH (Robey, 2014)

2.3 Effects of iron and manganese on groundwater supplies

Borehole clogging is a world-wide issue reducing drinking water supplies from borehole pumping activities (Engelbrecht, 1998). This has been evident in Israel's coastal aquifer where a total of 460 operational observation- and pumping-boreholes has decreased to 200 boreholes as a consequence of clogging. River regions in the Netherlands wellfields extract anaerobic water, also resulting in aquifer clogging issues. With South Africa's different aquifers having been, abandoned, rehabilitated, and re-drilled into, the addition of boreholes into these aquifers have contributed to the cause of borehole clogging (Engelbrecht, 1998).

Iron oxide, manganese oxide, and calcium carbonate precipitates have been recognized as a global concern (Kinsbergen, 2019). Iron and manganese concentrations exceeding natural levels impose aesthetic and potable issues to public and industrial water consumers (Silveria, 1988; Robey, 2014). Organoleptic properties associated with the presence of iron and manganese include water discolouration's ranging from reddish-brown or greyish-black, turbid water, and an undesirable taste and appearance to drinking water (Mettler *et al.*, 2001; Edition, 2011; Robey, 2014). It also causes paper, cloth, plastic, and water receptacle staining, clogging of home softeners, pressure tanks and heaters, and corrosion in distribution systems (Clark, 1988; Robey, 2014). Consistencies in the occurrence of iron-related and, by extension, manganese-related clogging of boreholes in primary and fractured rock aquifers are considered a well-known phenomenon in South Africa's potable water supply schemes (Robey, 2014). Clogged production boreholes have threatened water quality and production yields of groundwater schemes, and is of great concern for future groundwater developments (Robey, 2014; Robey *et al.*, 2014).

The World Health Organization (WHO) endorses the treatment of water internationally if iron and manganese concentrations are above 0.3 mg/L and 0.1 mg/L respectively, before distribution (Clark, 1988; Mettler *et al.*, 2001; Edition, 2011). Although no health-based guidelines are stipulated in the WHO guidelines, health-based risks associated with prolonged iron and manganese ingestion have been reported. This includes effects on adults such as memory attenuation and muscle movement effects and in minors such as neurological development, intellectual function, and hyperactive classroom behaviour (Bouchard *et al.*, 2007; Homoncik *et al.*, 2010; Robey, 2014; Islam *et al.*, 2015).

2.4 Borehole clogging

Clogged borehole screens and the immediate aquifer is facilitated by fluctuating borehole yields, aquifer transmissivity (T) and the presence of biological residue (biofilm) and excessive oxide accumulations (Robey, 2014). Bugan *et al.* (2016) identified four possible attributing factors of production borehole clogging:

- Chemical clogging: The natural existence of both iron and manganese in aquifers
- Microbiological clogging: Naturally occurring bacteria which assist in the accumulation of iron and manganese elements

- Physical clogging: New borehole developments and variable pumping schedules and/or pumping regimes

2.4.1 Chemical clogging

Iron hydroxide minerals, such as ferrihydrite, goethite, and haematite, have been found to contribute to chemical clogging by increasing the rate of iron oxidation (Smith, 2006). Manganese oxides, iron sulphides, iron oxyhydroxides, and calcium carbonates form part of clogging occurrences in boreholes (Walter, 1997; Smith, 2006). Oxide precipitate solution properties change both chemical and physical morphological properties of natural iron oxides (Smith, 2006). In the event of these occurrences, properties of the solution consequently affect Fe^{2+} and Fe^{3+} concentrations, temperatures, pH levels, Eh and the ionic strength and composition of the affected solution (Lo *et al.*, 1996; Smith, 2006). Iron clogging in boreholes is enhanced by near-neutral pH levels between 6.3 – 6.8 of groundwater, iron concentrations that exceed 0.1 mg/L, and the presence of oxygen in groundwater (Smith, 2006). Layering of various oxygen levels within the borehole casing also facilitates iron clogging procedures (Smith, 2006). This typically occurs due to the presence of oxygen located closer to the surface of the borehole casing. Once soluble iron is exposed to oxygen it facilitates the oxidation process, precipitating iron into its insoluble state of ferric iron, ultimately contributing to clogging occurrences.

2.4.2 Microbiological clogging

Bacteriological colonies bearing slimy matrices recognized as biofilms precipitate ions, such as iron and manganese. These deposits surround production borehole screens, pumps, distribution pipelines, the surrounding aquifer, and borehole gravel packs (Tredoux *et al.*, 2004; Department Water Affairs and Forestry, 2009; Robey, 2014). Microbiological clogging is the most common form of clogging of boreholes and aquifers, with 80% of boreholes experiencing clogging due to biological activity (Engelbrecht, 1998). This biological condition is identified as biofouling. It is characterized by its difficult elimination resistance to chemicals and fast reproductive abilities in high turbulent pumping regimes which introduce atmospheric oxygen and pressure fluctuations assisting in production borehole clogging (DWAF, 2009; Robey, 2014). Decreasing water levels introduces atmospheric oxygen or aeration into the water-bearing formation, accelerating bacterial-related borehole clogging (DWAF, 2009).

Production borehole clogging influenced by the natural occurrence of iron in groundwater and biofouling introduces operational performance difficulties. *Gallionella ferruginea* is a common species of iron bacteria susceptible to low, yet detectable, DO concentrations and acts as an effective biofouling agent (Walter, 1997). This iron bacteria species exists in filamentous colonies and thrives off oxidation reactions from Fe^{2+} to Fe^{3+} (Clark, 1988). Biofilms contribute to increased pH levels of well water, either influenced by organic acid consumption or carbon dioxide (CO_2) removal in solution (Walter, 1997). Biologically induced precipitates are mainly comprised of carbonate minerals that crystallize and densify over time (Clark, 1988). pH variations introduced by groundwater aeration disturbances impose solubility effects of these carbonate minerals (Mettler *et al.*, 2001). Favourable conditions of iron biofouling are dependent on high nutrient concentrations such as Fe^{2+} and phosphorus, of approximately 1 m/s of water flow velocity, high redox gradients, oxic and anoxic water boundaries, and near-neutral pH ranges (Walter, 1997; Brown *et al.*, 1998; Smith, 2006).

2.4.3 Physical clogging

Physical factors associated with the rate of borehole clogging are related to borehole design and construction thereof (Smith, 2006). Screen displacement, unfavourable construction materials and equipment used in borehole construction are common factors influencing corrosion rates (Smith, 2006). Equipment failure usually occurs during the solidification of deposits. Declining borehole yields, operational procedures, and defective equipment are influenced by production borehole clogging due to high water demands and over-abstraction occurrences (DWAF, 2009; Robey, 2014). Over-abstractions occur during increasing supplementary production borehole pressures that maintain water supplies to water distribution demands (Robey, 2014). These issues impose operational problems and maintenance costs to production boreholes for potable water management supplies, imposing futuristic concerns on groundwater developments (Robey, 2014). Declining borehole yields highlights the need to enhance borehole operational efficiency and service delivery.

2.5 Characteristics affecting iron and manganese treatment

Subsurface properties have the greatest influence on the mobility and treatability characteristics of ISIR technologies (DEP, 2017). ISIR technology has been applied for decades on both an international and local level (Karakish, 2005). To ensure effective ISIR treatment applications

a well-defined design criteria, method application, and operational performance should be evaluated according to site characteristics (Karakish, 2005; Robey, 2014). Background data on investigated boreholes such as borehole construction, local geology and hydrology, soil characteristics, hydrogeological parameters, water quality or chemistry, contaminant type, transmissivity, storativity, groundwater flow rates or direction and aquifer conditions should be clearly understood (Robey, 2014; DEP, 2017). Understanding these properties provides valuable information to ISIR design, methodology suitability, and performance efficiency (DEP, 2017).

Oxidation and precipitation assist in the removal of dissolved iron and manganese in groundwater (Ahmad, 2012). Key physical and chemical parameters to be considered during ISIR treatment include pH, Eh, temperature, total organic carbon (TOC) or dissolved organic carbon (DOC), electrical conductivity (EC), dissolved oxygen (DO) concentrations, ammonia (NH_3), CO_2, hydrogen sulphide (H_2S), iron bacteria and soil characteristics (Filtronics, 1993; Vance, 1994; Ahmad, 2012). These parameters are essential in mobilizing and controlling iron and manganese concentrations, and removal efficiency rates and should be considered at any site to determine ISIR treatment suitability (Homoncik *et al.*, 2010).

2.5.1 pH and Redox potential (Eh)

Soluble iron and manganese exist in high concentrations in anoxic groundwater sources (Appelo and Postma, 2005; Robey, 2014). Ferrous iron typically occurs under pH values greater than 8 and Eh between 420 and 790 millivolts (mV) (Smith, 2006; Ahmad, 2012). Ferrous iron is easier and faster to oxidize in relation to manganese (Ahmad, 2012). Under favourable groundwater conditions, soluble iron and manganese are vulnerable to movement between pH ranges of 5.5 and 8.2 and in an area of low Eh (Ahmad, 2012; Robey, 2014). Oxidation of Fe^{2+} occurs optimally at a near-neutral pH level of greater than 6 and ideally between 7 and 8, while Mn^{2+} oxidation oxidizes optimally at a pH greater than 8 (Robey, 2014). In the event of ISIR, low pH conditions, generally lower than 7, requires higher oxygenated volumes to be injected into the aquifer for optimum iron remediation (Braester and Martinell, 1988).

Redox potential values in an aquifer setting with pH levels close to 7 can reach up to 700 mV if the precipitation zone is exceeded (Braester and Martinell, 1988). Tredoux *et al.* (2011) identified that Fe^{2+} was converted to Fe^{3+} with manganese remaining in solution during

increasing redox potentials. At pH values lower than 7 and Eh as high as 800 mV, manganese usually occurs in its soluble state (Mn^{2+}) (Homoncik *et al.*, 2010). Sufficient oxidation of metals, such as manganese, requires high Eh values of around 1000 mV if pH levels are very low (Braester and Martinell, 1988). In the presence of oxygen and high pH conditions, manganese is oxidized to Mn^{4+} (Homoncik *et al.*, 2010). Redox potentials in aquifers are dependent on many environmental factors (Braester and Martinell, 1988). Groundwater containing high amounts of methane, H_2S, dissolved iron and manganese and low pH levels express Eh to be low in value (Braester and Martinell, 1988). As a result, iron and manganese oxidation occur in groundwater environments with pH values greater than 8. Furthermore, Eh between 420 and 790 mV facilitates iron and manganese oxidation.

2.5.2 Temperature

The rate of iron oxidation presents effects between temperatures of 5 to 35˚C (Walter, 1997; Smith, 2006). Faster iron and manganese oxidation rates are greater at higher water temperatures and slower at lower water temperatures (Filtronics, 1993; Vance, 1994).

2.5.3 Total organic carbon (TOC) or Dissolved organic carbon (DOC)

Inorganic and organic complexes in waters possess inhibiting factors to oxidation reactions as increasing iron and manganese concentrations causes oxidation difficulties (Silveria, 1988). As described by Clark (1988), the exposure of groundwater to high organic matter, low pH levels, reducing Eh and percolation through ferruginous minerals introduce iron-rich groundwater conditions. According to Cromley and O'Connor (1976), organic matter presents interferences with the iron removal process in groundwater by concepts of peptizing ferric hydroxide precipitates, oxidation retardation, or complexation. Organic's ability to form a dissolved complex compound with iron is possible. However, it relies on water alkalinity, the molecular weight and hydroxyl group quantities of the organic matter (Sallanko *et al.*, 2007). High organic matter quantities introduce separation difficulties to oxidized iron (Sallanko *et al.*, 2007).

Dissolved organic carbon is defined as the fraction of organic matter which can pass through a pore size membrane ranging between 0.7 and 0.22 µm (Bruckner, 2016). Elevated DOC levels in groundwater are influenced by the presence of organic matter, it bears the capacity to

mobilize iron and assists in complexed iron molecule formation. These factors ultimately contribute to production borehole clogging (Tredoux *et al.*, 2009; Robey, 2014). It serves as a parameter of organic pollution in wastewater and water sources (Katsoyiannis and Samara, 2007). As a result, increased TOC and DOC concentrations mobilises iron and manganese oxidation rates that cause clogging of production boreholes (Tredoux *et al.*, 2011).

2.5.4 Dissolved Oxygen (DO)

Dissolved oxygen is a measure of the amount of oxygen dissolved in water and an indication of the amount of oxygen available to aquatic organisms and chemical reactions. Increasing concentrations accelerates oxidation reaction times of iron and manganese (Filtronics, 1993; Vance, 1994).

2.5.5 Hydrogen Sulphide (H_2S)

Hydrogen Sulphide is a gas associated with the presence of iron and manganese in groundwater (Filtronics, 1993). In addition to its "rotten egg" odour, sulphide fosters sulphur bacteria, causing corrosion to pipelines, irons and reservoirs. Anaerobic sulphate and organic matter reduction form sulphides and bisulfides, which is pH-dependent. Hydrogen sulphide dominates at pH levels less than 7, hydrogen bisulphide dominates between pH ranges of 7 and 9.5 and sulphide dominates at pH levels greater than 9.5. In the presence of sulphides, reactions with injected oxygen pose adverse effects on water quality, ranging from decreased pH levels to increasing heavy metal concentrations (Appelo and De Vet, 2003). Oxidants such as Cl_2, O_3, ClO_2 and H_2O_2 are highly reactive with H_2S. Organic complexes and substances possessing an oxidation demand must be treated before the oxidant effectively oxidizing iron and manganese (Filtronics, 1993). Sulphide oxidation is highly important in treatment procedures for effective iron and manganese removal. As a result, increasing concentrations of H_2S decreases the rate of iron and manganese oxidation.

2.5.6 Iron bacteria

Iron bacteria are usually present in pH ranges of 6 to 10 and bare a DO tolerance between 0.01 and 4.0 mg/L (Filtronics, 1993). The most common forms of iron bacteria in water are *Gallionella* and *Crenothrix* which use Fe^{2+} as an energy source to oxidize it into Fe^{3+}

(Filtronics, 1993). Iron bacteria contribute to corrosive abilities of well piping and casings of distribution systems by reducing well capacities and pipe diameters, causing staining and aesthetic issues due to their reddish-brown slime and stringy masses.

Microbiological activity from bacteria can oxidize reduced iron and manganese states under poor oxygen conditions and/or at increased Eh (Silveria, 1988; Vance, 1994). Under anaerobic conditions and suitable Fe^{3+} states, Fe^{3+} crystallinity increases with decreasing microbiological availability (Vance, 1994). The presence of these biofilm matrices is bacteriologically induced and contribute to mineral deposits of iron and manganese oxides that assist in pumping inefficiencies (Kinsbergen, 2019). Iron bacteria treatment involves material disinfections that are in contact with boreholes, such as chlorine or stronger chemical applications (Filtronics, 1993). As a result, iron and manganese oxidation increases in the presence of iron bacteria.

2.5.7 Soil characteristics

Highly permeable soils generally require higher volumes of fluid reagent injection for effective removal and treatment rates (Robey, 2014; DEP, 2017). Granular soils have uniform infiltrations of fluid characteristics, during sufficient fluid injection rates and injection durations (DEP, 2017). Calculations to determine minimum volume fluid injections of a treatment area can be calculated by using identified site-specific parameters of soil porosity (n), soil effective porosity (ne), soil hydraulic conductivity (K), soil fraction organic carbon (FOC), and treatment reagent(s) viscosity (μ) (DEP, 2017). Even though highly permeable formations have readily accepting fluid characteristics and a larger radius of influence, the number of injection boreholes should always be considered to effectively distribute sufficient volumes of injections throughout the designated treatment area (DEP, 2017).

Low permeable soils have reduced infiltration fluid volumes compared to high permeability soils (DEP, 2017). The establishment of flow paths is created under increased subsurface pressures to distribute injection fluid within a treatment area (DEP, 2017). To establish the most effective fluid delivery systems, closely spaced injection boreholes will promote fluid injection distribution effectively, which will target contaminant migration pathways (DEP, 2017). More fluid injection events will be required for effective contaminant removal. Alternatively, the use of a gaseous reagent such as O_3, hydrofracturing or pulsed pumping could be applied for effective removal rates (New Jersey DEP, 2017; Gale *et al.*, 2015). Hydrofracturing increases soil permeability and pulsed pumping allows for the injection pump

to be cycled on and off creating a back and forth motion to the reagent and improving contact with the contaminant (Gale *et al.*, 2015).

Histols (peat and marsh mats) are identified by poor drainage and high organic carbon content characteristics (DEP, 2017). Poor drainage properties restrict injection volumes of fluids to penetrate the subsurface during each injection cycle (DEP, 2017). High organic carbon content soils imply additional reagent fluid injection demands, as organic materials in the soils will easily react and consume reagent fluids, reducing reagent strength and availability during injections (DEP, 2017).

Heterogeneous soils are characterized by high permeability surface soils and lower permeable soils with increasing depth, retaining contaminants more easily (DEP, 2017). As a result, contamination retention is prone to increasing depth due to limited injection reagent injection accessibility (DEP, 2017). The importance of site characterization is reiterated, especially in heterogeneous soils, as specific contaminant locations should be known to target those areas directly for effective remediation results (DEP, 2017).

Groundwater flow in bedrock formations is generally fractured and bedding plane controlled, except for change caused by weathering and mineral dissolution which adds additional pathways in the subsurface (DEP, 2017). Contaminant distribution, migration paths and injection well design and location are of critical importance and should be determined by a detailed site characterization (DEP, 2017). Alterations in injection volumes and the extent of influence are determined by bedrock formations, treatment applications, site characterisation and pilot testing to establish effective treatment procedures (DEP, 2017).

2.6 Factors affecting iron and manganese removal in groundwater

Oxidation, precipitation and sorption processes affect the concentration of iron and manganese (Van Der Laan, 2008). Iron and manganese in groundwater can be removed by oxidation or sorption methods (Ezzat *et al.*, 2016). Oxygen transportation in groundwater is dependent on groundwater velocity and sorption and dispersion processes (Boochs and Barovic, 1981). These processes are identified in Figure 2.4.

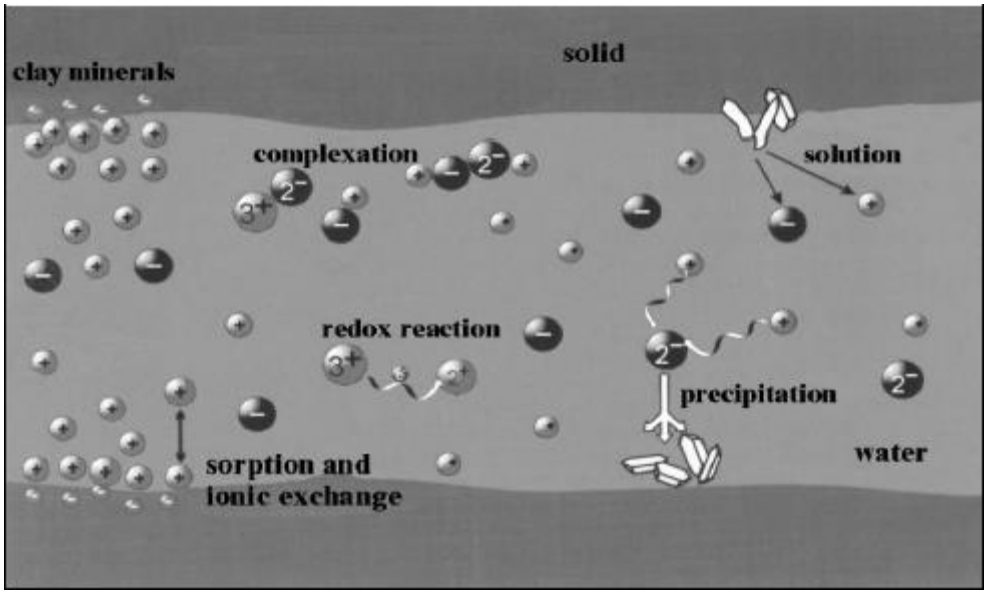

Figure 2.4: Different processes influencing iron concentrations in the subsurface (Ahmad, 2012). The process includes clay minerals, complexation, redox reactions, sorption and ionic exchange, and precipitation.

2.6.1 Sorption

Sorption is a general term that populates three different process descriptions; adsorption, absorption and ion exchange (Ahmad, 2012). Adsorption is the process whereby a chemical adheres to the surface of a solid, whereas absorption identifies chemical specie penetration into a solid, and ion exchange is the replacement of ions between chemicals along a solids surface (Ahmad, 2012). These processes regulate the transport of contaminants in soils and aquifers (Figure 2.5) (Appelo and Postma, 2005; Ahmad, 2012). Sorption in aquifers is modelled according to a solid's properties and generally occurs on clay minerals, oxides, or organic matter (Appelo and De Vet, 2003). Contaminant properties influence sorption behaviour and are classified according to water solubility, polar or ionic character, acid-base chemistry, redox chemistry and octanol or water partition coefficients (Piwoni and Keeley, 1990; Ahmad, 2012). Adsorption of dissolved iron and manganese are favoured when iron and manganese precipitate in the aquifer, as it provides suitable pH conditions for the removal of iron and manganese. A combination of both phase processes of oxidation and adsorption speeds up the removal of iron and manganese (Ahmad, 2012).

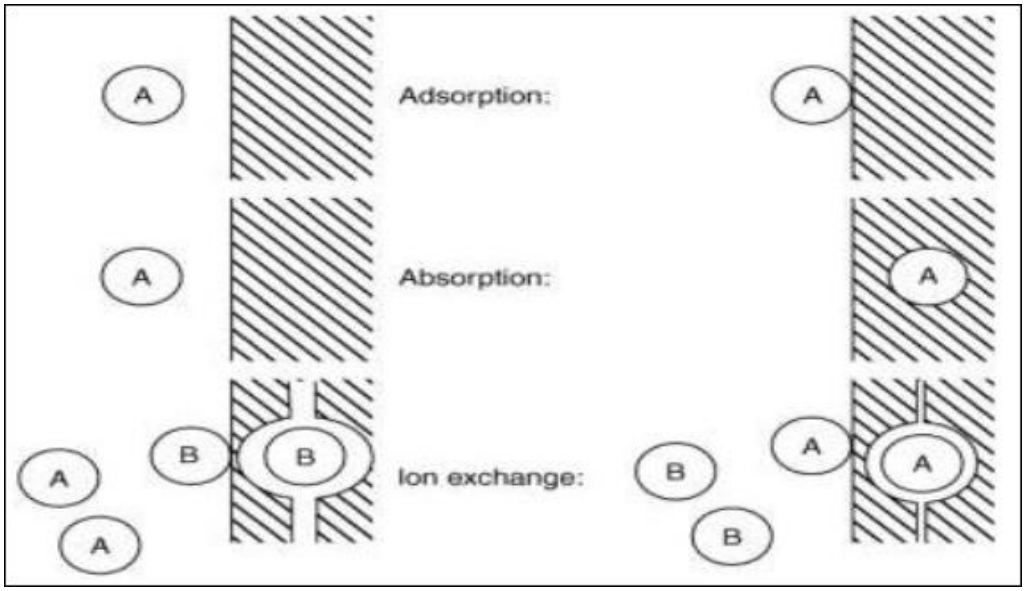

Figure 2.5: A demonstration of three sorption processes involving adsorption, absorption, and ion exchange (Ahmad, 2012).

2.6.2 Oxidation-reduction (redox) processes

Contaminants chemical oxidation involves the breaking of bonds of a contaminant compound in the presence of injecting or adding a highly reactive substance to stimulate the reaction (IDEM, 2005). Oxidation processes promote the transfer of contaminants to dissolved phases to easily treat contaminants *in situ* (IDEM, 2005). Once iron and manganese are converted to its dissolved states, these concentrations in groundwater can easily be reduced. Oxidation-reduction (redox) zones, oxic, hypoxic, anoxic and anaerobic, in the subsurface under natural groundwater conditions describes the oxidation processes that occur as oxygen levels decreases in the subsurface with increasing time (Figure 2.6). The root, intermediate, capillary fringe, and saturated zones within the vadose zone determines the redox state for both iron and manganese (Zhang and Furman, 2020). For iron, $Fe(OH)_2$ / Fe^{2+} occurs at the redox potential (Eh) of 0 mV at pH levels of 7.25, whereas for MnO_2 / Mn^{2+} it occurs at Eh values of 550 mV at a pH of 7.25 (Figure 2.6) (Zhang and Furman, 2020).

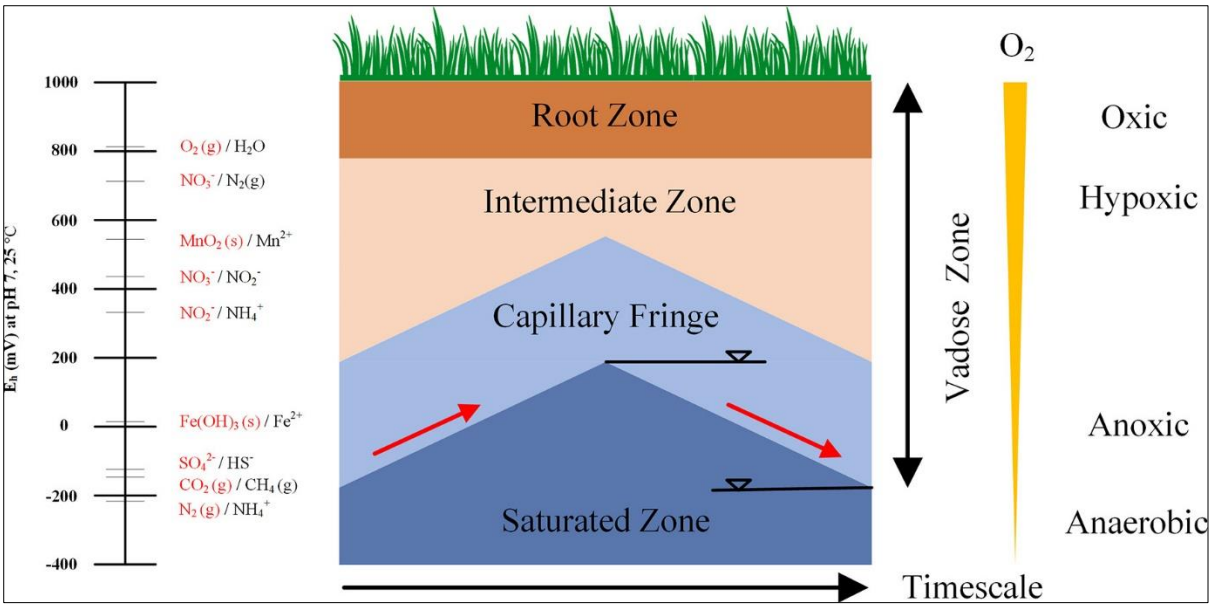

Figure 2.6: Natural reduction-oxidation (redox) zones in the subsurface in a saturated soil environment indicating reduced oxygen levels with increasing time. Includes redox potential (Eh, mV) at pH levels of 7.25 of chemical species (Zhang and Furman, 2020).

2.6.3 Chemical oxidants

The behaviour of oxidation agents used in aquifers during ISIR contributes to understanding the design of injection boreholes and injection regimes (Boochs and Barovic, 1981). Chemical oxidant strength, type and pH levels are measurable factors associated with the removal of iron and manganese (Robey, 2014). Various oxidant quantities required to remove 1 mg of Fe^{2+} and Mn^{2+} is identified in Table 2.1.

Table 2.1: Various oxidant quantities required to remove 1 mg of Fe^{2+} and Mn^{2+}. Oxidant quantities (mg), oxidation times (minutes or hours), necessary pH levels, and other information are included (Robey, 2014).

	Stoichiometric Reaction	Amount	Oxidation time	pH	Other information
O_2	$4Fe^{2+} + O_2 + 10H_2O \rightarrow 4Fe(OH)_3 + 8H^+$	0.14 mg	10 minutes	≥ 7.2	Application successful at lower concentrations but pH > 8.5 is necessary for dual oxidation of iron and manganese. If > 5mg/ℓ or complexed, oxygen should be used as a pre-oxidant step to reduce chemical costs.
	$2Mn^{2+} + O_2 + 2H_2O \rightarrow 2MnO_2 + 4H^+$	0.29 mg	1 hour	≥ 9.5	
O_3	$2Fe^{2+} + O_3 + 5H_2O \rightarrow 2Fe(OH)_3 + O_2 + 4H^+$	0.43 mg	< 1 minute	≥ 5.5	Instantaneous oxidation of uncomplexed ions and can oxidise complexes, however higher doses of ozone are required.
	$Mn^{2+} + O_3 + H_2O \rightarrow MnO_2 + O_2 + 2H^+$	0.87 mg		≥ 8	
$KMnO_4$	$3Fe^{2+} + MnO_4^- + 7H_2O \rightarrow 3Fe(OH)_3 + MnO_2 + 5H^+$	0.94 mg	< 5 minutes	≥ 7.5	Efficient for uncomplexed ions at low concentrations but is ineffective when ions are complexed.
	$3Mn^{2+} + 2MnO_4^- + 2H_2O \rightarrow 5MnO_2 + 4H^+$	1.92 mg		5.5-9.0	
ClO_2	$5Fe^{2+} + ClO_2 + 13H_2O \rightarrow 5Fe(OH)_3 + Cl^- + 11H^+$	0.24 mg	< 1 minute	6.8-8.4	Rapid oxidation of uncomplexed ions and effective to some extent with complexed iron or high NH_4^+ concentrations. Reacts faster with uncomplexed manganese than Cl_2 but is more expensive.
	$Mn^{2+} + 2ClO_2 + 2H_2O \rightarrow MnO_2 + 2ClO_2^- + 4H^+$	2.45 mg		5.5-9.0	
HOCl	$2Fe^{2+} + OCl^- + 5H_2O \rightarrow 2Fe(OH)_3 + Cl^- + 4H^+$	0.47 mg	< 1 minute	≥ 8.0	Rapid oxidation of uncomplexed iron but less efficient with manganese in near-neutral conditions and cannot be used for organic-rich water.
	$Mn^{2+} + OCl^- + H_2O \rightarrow MnO_2 + Cl^- + 2H^+$	0.96 mg	2 to 3 hours	≥ 8.5	
H_2O_2	$2Fe^{2+} + H_2O_2 + 4H_2O \rightarrow 2Fe(OH)_3 + 4H^+$	0.30 mg	< 1 minute	5.5-9.0	Rapid oxidation of iron but inefficient for removal of complexed iron and uncomplexed manganese.
	$Mn^{2+} + H_2O_2 \rightarrow MnO_2 + 2H^+$	0.62 mg	> 5 hours	≥ 8.5	

2.7 Ozone as an oxidant

The use of O_3 commercialized in France in 1906 with its first uses in water treatment immerging during 1893 in the Netherlands (Rice, 2002; Robey, 2014). Its non-toxic abilities are presented most effectively when dissolved in water, and during rapid conversions when exposed to oxygen (Robey *et al.*, 2014). Its harmless characteristics to safety regulations, hazard control and practical uses to variable industrial applications are widely utilized (Rice, 2002). Ozone is an unstable chemical oxidant agent that promotes oxidation and substitutes chlorine for its sterile attributes in water treatment procedures, considering its third-highest oxidant power characteristics (Nimmer *et al.*, 2000; Rice, 2002; Robey, 2014). It easily reacts with double bonds, activated aromatic systems, sulphides and non-protonated amines (Von Gunten, 2003). Direct O_3 reactions are dependent on acid-base and metal complexation (Von Gunten, 2003). Dominant oxidant abilities are characterized by its decomposing abilities, forming hydroxide and DO concentrations, improving oxidation reactions. Furthermore, its doses in drinking water and wastewater treatment allows for effective uncomplexed and

complexed iron, and DOC elimination (Robey, 2014; Rajagopaul *et al.*, 2008; Nimmer *et al.*, 2000; von Gunten, 2013). Common applications are involved in potable- and waste-water treatment procedures, agricultural, mining and food-processing industries (Rice, 2002).

Ferric hydroxide and manganese oxide precipitants will enable acceptable drinking water standards under suitable temperature and pH levels during O_3 dosage in groundwater (El Araby *et al.*, 2009). Ozone is emerging as a suitable *in situ* chemical oxidizing (ISCO) compound used as a remediation technique, characterized by its benefits of continuous oxidation application (Plummer *et al.*, 2005). Apart from other chemical oxidation techniques, O_3 can be injected as a gas into the vadose zone (Plummer *et al.*, 2005). Introducing O_3 gas into drinking water has characteristics to improve aesthetics and serve as a disinfecting agent to contaminants such as H_2S, iron and manganese, and microorganisms (El Araby *et al.*, 2009). The main secondary oxidant formed by O_3 decomposition in water is the OH radical (Von Gunten, 2003). Most unique to O_3, compared to other disinfectants of drinking water treatment such as chlorine, is its decomposition into OH radicals, which are the strongest oxidants in water (Von Gunten, 2003).

Using ozone (O_3) as an oxidant in the removal of 1 mg of soluble iron and manganese requires less than a minute for these ions to be oxidized (Robey, 2014). The reaction between Fe^{2+} to $Fe(OH)_3$ requires 0.43 mg of O_3 per 1 mg iron. However, the reaction from Mn^{2+} to MnO_2 requires 0.87 mg of O_3 per 1 mg of manganese. According to Table 2.1, the application of O_3 within water systems requires almost double the quantity of dosed O_3 used in iron removal to remove manganese (Robey, 2014). As evident, the oxidation of these uncomplexed ions generally occurs at much faster rates as opposed to complexed ions which require higher doses of O_3 and greater favourable conditions for improved removal efficiency (Robey, 2014). The oxidation rate of Fe^{2+} is influenced by abiotic factors such as the concentration of anionic species, such as chlorine, reducing the oxidation rate of Fe^{2+} and promotes increased concentrations (Lefevre *et al.*, 2016). pH dependency, DO and oxidants such as oxygen, chlorine and potassium permanganate $(KMnO_4)_3$ are additional factors associated to altered oxidation rates of Fe^{2+} (Walter, 1997; Ellis *et al.*, 2000; Lefevre *et al.*, 2016).

2.8 ISIR efficiency rates

ISIR efficiency is described by the extracted volume in the absence of iron and manganese to the injected volume of aerated groundwater (Olsthoorn, 2000). Observations indicating

increasing oxidant concentration in injectant water is pointless when efficiency is limited to exchangeable Fe^{2+} quantities that can consume the oxidant during the injection stage (Appelo *et al.*, 1999). One of several theories identified by Appelo *et al.* (1999) is that of Boochs and Barovic (1981), who considered ISIR treatment efficiency equivalent to the mixing ratio of groundwater and injected water volumes. However, this theory was unable to distinguish why treatment efficiency increases with increasing runs (Figure 2.7) by Appelo *et al.* (1999). indicates The efficiency rate is explained by the ISIR treatment as for every litre of injected water, the removal efficiency value (in litres) represents the iron-free groundwater that can be abstracted (Appelo and De Vet, 2003).

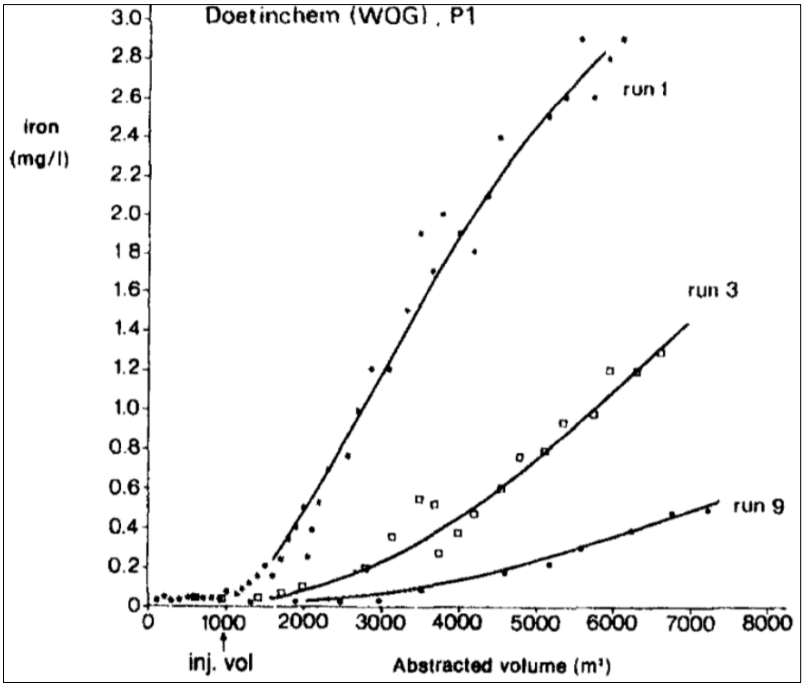

Figure 2.7: Iron concentrations in groundwater relative to increasing iron-free groundwater abstraction volumes over 3 abstraction periods after oxygenated water injection (Appelo et al., 1999). Iron concentrations (mg/L), abstraction volumes (m^2), and abstraction periods (1^{st}, 3^{rd}, and 9^{th}) are included.

Performed in many European countries, ISIR is a viable option to decrease iron concentrations in groundwater (Appelo *et al.*, 1999). Involving cyclic oxygenated water injection into the groundwater source, abstracted groundwater pumped after treatment from the aquifer has decreased iron and manganese concentrations, which assists in the absence of clogging occurrences (Appelo *et al.*, 1999). To determine removal efficiency, the volumetric ratio of the

abstracted volume of groundwater with reduced iron (V_{gw}) over the volume of injected volume (V_{inj}) is calculated (Appelo *et al.*, 1999). This is expressed by Equation 5:

$$E = \frac{Vgw}{Vinj} \qquad \text{(Equation 5)}$$

According to Hallberg and Martinell (1976) and Rott and Lamberth (1993), bacteria play a decisive role in efficiency determination. The repeated injection of oxygenated water and abstraction of reduced groundwater nutrients (injection-abstraction cycles) creates a favourable condition for bacterial community growth (Appelo *et al.*, 1999). Efficiency increasing with successive runs were related to bacterial community growth (Appelo *et al.*, 1999). This is explained by micro-organisms removing and storing the chemical oxidant, and implement usage when flow is inverted, allowing iron-rich groundwater to pass through (Appelo *et al.*, 1999). This process is dependent on the oxidation state of organic matter, and the ability of organic matter reactions to obtain sufficient oxidant concentrations in the injection fluid to attain higher efficiencies, which are more favourable when using oxygen (Van Beek and Vaessen, 1979; Appelo *et al.*, 1999).

The removal efficiency (V_{gw}/V_{inj}) of ISIR plants ranges between 3-22 and is dependent on site characteristics. However, the efficiency of ISIR is dependent on the sorption capacity of iron in an aquifer and is generally low on coarse, gravel aquifer types (Appelo and De Vet, 2003). Due to combined effects of chemical transportation and reaction, as well as the dispersion of chemicals within the aquifer, iron concentrations in the well will increase steadily with pumping (Appelo *et al.*, 1999). Iron remediation efficiency is dependent on decreasing Fe^{3+} concentrations in the event of newly injected aerated water in the aquifer (Appelo *et al.*, 1999). A case study in the Netherlands, a theory modified by Van Beek and Vaessen (1979), revealed that aerated water injections are proportionate to iron-reducing groundwater extraction at a 1:7 ratio respectively (Appelo *et al.*, 1999). Furthermore, successive runs of pumped oxygenated water sources derived from a nearby production borehole or treated groundwater from a reservoir revealed decreasing iron concentrations, illustrating increasing efficiency, which is a common feature in ISIR treatment procedures (Appelo *et al.*, 1999).

Apart from determining removal efficiencies using the volumetric ratio, the specific capacity (Sc) is used as an indicator of borehole efficiency (Robey, 2014). Comparing the specific capacity over time with the highest specific capacity obtained after a newly drilled and correctly developed borehole, borehole efficiency can be determined (Driscoll, 1986; Johnson,

2005; Robey, 2014). This specific capacity value is generally considered the standard value, with which to compare future values to (Driscoll, 1986; Johnson, 2005). Declines in calculated specific capacity indicates the occurrence of clogging activities on the borehole screen and/or gravel pack, pump failure, or decreased water levels (Driscoll, 1986; Johnson, 2005; Robey, 2014). Clogged boreholes should be remediated if a 25% decline in specific capacity is observed, as a specific capacity loss of 40% or higher will be difficult to restore borehole performance (Anderson *et al.*, 2010). Although specific capacity is a measure of borehole performance, it describes the productivity of the borehole and aquifer (Kruseman *et al.*, 1970; Robey, 2014). The abstraction rate (Q) is measured by dividing the amount of litres of water abstracted (L) by the duration of the step-drawdown test step in seconds (s). Dividing the abstraction rate (Q) by the drawdown (Sw) from step-drawdown tests, the specific capacity is calculated and expressed in Equation 6 (Anderson *et al.*, 2010):

$$Sc = \frac{Q}{Sw} \qquad \text{(Equation 6)}$$

An evaluation of specific capacity in boreholes has previous been tested in the study by Robey (2014) indicating that the specific capacity of a borehole is inversely proportional to the increasing abstraction rate with time. Specific capacity decreases in proportion to the drawdown in unconfined aquifers, such as in the Atlantis aquifer. These findings correlate to the conditions outlined by Driscoll (1986). Specific capacity declines have also been experienced in Suffolk Count in Long Island, New York production boreholes (Walter, 1997; Smith, 2006).

2.9 Iron and manganese removal techniques

The removal of iron and manganese in groundwater is made possible by *ex situ* and *in situ* iron and manganese removal. *Ex situ* techniques are techniques that involve treatment after groundwater extraction above ground while *in situ* techniques are techniques that involve direct subsurface treatment into an aquifer through boreholes. This work focuses on ISIR techniques and highlights the Vyredox principle applied in this study. Identified *in situ* techniques in this study includes the *in situ* deferrization experiment, *in situ* magnetic treatment method, Blended Chemical Heat Treatment (BCHT), Electrochemically Activated Water (EAW), Radical Water Treatment (RWT), BURMAN treatment, SIDKO system, and the two- or three-production borehole method. The identified international case studies explain how methods work, how

well they work and where they have been applied internationally. A comparative analysis between case studies identifying ISIR techniques, oxidant type, design, injection regime, baseline water quality, iron and manganese levels after ISIR, geological settings and aquifer types, efficiency coefficients, drinking water quality standards, and injection-abstraction cycles are summarized in Table 2.2. Identified case studies that could not be compared Table 2.2 are further discussed under headings in terms of Additional ISIR case studies; ISIR techniques, designs and oxidants; Injection regime and geological and/or aquifer types; Pre- and post-ISIR treatment and drinking water limits; Efficiency coefficients and injection-abstraction cycles; Removal efficiencies; and Conditions for oxidation and iron and manganese removal.

2.9.1 *In situ* iron remediation (ISIR) case study summary

Table 2.2: Comparative analysis between recognized in situ iron remediation (ISIR) technologies implemented internationally.

Source/reference	AWWA, 1984	Braester and Martinell, 1988	Dumousseau *et al.*, 1990	Olsthoorn, 2000	Mettler *et al.*, 2001	Appelo and de Vet, 2003	van Halem *et al.*,2010	Ebermann *et al.*, 2012
Location	Newman Avenue wellfield, Seekonk, Massachusetts	Drösing WTP, Lower Austria	Beaucaire WTP, south of France	El-Beheira, Egypt	Le Neuveville, western Switzerland	Lekkerkerk WTP, the Netherlands	Manikganj district, Bangladesh	Dobra, northern Saxony, Germany
ISIR treatment	Vyredox	Three production borehole method	Two-production borehole method	BURMAN treatment	Vyredox	Modified production borehole	SIDKO System	Two-production borehole method
Oxidant	Aerated treated groundwater from the distribution system	Aerated groundwater	Aerated groundwater	Cl_2 or $KMnO_4$	Aerated groundwater	Aerated groundwater	Aerated treated groundwater from the Bengal Delta Aquifer	Oxygen gas
ISIR Design	Two production boreholes surrounded by six injection well-points, and the third production borehole surrounded by four injection boreholes	Five well-points were constructed around each of the three production boreholes	Two-production borehole without additional boreholes	Two production borehole method	Two production boreholes were surrounded by five well-points at a 7 m radius around the production boreholes	The production borehole was the source of the recharge water and used for injection.	Water was aerated to DO concentrations between 1 to 6 mg/L and then filtrated through a sand and Fe(III)-hydroxide media	Pumping well 1 (PW1) was the injection borehole and PW2 was the source of water

Injection regime	24-hour injections occur every 2 to 3 weeks	One production borehole was used as the main water supply. Aerated water from the second borehole was infiltrated into the well-points of the third borehole. The treated borehole is then in production during treatment of another borehole.	Groundwater was pumped from one of the production boreholes and diverted for injection (2 500 m^3 for 18 hours) in the second borehole. After six hours, the operation was reversed and injection occurred in the second production borehole.	Intermittent injection of approximately 2 000 m^3 per cycle	Injection in the well-points took place for 24 hours at 8 L/s every five to ten days	6 % of the abstracted water volume was injected at 8.33 L/s for two days and immediately thereafter, pumping was resumed at 6.4 L/s for approximately 40 days.	Injection volume per cycle was < 1 m^3 at an injection rate of 1.2 m^3/h	Groundwater abstracted from PW2 (300 m^3) was injected into PW1 at 0.33 L/s
Baseline/initial water quality	Fe = 2.6 mg/L Mn = 6.2 mg/L	Fe = 0.27 - 0.35 mg/L Mn = 0.32 - 0.48 mg/L	Fe = 0.18 mg/L Mn > 0.05 mg/L	Fe = 0.38 mg/L Mn = 1.00 mg/L	Fe = 0.3 - 1.0 mg/L Mn = 0.1 - 0.2 mg/L	Fe = 6 - 7 mg/L	As = 0.145 mg/L Fe = 15.0 mg/L Mn = 0.3 mg/L	Fe = 9.8 mg/L (PW1) and 4.5 mg/L (PW2) Mn = 0.43 mg/L (PW1) and 0.29 mg/L (PW2)

Fe and/or Mn levels after ISIR	Fe < 0.5 mg/L Mn < 0.05 mg/L	Fe ≤ 0.1 mg/L Mn ≤ 0.05 mg/L	Fe < 0.05 mg/L Mn < 0.02 mg/L	Fe = 0.38 mg/L Mn < 0.4 mg/L	Fe < 0.2 mg/L Mn < 0.2 mg/L	Fe = 3 - 4 mg/L		Fe < 0.2 mg/L
Geological setting or Aquifer type	Glacial deposit	Gravel-sand aquifer with high clay content	Alluvial sand aquifer, clay-rich loam coverage (semi-confined)	300 m aquifer thickness with a semi-confined clay layer above the aquifer	Alluvial-deltaic aquifer	Coarse-grained sandy aquifer (20 -30 m thick)	Alluvial sands, anoxic aquifer	Aquifer of Pleistocene-age (14 m thick fine to medium-grained sands)
Efficiency coefficient (V/Vi)		2		4			Increased with each injection-abstraction cycle	2
Drinking water limits		Fe ≤ 0.1 mg/L Mn ≤ 0.05 mg/L	Fe < 0.05 mg/L Mn < 0.02 mg/L	Fe < 1.0 mg/L Mn < 0.5 mg/L			As = 0.001 mg/L Fe =0.3 mg/L Mn = 0.2 mg/L	Fe = 0.5 mg/L
Injection-abstraction cycles	A total of 19 cycles were performed for Mn removal to be established	1 after every 24 hours	4	19		18	20	4 (within a week) and 8 (within a few months)
Additional comments		Mn removal took longer and was only achieved after 20 days of application	Lowered pH values were noted during the treatment procedure in this aquifer setting	Conditions of the Nile Delta Aquifer groundwater has high Mn concentrations and low DO	Abstraction rate of 40 L/s.		Subterranean environment area	

2.9.2 Additional i*n situ* iron remediation (ISIR) case studies

2.9.2.1 Cromley and O'Connor (1976)

Although this case study didn't highlight a specific study related to ISIR, it compared the effects of ozonation and aeration on iron- and organic matter-containing groundwater. Results from the application of ozonation in groundwater demonstrated events whereby organic compounds are destroyed in the presence of O_3. However, in the absence of complete organic compound destruction, these compounds can possess aggressive traits by forming additional organic compounds, generating additional iron removal interferences in groundwater. Effects of ozonation in comparison to simple aeration identified three key aspects. Firstly, the oxidation of Fe^{2+} was performed at much faster rates and more extensively using ozonation. Secondly, TOC concentrations were greatly decreased by ozonation, whereas simple aeration barely affected these concentrations. Lastly, iron removal was significantly reduced by ozonation during the first reaction phase compared to simple aeration. During the second phase, ozonation depleted removal efficiencies immensely, possibly due to increasing organic compound interferences. Despite the interference from organic compounds, a preference of ozonation over simple aeration holds promising results in terms of effective iron removal from groundwater sources.

2.9.2.2 Hallberg and Martinell (1976)

This case study explains the Vyredox method applied in Herajoki at Rihimaki, Finland, which was the first Vyredox method developed, installed and considered a treatment plant to reduce iron concentrations *in situ*. With 2 different boreholes used in the treatment process, at 10 m apart, iron and manganese concentrations were vastly different. Both boreholes yielded similar water levels and supplied more than 7 000 m^3 over many years. The use of aerated water allowed for suitable conditions for iron-oxidizing bacteria to assist with iron oxidation *in situ*. Iron concentrations in borehole 1 and borehole 2 were recorded as 0.4 and 3.5 mg/L respectively, noting a great change in groundwater quality over a 10 m separation. This is due to variations in geological strata, groundwater composition, seepage conditions into the subsurface and fluctuations in the oxygen content of groundwater. Repetitions of in situ injections at the study site at specific time periods promoted the decrease in iron concentrations.

2.9.2.3 Boochs and Barovic (1981)

This case study addressed the ISIR conditions of the experiment performed in Ostfriesland, northern Germany that injected oxygen-rich water *in situ* to treat high iron and manganese concentrations in groundwater of coastal areas. The borehole used for abstraction and injection purposes was 80 m in depth and screened between 64 to 78 m. Treated water was saturated with oxygen from the air and injected at a rate of 50 m^3/h for 48 hours. Thereafter, abstraction occurred and re-injection shortly after. A ratio of injection to abstraction phases increased from 1:1 to 1:3. Before treatment, iron concentrations were roughly 10 mg/L. During the injection-abstraction cycles, an oxidation zone was created around the well, decreasing iron concentrations of the abstracted water during each injection phase, as abstraction durations increased.

The study also recommended suggestions that were drawn from the experiment, taking into consideration its conclusion that groundwater quality can be improved by recharging water containing oxygen *in situ*. The water source should be saturated with oxygen and recharged *in situ* through discharge boreholes to ensure that recharged water is distributed in the same pores during injection and abstraction. Water sources from reservoirs, boreholes, or from integrated water supplies should be pre-treated to improve operation time of the well. Recharge time is dependent on dispersion, influenced by tectonics and aquifer structure.

2.9.2.4 Walter (1997)

Suffolk County in Long Island, New York is a project that demonstrated the roles of iron-related bacteria and chemical conditions which affect capacity declines in production boreholes. According to this study, the effects of iron-related well-screen and casing encrustation and aquifer biofouling initiated the occurrence of production borehole clogging and declined borehole yields (Walter, 1997; Smith, 2006). Borehole operations were considered a determinant in clogging occurrences, as this study recognized increased effects during shut down periods. This was described by mineralogical and chemical procedures of precipitated iron oxyhydroxides and iron bacteria growth, hindering pore space surrounding the formation, pumps, pipes, and well screens (Walter, 1997; Smith, 2006). Furthermore, elevated iron and phosphate levels and low DO concentrations were associated effects related to iron-related well-screen encrustation in this study area. Conditions contributing to redox disequilibrium is said to originate from combining oxygenated groundwater with low DO

concentrations and low groundwater pH ranges that reduce the rate of iron oxidation after introducing oxygen into the system. According to the study of Walter (1997), it considers iron-related bacteria and elevated iron concentrations in groundwater as a source of clogging incidences that decrease well yields and specific capacity. This typically occurs due to precipitates during oxidation to iron oxyhydroxides. This project recommended suggestions and concerns of geochemistry and microbiology associated with iron-related well-screen encrustation. However, the role of ISIR treatments to these conditions are not determined in this project.

Suffolk Count in Long Island, New York has experienced specific capacity declines in several production boreholes during shut down periods. It is said that the effects of iron-related well-screen and casing encrustation and aquifer biofouling initiated the occurrence of production well clogging and declined well yields (Walter, 1997; Smith, 2006). This is described by mineralogical and chemical procedures of precipitated iron oxyhydroxides and iron bacteria growth, hindering pore space surrounding the formation, pumps, pipes, and well screens (Walter, 1997; Smith, 2006). Furthermore, elevated iron and phosphate levels and low DO concentrations are associated effects to iron-related well-screen encrustation. Conditions contributing to redox disequilibrium is said to originate from combining oxygenated groundwater with low DO concentrations and low groundwater pH ranges. These conditions reduce the rate of iron oxidation after introducing oxygen into the system.

Increased pH levels increase the rate of Fe^{2+} oxidation, due to ferric hydroxide autocatalytic effect, ultimately increasing saturation and precipitation of ferric hydroxide in production boreholes. Parameters such as pH, concentration, feed rate, and anion nature determine the composition of precipitate formation (Alıcılar *et al.*, 2008). According to Equilibrium modelling, treated water was saturated with ferric hydroxide and possessed an average half-time of oxidation of 11.9 minutes at pH ranges between 7 and 8. On the contrary, untreated well water was unsaturated with ferric hydroxide and possessed an average half-time of oxidation of 4.19 days at pH ranges between 4 and 5. Ferric hydroxide would not precipitate during production well operations, as pumping practices preserve groundwater's pH at naturally low levels and ultimately maintaining undersaturation. The removal of iron, manganese, and sulphate and increasing the pH of solutions alter well water chemistry. Well-screen encrustation materials sampled the presence of sulphur-reducing bacteria and iron-sulphide mineralogy, which promotes well-screen encrustation in certain geochemical

environments. Suffolk County bears a hydrogeological environment characterized by unconsolidated sand and gravel aquifers underlying this suburban county.

According to the data obtained for the study, Fe^{2+} was the most abundant iron species in the production boreholes and constituted between 81.6 – 99.4% of the total iron (Fe^{T}) composition from the groundwater sources. A relatively intriguing finding documented by Walter (1997), mentions that according to the Fe^{2+} and Fe^{3+} data obtained, conditions between iron and oxygen at concentrations equal to or greater than 0.1 mg/L within the boreholes are reducing and oxidizing respectively. A corroboration by Walter (1997) stated that the well water was in a state of redox disequilibrium in its most natural conditions during groundwater blending.

Eh values of groundwater from the Fe^{2+} or Fe^{3+} redox couple averaged to 390 mV and the DO or water redox couple averaged to 810 mV. The disequilibrium formed between iron and oxygen indicates the blend between oxygenated water and Fe^{2+} water generally occurs near the well screen. This occurrence could either be influenced by variable geochemical water characteristics along the well screen or within the aquifer in response to oxygenated drawdown surrounding the pumping well. According to the equation, an expectation that iron oxidation would likely occur faster at high pH values and high DO concentrations are deduced, with pH contributing to the greatest effect. The oxidation of Fe^{2+} increases along with the occurrence of precipitating ferric hydroxide in treated water due to its elevated pH levels and pH-dependency. The oxidation rate of iron decreases the presence of high concentrations of sulphate, chloride, nitrate, and bromide, through the complexation of free Fe^{2+}. In addition, low concentrations of DO slow down the rate of chemical iron oxidation within boreholes (Smith, 2006).

2.9.2.5 Teutsch *et al.* (2005)

Ron River in central Switzerland is an example of a small-scale *in situ* deferrization experiment performed in the Ron River valley aquifer setting reaching up to thicknesses of 10 m. This case study highlighted the environmental conditions and treatment procedure specific to this study area. Groundwater recharge is fed by lateral flows from valley planes and precipitation within the area and percolates between glaciofluvial gravel and sand deposits. Using a three-stage experiment, repeated simultaneous oxygenated water injection using 8 mg of oxygen per litre over a two-hour period was performed. A stable reaction time of one hour and groundwater extraction regimes of 45 litres per minute between two and six days was achieved. With

increased runs of oxygenated water injections and groundwater abstraction cycles, it was observed by breakthrough curves that after the 6th and 7th cycle, iron concentrations decreased most significantly. The duration of the experiment observed that Fe^{2+} is adsorbed from native groundwater and drawn into an oxidation zone where oxidation occurs, forming ferric hydroxide. The experiment demonstrated increasing removal rates of dissolved iron concentration with respect to increased oxygenated water injection cycles temporally. However, the aquifer setting of the Ron River project differs from the current study, thereby depicting variable reactive conditions.

2.9.2.6 Diliūnas *et al.* (2006)

Diliūnas *et al.* (2006) investigated the effects of *in situ* magnetic activation of iron and thinly dispersed compounds in groundwater aquifers of quaternary and alluvial deposit composition. The magnetic treatment method incorporates groundwater aeration and abstraction thereafter to emit improved drinking water quality standards. This method considers improved and effective ISIR strategies in groundwater. Although magnetic conditioning is generally used for surface water, groundwater implementations have only been investigated in Lithuania. The oxidation environment of aquifers promotes almost complete elimination of iron under the following conditions: Eh > 190 mV, pH > 7.5, oxygen levels > 0.4 mg/L and CO_2 < 50 mg/L.

2.9.2.7 Smith (2006)

From a South African context, this study mentions ISIR technologies that have been implemented at smaller scales to the current project to investigate the rehabilitation of clogged boreholes. Rehabilitation methods previously conducted on the majority of the production boreholes in South Africa have considered the concepts of patent Blended Chemical Heat Treatment (BCHT), Electrochemically Activated Water (EAW) and Radical Water Treatment (RWT) (Bishop, 2006; Smith, 2006; Robey, 2014). The Klein Karoo Rural Water Supply Scheme (KKRWSS) supplies domestic and farmers with water in the Oudtshoorn valley area of the Western Cape, South Africa (Bishop, 2006). The KKRWSS demonstrated the application of BCHT to iron-clogged production boreholes using a three-phase treatment approach (Walter, 1997; Smith, 2006). The Atlantis Water Resource Management Scheme (AWRMS) is also an example of ISIR implementation using BCHT. The three-phase application involves heating chemical blends around temperatures of 65 - 95˚C to shock and disrupt the clogging

material in screens and casings of the borehole, which is mechanically dispersed (Flower and Bishop, 2003). Secondly, pH levels are dropped to less than 1.5 along with high-pressure cleaning applied within the borehole (Robey, 2014). Lastly, further high-pressure cleaning is performed once again and the neutralization of water chemistry is performed to prevent the reoccurrence of borehole clogging. The project demonstrated successful returning yields within three days after treatment, having injected 10 m^3 of chemical blends into the production boreholes (Smith, 2006; Robey, 2014).

Although this belligerent remediation technique is available in South Africa, its long-term approach to the prevention of borehole clogging is short-lived due to exorbitant expenses, skilled operators, equipment requirements, and toxic chemical hazardous environments (DWAF, 2009; Robey and Tredoux, 2013). According to Smith (2006), the combination of mechanical and chemical applications coordinates the successful implementation of the BCHT method. Clearly outlined prospects of the project developed evidence that sustainable production yields are actively maintained through coupled routine maintenance, well-developed management strategies that initiate progressive improvements, sufficient project funding, and competent operational staff which optimize borehole rehabilitation (DWAF, 2009).

2.9.2.8 Kinsbergen (2019)

Harsonic, based in Belgium, has created a useful ultrasonic device to provide an effective solution to prevent borehole clogging as a consequence of iron oxide, manganese oxide, and calcium carbonate contamination (Kinsbergen, 2019). The ultrasonic device uses an ultrasound transducer above-ground to emit ultrasound waves at specific resonant frequencies within the borehole, decomposing the bacteriological-induced biofilm matrix (Kinsbergen, 2019). The use of water as the carrying medium allows ultrasound waves to penetrate open check valves, pump heads, and borehole screens (Kinsbergen, 2019). After the decomposition of biofilm in the borehole, frequent operation during borehole abstraction removes biofilm matrix impurities (Kinsbergen, 2019). The application of the ultrasonic device has been used over the past 10-years in ship hulls, cooling systems, and well-point distribution systems worldwide to prevent biofilm formation (Kinsbergen, 2019). The reduction in pumping efficiencies, as a consequence of iron oxide deposits in Koo Valley generally occur within 3 months of production, has been estimated at 90% (Kinsbergen, 2019). A summary of results indicated

that after 2 years of borehole operation with the installed ultrasonic device, borehole performance was consistent and had a 50% reduction in energy consumption per cubic metre of pumped groundwater. Similar testimonies were recorded in Texas (iron oxide deposits) and Burkina Faso (calcium carbonate deposits). This is a new and emerging ISIR technology.

2.9.3 *In situ* iron removal (ISIR) techniques, designs and oxidants

Since the 1970s, several different ISIR techniques have been implemented with the main two including single well that uses a single well for injection-abstraction cycles, and multiple boreholes that use separate boreholes for injection-abstraction cycles. Multiple well techniques are known as the Vyredox method (Robey, 2014). Vyredox treatment methods in this study review implementations in Massachusetts, Switzerland, South Africa, and Austria and other ISIR methods (American Water Works Association, 1984; Braester and Martinell, 1988; Mettler *et al.*, 2001; Robey, 2014). Although Massachusetts, Switzerland, and Austria have used aerated water as its preferred oxidant during its Vyredox treatment, South Africa has incorporated the use of O_3 as an oxidant which has yielded promising results (American Water Works Association, 1984; Braester and Martinell, 1988; Mettler *et al.*, 2001).

In addition to the common Vyredox method, other ISIR treatment methods include the BURMAN, SIDKO system, magnetic treatment, *in situ* deferrization experiment, single well, two- and three-production borehole that adopts the Vyredox methodology, BCHT, liquid CO_2 process, EAW, RWT, and the BoreSaver Ultra C Treatment methods, that have been implemented in Egypt, Bangladesh, Europe, Switzerland, India, France, Netherlands, Germany, and South Africa (Olsthoorn, 2000; Mettler *et al*., 2001; Smith, 2002; Flower and Bishop, 2003; Teutsch *et al.*, 2004; Diliūnas *et al.*, 2006; Smith, 2006; Sen Gupta *et al.*, 2009; van Halem *et al.*, 2010; Deed and Preene, 2013; Ebermann *et al.*, 2013).

Most of these treatment methods use aerated water as an oxidant. Certain treatment methods have adopted very different oxidant applications in their techniques. The Magnetic treatment method improves drinking water quality and the removal of iron and thinly dispersed compounds in groundwater aquifers of Quaternary and alluvial deposit composition (Diliūnas *et al.*, 2006). The BoreSaver Ultra C treatment method is another example of a rarely used oxidant in this ISIR treatment (Deed and Preene, 2013). In this treatment, oxalic acid and biocidal copper compounds are injected in mild acidic aquifer conditions *in situ*, disrupting iron deposits in boreholes (Deed and Preene, 2013). In addition to oxidant variability, although

using the two-production borehole method adopted from the Vyredox method, Ebermann *et al.* (2012) use oxygen gas as an oxidant. The ISIR treatment of Robey (2014) used O_3 as the selected oxidant because aeration was not feasible for the organic-rich groundwater present at the study site. The effects of ozonation and aeration on iron- and organic matter-containing groundwater was further investigated and discussed by Cromley and O'Connor (1976).

2.9.3.1 The SIDKO System

A community scaled test facility was created in Manikganj district, Bangladesh to injected aerated water into anoxic aquifer conditions in hopes to oxidize and precipitate iron (Fe) and arsenic (As) concentrations in shallow tube boreholes, reducing these concentrations. One of the objectives of the study was to determine the dominant process in subsurface Fe and As removal to meet WHO standards applicable for rural Bangladesh groundwater sources. Using an anoxic column experiment using natural groundwater, simulating a change in redox conditions in the oxidation zone during Fe and As removal was aimed at being achieved. The column experiments were conducted under controlled conditions for adsorptive-catalytic oxidation procedures, with the test facility providing insight on the subsurface treatment in the complex subterranean environments in the area.

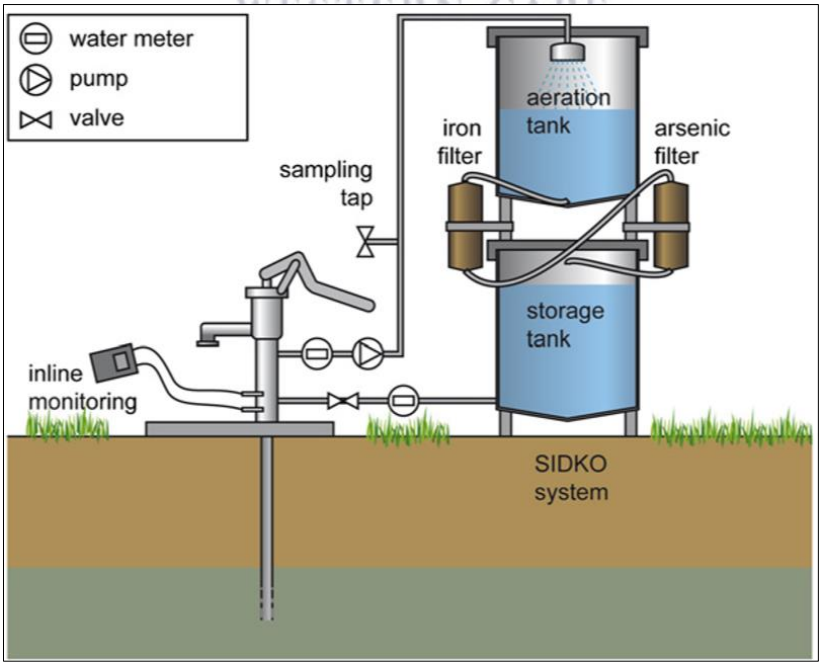

Figure 2.8: The small-scale test facility in Manikganj, Bangladesh using the SIDKO system to remove iron (Fe) and arsenic (As) from groundwater

The principle outlined by the small-scale subsurface Fe and As removal technique is that aerated water is injected in the subsurface periodically (Figure 2.8). When Fe^{2+} is oxidized, an iron hydroxide surface area along soil grains is created and available for adsorbing Fe^{2+} and oxyanions such as As. During abstraction, Fe^{3+} coated soil grains adsorbs the Fe^{2+} and As (III), resulting in reduced Fe and As concentrated groundwater. Once iron oxyhydroxide is exhausted, the reoccurrence of high Fe and As concentrations prevail as no Fe^{2+} or As (III) will be adsorbed along soil particles. As a result, the injection phase commences with the abstraction phase to follow (Figure 2.9).

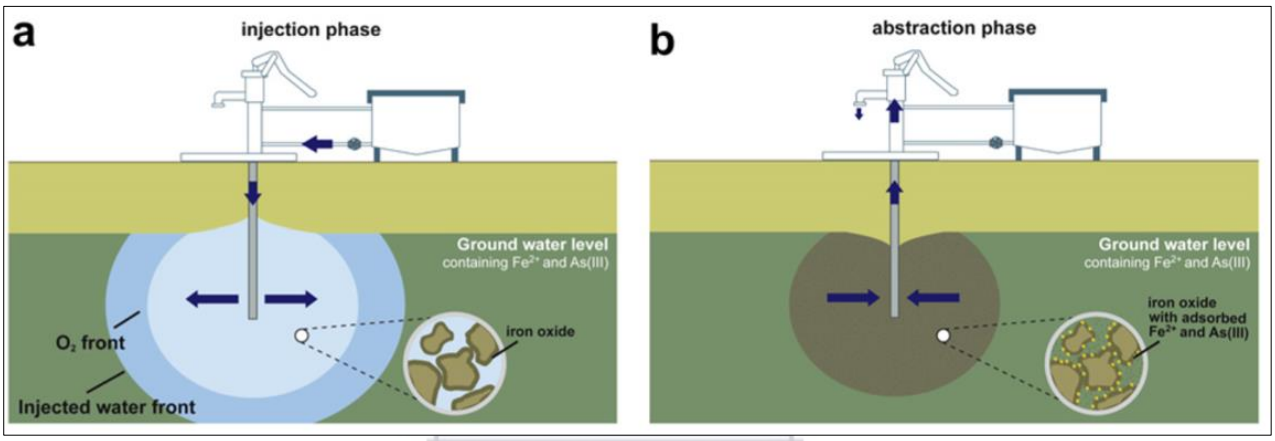

Figure 2.9: Subsurface iron removal using aerated water as the oxidant during (a) the injection phase, when aerated water is injected into the subsurface, creating an oxygen zone for oxidation of iron oxides to form in the zone and (b) during groundwater abstraction, treated water free of ferrous iron (Fe^{2+}) is abstracted, leaving precipitated iron oxides in the subsurface.

2.9.3.2 The Vyredox Method

During the 1960's, an alternative to the removal of iron and manganese in groundwater treatment has been applied, through *in situ* treatment methods such as the Vyredox Method (Braester and Martinell, 1988). The first commercial Vyredox plant was developed in 1969, and today more than one hundred plants in over ten countries have been developed, adopting the Vyredox I and/or Vyredox II principle (Braester and Martinell, 1988). The injection of degassed and oxygenated water in the subsurface establishes an oxidation zone and redox gradient around the injected well (Braester and Martinell, 1988). With increased pumping activities from the production well, iron and manganese precipitation zones usually occur closer to the well, thereby increasing iron and manganese concentrations yet again (Braester

and Martinell, 1988). Re-injection of oxygenated water is performed, allowing the redox gradient to expand and distribute iron and manganese concentrations throughout the oxygenated and precipitation zone around the well (Braester and Martinell, 1988).

The "daisy-wheel" approach (Figure 2.8) adapts the concept derived from Hallberg and Martinell (1976), which injects oxygen-rich water into injection boreholes surrounding the borehole. Alternatively, the approach developed by Diliūnas *et al.* (2006) injects oxygen-rich water directly into the production borehole. Numerous factors should be considered before the commencement of water injection, as the application of *in situ* treatments aims to promote reducing conditions to iron-related clogging before abstraction (Braester and Martinell, 1988). These factors include the removal of Fe^{2+}, CO_2 and methane on water retrieved from a surrounding borehole before oxygenation (Hallberg and Martinell, 1976), and pH levels should be equal to or not exceed 7, considering Fe^{2+} oxidation conditions (Cavé *et al.*, 2004).

The Vyredox method reduces groundwater conditions bearing high iron and manganese concentrations (Braester and Martinell, 1988). With iron and manganese characterized as abundant elements in the composition of the earth's crust, their natural existence in groundwater is a concerning aspect when considering groundwater practices as a potable water source (Braester and Martinell, 1988). Ferrous iron in its natural state is highly soluble. However, Fe^{3+} is usually precipitated as an oxide (Fe_2O_3) or oxyhydroxide (FeOOH) (Braester and Martinell, 1988). Oxidation is highly dependent on DO (Braester and Martinell, 1988). Redox potential values are dependent on pH levels typical for aquifer systems of around 7 that facilitate sufficient manganese oxidation and generally occupy values of 600 to 1000 mV moving outwardly from the production well (Braester and Martinell, 1988). With lower pH levels, iron removal is reluctant to reducing conditions and requires continuous O_3 injection into an aquifer system to meet satisfactory iron remediation results (Braester and Martinell, 1988).

The derivative of oxygen is generated either by aeration or dosing mechanisms using oxygen gas. Dissolved oxygen concentrations of the injected water using aeration decreases to approximately 6 – 8 mg/L, whereas dosing oxygen gas maintains concentrations at 20 – 30 mg/L (Diliūnas *et al.*, 2006). Water abstraction from an unclogged production borehole is oxygenated and injected at a phase time of between 20 – 30 hours according to site specifications (Robey *et al.*, 2014). Thereafter, abstraction from the production borehole

requiring treatment is initiated and once iron levels increase, abstraction is terminated and oxygenated water is reinjected, repeatedly (Tredoux *et al.*, 2004; Robey *et al.*, 2014).

The Vyredox I principle is when injections boreholes are used solely for injections (Braester and Martinell, 1988). Injected water is either supplied by a supply well or a nearby reservoir (Braester and Martinell, 1988). During injections, the supply well pump is switched off and injection commences for 20 – 30 hours once stopped, allowing a contact time of a further 4 – 10 hours and a precipitation zone around the well to be developed (Braester and Martinell, 1988). The efficiency ratio of a plant requires ten or more injection cycles and is expressed as the ratio between the amount of pure water pumped out after aeration and the amount of injection water used for aeration (Braester and Martinell, 1988). Chemical and hydrological conditions are contributing factors varying efficiency values (Braester and Martinell, 1988). Efficiency ratio values usually range from 3 to 50, with normal values around 10 and abnormal values above 50 (Braester and Martinell, 1988).

The Vyredox II design was developed to compensate for expensive small well sites (Braester and Martinell, 1988). The guiding principle is that each injection well is installed with a submersible pump and cyclic injection pumping in the injection boreholes is independent of whether the supply well pump is switched on or not (Braester and Martinell, 1988). Pumping and/or injection boreholes are dependent on-site conditions with previous site examples of 3 up to 16 (Braester and Martinell, 1988). The cyclic pattern of pumping and/or injecting is expressed in Figure 2.10.

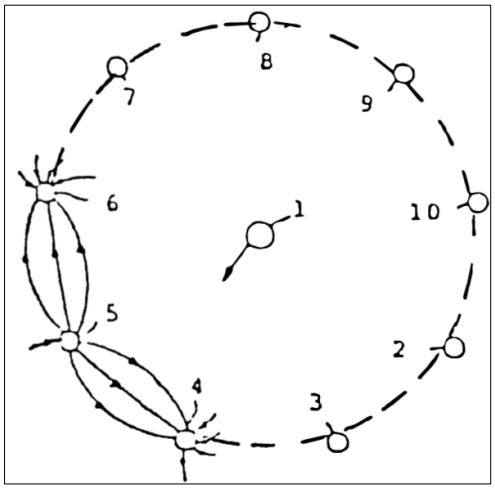

Figure 2.10: Illustration of the Vyredox II design in a cyclic design representing injection and/or pumping boreholes (°) from 1 to 10 (Braester and Martinell, 1988)

Injection or pumping boreholes 4 and 6 are pumped using an oxygenator allowing water to be degassed, aerated and then injected into intermediate well 5 (Braester and Martinell, 1988). Once an allocated period of contact time is assigned, pumping of injection and/or pumping boreholes 5 and 7 occurs and then injected into well 6, developing a cyclic injection and/or pumping regime (Braester and Martinell, 1988). This injection or pumping regime creates a superimposed hydraulic gradient fit for the supply well (Braester and Martinell, 1988). Once the supply well is operational, a "curtain" is formed between the hydraulic gradient and the injection and/or pumping boreholes, and an oxidation zone for iron and manganese is created to create precipitates (Braester and Martinell, 1988).

Aquifer clogging by these precipitated metals is of great concern. However, combined properties of a well-developed oxygenation zone and a well-maintained plant yields promising pore volumes in aquifers that are affected minimally and at slow rates (Braester and Martinell, 1988). This is proven by the oldest Vyredox plant in Grimsa's, Sweden built in 1971, which yielded no severe precipitation in interstitial pore spaces and around 1% of precipitates in the central well screen (Braester and Martinell, 1988). Based on these findings, the Vyredox method is selected as the preferred method used in this study.

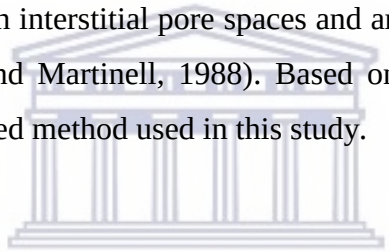

2.9.4 Injection regime and geological and/or aquifer types

ISIR designs and injection regimes differ vastly in each country. These differences are largely influenced by geological settings or aquifer conditions world-wide. ISIR treatments have successfully been implemented in geological conditions and/or aquifer types of semi-consolidated and unconsolidated, gravel-sand aquifers, glacial and alluvial deposits, and fractured aquifers (Mettler *et al.*, 2001; Diliūnas *et al.*, 2006; Robey, 2014). The Vyredox method using aerated water as an oxidant indicates similar ISIR treatment methods with various ISIR designs and injection regimes based on different geological and aquifer types in different countries. For example, the concept implemented by Braester and Martinell (1988) in Drösing, Lower Austria adopted the Vyredox I principle. This design and injection regime were performed on a large scale, compared to many other countries. This principle indicates the design and injection regime suitability for this geological setting and aquifer type.

Another case study providing geological and aquifer suitability implementing the Vyredox method using aerated water as an oxidant is that of Mettler *et al.* (2001). Under these conditions, a suitable design and injection regime was executed, as this study area not only has

one but two identical well systems, which indicates suitability based on the implementation scale for this study area (Mettler *et al.*, 2001). In addition, Switzerland has also applied a small-scaled *in situ* deferrization experiment performed in the Ron River valley aquifer, characterized by its aquifer thickness of 10 m and its glaciofluvial gravel and sand deposit geological settings (Teutsch *et al.*, 2005). Although both studies were performed in Switzerland with reducing conditions of iron and manganese, differences in ISIR treatment methods, aquifer type and geological settings, and injection regimes were noticed.

Similar aquifer conditions to Mettler *et al.* (2001) has been identified in Manikganj district, Bangladesh, that used and injected aerated water as its preferred oxidant using the SIDKO system into its alluvial sands and anoxic aquifer conditions in the subterranean area (Van Halem *et al.*, 2010). Although similar aquifer conditions have been identified in both case studies of Mettler *et al.* (2001) and Van Halem *et al.* (2010), different ISIR designs and injection regimes have been implemented. This could indicate design and injection flexibility in these geological and aquifer conditions.

The case study of Dumousseau *et al.* (1990) in France investigated the implementation of the two-production borehole method adopted from the Vyredox method (Ahmad, 2012). This case study considers similar aquifer and/or geological settings expressed in Bangladesh and Switzerland, based on its alluvial semi-confined sand aquifer, with clay-rich and loam coverage (Dumousseau *et al.*, 1990; Ahmad, 2012). Similar ISIR designs, incorporating the two-production borehole system has been implemented in Germany which had a geological region of 14 m thick fine to medium-grained sands and of Pleistocene age, Egypt with geological conditions of the Nile Delta Aquifers 300 m aquifer thickness with a semi-confined clay layer above the aquifer, and in Massachusetts with a geological setting of Glacial deposits ((AWWA), 1984; Olsthoorn, 2000; Ebermann *et al.*, 2013).

2.9.5 Pre- and post-ISIR treatment and drinking water limits

Almost all ISIR treatment methods with suitable oxidants, designs, injection regimes, and geological and/or aquifer types have achieved reduced iron and manganese concentrations. These concentrations are either country-specific or according to the international WHO standards. In Bangladesh, baseline iron concentrations reduced from 15.0 mg/L to 0.3 mg/L, well within the country-specific iron drinking water quality guideline values of 0.3 mg/L. Other ISIR treatments that have achieved reduced iron and manganese concentrations within country-

specific and/or WHO standards are treatments in Austria where iron was reduced to ≤ 0.05 and manganese to ≤ 0.03 mg/L, well within Austria's drinking water standards of ≤ 0.1 mg/L and ≤ 0.05 mg/L respectively). In Egypt, iron and manganese was reduced to 0.38 mg/L and 0.4 mg/L, within drinking water guideline limits of < 1.0 mg/L and < 0.5 mg/L respectively. France reduced iron and manganese to specified limits of below 0.05 mg/L and 0.02 mg/L respectively. Germany reduced iron to < 0.2 mg/L, within the 0.5 mg/L threshold, and Switzerland which reduced both iron and manganese concentrations to below 0.2 mg/L, within country limits. (Braester and Martinell, 1988; Dumousseau *et al.*, 1990; Olsthoorn, 2000; Mettler *et al.*, 2001; Van Halem *et al.*, 2010; Ahmad, 2012; Ebermann *et al.*, 2012). Although minor differences in the drinking water guideline values has been observed in different countries, the slight difference is also compared to South Africa's drinking water guideline values of 0.3 mg/L and 0.1 mg/L for iron and manganese respectively.

2.9.6 Efficiency coefficients and injection-abstraction cycles

As described by Olsthoorn (2000), the efficiency coefficient determines the ratio of extracted volume in the absence of iron and manganese to the injected volume of aerated water (Olsthoorn, 2000). Removal efficiency increases with increasing injection-abstraction cycles, dependent on the contact time following the injection and abstraction phase. The volume of injected water is dependent on aquifer hydraulic properties and the treatment area (Robey, 2014). The desired treatment zone is determined by the average volume that the borehole is pumped from per day (Hallberg and Martinell, 1976). Efficiency coefficients determined by ISIR treatments has been calculated as 4 in Egypt and 2 in Austria and Germany (Braester and Martinell, 1988; Olsthoorn, 2000; Ebermann *et al.*, 2012).

Every period of injection-abstraction is referred to as a cycle (Van Halem *et al.*, 2010). Injection-abstraction cycles indicated that after the fifth ISIR cycle in Egypt, manganese was reduced to even lower concentrations (Olsthoorn, 2000). In Switzerland, increased runs of oxygenated water cycles were performed (Teutsch *et al.*, 2005). Injection rates using 8 mg of oxygen per litre over two hours, a stable reaction time of one hour, and groundwater abstraction regimes of 45 L/min between two and six days observed breakthrough curves after the sixth and seventh cycles that reduced iron concentrations significantly (Teutsch *et al.*, 2005). In Massachusetts, a total of nineteen cycles was performed for manganese removal to be established ((AWWA), 1984). Similar manganese removal difficulties were raised in Austria,

which required a total of 20 cycles over 20 days for manganese removal to be achieved (Braester and Martinell, 1988). High quantities of injection-abstraction cycles for efficient iron and manganese removal have also been reported in Bangladesh and Netherlands with 20 and 18 cycles respectively. Lower cycles of iron and manganese removal efficiencies were noted in France and Germany with 4 cycles in each country. However, in Germany 4 cycles occurred within a week, and 8 cycles within a few months (Dumousseau *et al.*, 1990; Appelo and De Vet, 2003; Van Der Laan, 2008; Van Halem *et al.*, 2010; Ahmad, 2012; Ebermann *et al.*, 2012).

The majority of injection-abstraction cycles are determined by Fe^{3+} and Mn^{4+} phases that become exhausted. In an aquifer, soluble iron and manganese ions are oxidized in the presence of a suitable oxidant and correct dosage to form iron and manganese oxyhydroxides on the mineral surfaces. These can take up to 20 to 30 hours and in some cases up to 51 hours to create an oxidation zone (Robey, 2014). Oxidation zones are dependent on oxidant concentration, injection rate, injection volume, and the hydraulic properties of the aquifer (Van Halem *et al.*, 2010; Robey, 2014). A lag phase or contact time follows the injection phase of between 4 to 10 hours to allow for reactions to occur, allowing suspended iron and manganese precipitates to settle into the aquifer matrix (Hallberg and Martinell, 1976; Braester and Martinell, 1988). During abstraction, with time, groundwater transverses the oxidation zone that acts as a filter, adsorbing further insoluble iron and other dissolved ions such as manganese, As, etc. that delays the movement of ions towards the borehole (Robey, 2014). Over time the oxidation zone is exhausted, increasing iron and manganese concentrations in the abstracted water. Once the drinking water standard is exceeded, oxygenated water is injected with the abstraction phase to follow, to regenerate the oxidation zone (Van Halem *et al.*, 2010; Robey, 2014).

2.9.7 Removal efficiencies

2.9.7.1 Braester and Martinell (1988)

Braester and Martinell (1988) highlighted the Vyredox I principle that was applied in Drösing, Lower Austria, and identified the geological conditions related to ISIR identified as limestone, dolomite, clay, and marl strata. Operations of the plant stipulated a 4:1 ratio of the processed aerated water to returned purified water to be achieved. Maximum abstraction and purification from three supply boreholes supplying a yield of 30 L/s each are surrounded by six injection boreholes. The first supply well is used for the production of purified water, which was the main water supply. The second supply well was for purified water abstraction, which was

infiltrated into the injection boreholes of the third supply well. Maximum iron and manganese concentrations of around 0.35 mg/L and 0.48 mg/L respectively in the boreholes exceeded drinking water quality standards in Austria.

Reducing conditions in response to the injection oxygenated water of iron and manganese concentrations were indicated (Figure 2.11). Results monitoring iron concentrations indicated a rapid decrease by more than 0.2 mg/L in just two days of operations, in relation to manganese which only decreased around 0.15 mg/L after 2 days of operations. Iron and manganese concentrations remained stable just after 6 and 12 days of operations respectively. After a month of operations, iron reached satisfying results of ≤ 0.05 mg/L, receding stipulated iron concentrations of drinking water quality standards in Austria. Similar to iron, manganese concentrations too receded its stipulated concentrations of drinking water quality standards in Austria, reaching values of ≤ 0.03 mg/L. A ratio of 2:1 was observed during plant operations, showing the ratio between processed water delivered to the main supply and oxygenated water. Its ratio increased to 7:1 over the next few months, with no effects on iron and manganese removal rates.

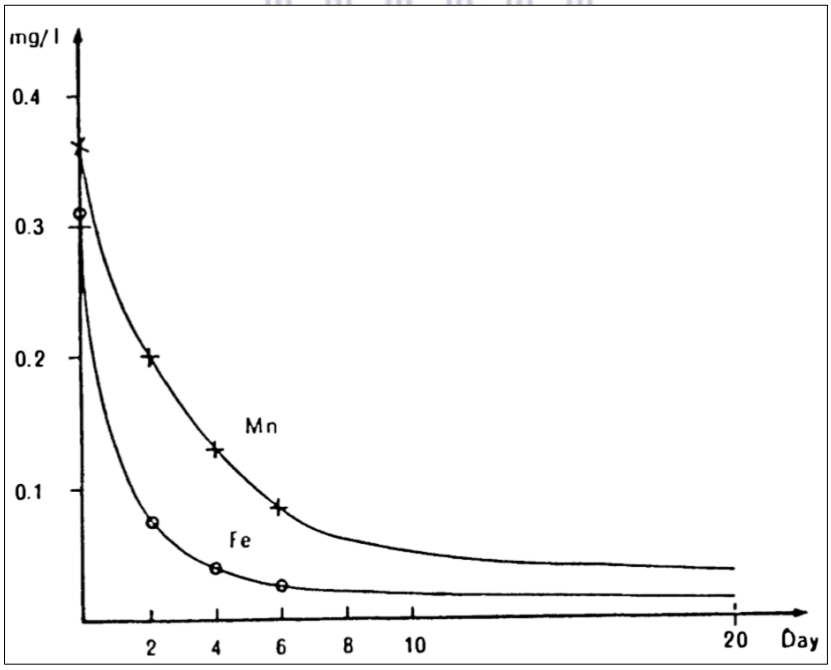

Figure 2.11: Reduced iron and manganese concentrations (mg/L) measured using the Vyredox I principle in Drösing, Lower Austria over a 20-day period (Braester and Martinell, 1988).

2.9.7.2 Van Halem *et al.* (2010)

The test facility observed that removal efficiency using the volumetric ratio (V_{gw}/V_{inj}), which represents the abstracted (V_{gw}) and injected (V_{inj}) volumes, increased with each injection-abstraction cycle. Associated abiotic factors along with adsorptive-catalytic oxidation contributed to efficiency levels of the experiment. Van Halem *et al.* (2010) also identified As adsorption during treatment is influenced by the amount of adsorbed iron that is oxidized, and not by the amount of removed iron.

2.9.8 Conditions for oxidation and iron and manganese removal

There is an expectation that iron oxidation would likely occur faster at high pH values and high DO concentrations, with pH contributing the greatest effect has been identified by Walter (1997). The oxidation of Fe^{2+} increases along with the occurrence of precipitating ferric hydroxide in treated water due to its elevated pH levels and pH-dependency (Walter, 1997). The oxidation rate of iron decreases the presence of high concentrations of sulphate, chloride, nitrate, and bromide, through the complexation of free Fe^{2+} (Walter, 1997). Also, low concentrations of DO slow down the rate of chemical iron oxidation within boreholes (Smith, 2006). Using aeration as a suitable oxidant in ISIR treatment, suitable DO concentrations between 8 and 10 mg/l should be achieved for successful removal rates (Robey, 2014). Except for organic-rich groundwater treatment, DO concentrations should be between 15 to 30 mg/L and consider using oxygen gas or O_3 as a suitable oxidant (Robey, 2014).

The reactions responsible for subsurface iron and manganese removal is described by oxidation of iron and manganese by oxygen through injection and adsorption of iron and manganese during extraction (Olsthoorn, 2000). *In situ* iron remediation (ISIR) methods are dependent on the concentration of DO in the injected water available to promote reactions with dissolved iron and manganese and groundwater pH in the aquifer, which dictates the rates of oxidation and removal efficiency (Robey, 2014). Oxidized iron and manganese minerals are reduced to its soluble ionic form in low redox potentials (Olsthoorn, 2000). Ideal monitoring conditions for O_3-based reactions include water temperatures between 15 and 20°C and pH ranges between 7.0 and 8.5 because a pH greater than 10 or high alkalinity (> 300 mg/L as $CaCO_3$) promotes the decomposition of O_3 into OH^- ions (EPA, 1999; Nimmer *et al.*, 2000; El Araby *et al.*, 2009). ISIR treatment must take into consideration that O_3 decomposes in water both during the contact stage with the recharge water and within water mixing in the aquifer, which

limits the O_3-based oxidation reactions (EPA, 1999; Robey, 2014). This is a crucial consideration in the case study in South Africa by Robey (2014).

Groundwater treatments performed in Finland are associated with high iron and manganese concentrations, and reduced pH levels (Sallanko *et al.*, 2007). Elevated iron and phosphate levels and low DO concentrations were associated effects related to iron-related well-screen encrustation in this study area (Walter, 1997). During the ISIR treatment in France, lowered pH values were noted during the treatment method in the alluvial sand aquifer conditions (Dumousseau *et al.*, 1990; Ahmad, 2012). The relationship between iron, organic content and chemical oxygen demand (COD) is expressed by Sallanko *et al.* (2007), who explains that the processes involved in iron removal are hindered by the presence of high organic matter and presents difficulties in the presence of COD levels greater than 3 mg/L. COD has a direct relationship in determining organic content in water (Cromley and O'Connor, 1976). The solubility of Fe^{3+} usually occurs in environments of pH levels below 3 (Sallanko *et al.*, 2007).

Relationships have been identified between the oxidation of iron and manganese and physico-chemical parameters. With regards to pH, water temperature, and DO concentrations, iron and manganese oxidation accelerates during high pH, temperature, and DO concentrations, with pH contributing to the greatest oxidation effects. On the contrary, high organic matter and low pH, DO, temperature, and Eh contribute to increasing dissolved iron concentrations in groundwater, reducing iron and manganese exposure to oxidizing. A relationship between DO concentrations and oxidant type was identified in this review, whereby DO differs greatly in the presence of different oxidant types. This was expressed in case studies using aeration and O_3, with a difference in DO concentrations varying up to 22 mg/L.

Chapter 3: Study area

3. Introduction

Chapter 3 describes the study area in terms of location, climate, geology, hydrology, hydrogeology, hydraulic properties, and groundwater quality.

3.1 Description of the study area

The town of Atlantis covers an area of approximately 28.84 km^2 located along the semi-arid to arid west coast of South Africa situated 50 km north of the Cape Town Central Business District (CBD) and forms part of this metropolitan area (Figure 3.1) (Tredoux *et al.*, 2011; Bugan *et al.*, 2016). Atlantis is an industrial town known for manufacturing textiles and clothing and possesses a range of land use activities. These activities include informal settlements, industrial areas, agricultural areas, and sand mining activities that impacts the groundwater quality of the sandy aquifer in the area.

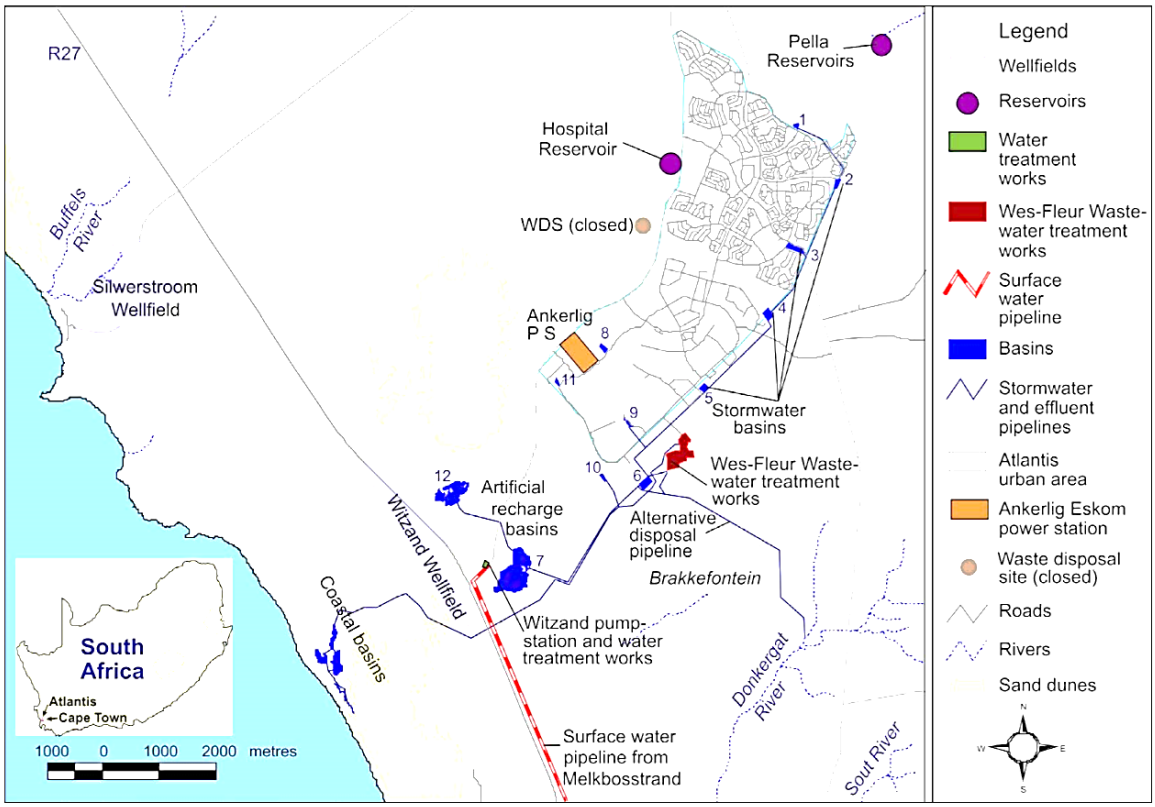

Figure 3.1: Geographical position of the town of Atlantis, layout of the Atlantis Water Supply Scheme (AWSS) and an indication of both wellfield (Witzand and Silwerstroom) locations (Bugan et al., 2016).

The study site (Figure 3.2) is located within an under-developed area vegetated by the Coastal Fynbos type and invaded by Rooikrans (*Acacia cyclops*), Port Jackson (*Acacia saligna*) and in certain areas, Bluegum trees (*Eucalyptus* spp.) and unconsolidated sediments, represented by its aquifer characteristics (Bugan *et al.*, 2018). Artificial recharge is mainly practiced in the south of the Witzand wellfield due to the sandy aquifer characteristics that allows infiltration in the subsurface with ease. (Tredoux *et al.*, 2009). However, groundwater abstraction is practiced in both Silwerstroom (southerly) and Witzand (northerly) wellfields (Tredoux *et al.*, 2009).

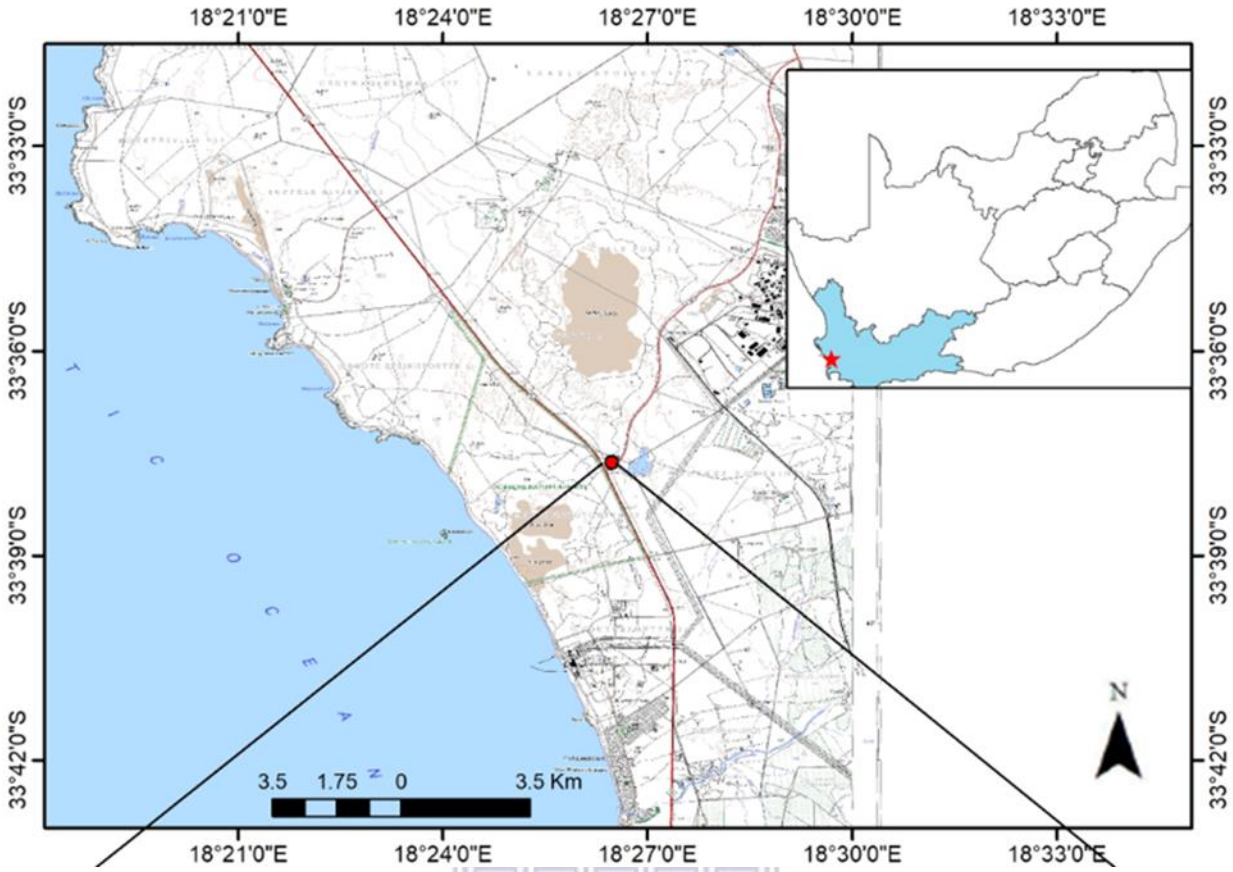

Figure 3.2: Locality map (•) of the study area in Atlantis, Western Cape, South Africa (Nhleko et al., 2020).

3.2 Climate

The mediterranean climate of Atlantis is characterised by its cool, wet winter seasons and dry, hot summer seasons (Tredoux *et al.*, 2002; Roberts *et al.*, 2009). Its dry summer periods typically occur between October and April and wet winter periods usually during May and September. Eight kilometres East of the study area, the Wesfleur Waste Water Treatment Works (WWTW) Station: 0020/846 Atlantis WWTW measures weather conditions. Atlantis receives an average annual precipitation of 457 mm (Figure 3.2) (Tredoux *et al.*, 2011; Robey, 2014; Jovanovic *et al.*, 2017; Bugan *et al.*, 2018). The average annual potential evaporation rates in the area are 1 613 mm/y with higher periods of potential evaporation during December and January and lower during July (Figure 3.3) (Parsons, 2007). The 33-year long-term mean annual precipitation from 1980 to 2013 indicates the highest precipitation periods from May to September (Table 3.1). These high precipitation periods range from 44.1 to 77.9 mm and low periods between October and April range from 10.9 to 37.2 mm (Table 3.1) (Parsons, 2007).

Table 3.1: Mean monthly precipitation (mm), and maximum and minimum temperatures (°C) between 1980 and 2013 measured at the Wesfleur Waste Water Treatment Works (WWWTW) in Atlantis. Mean monthly precipitation is recorded from January to December (Parsons, 2007).

Mean monthly values	January	February	March	April	May	June	July	August	September	October	November	December
Maximum temperature (°C)	27.5	27.9	26.7	24.1	21.0	18.4	18.0	18.2	19.8	22.6	24.3	26.3
Minimum temperature (°C)	14.4	14.7	13.3	10.9	8.8	6.7	6.0	6.4	8.0	9.8	11.5	13.7
Precipitation (mm)	10.9	12.4	14.5	37.2	56.5	77.9	76.5	68.7	44.1	23.6	20.5	14.0

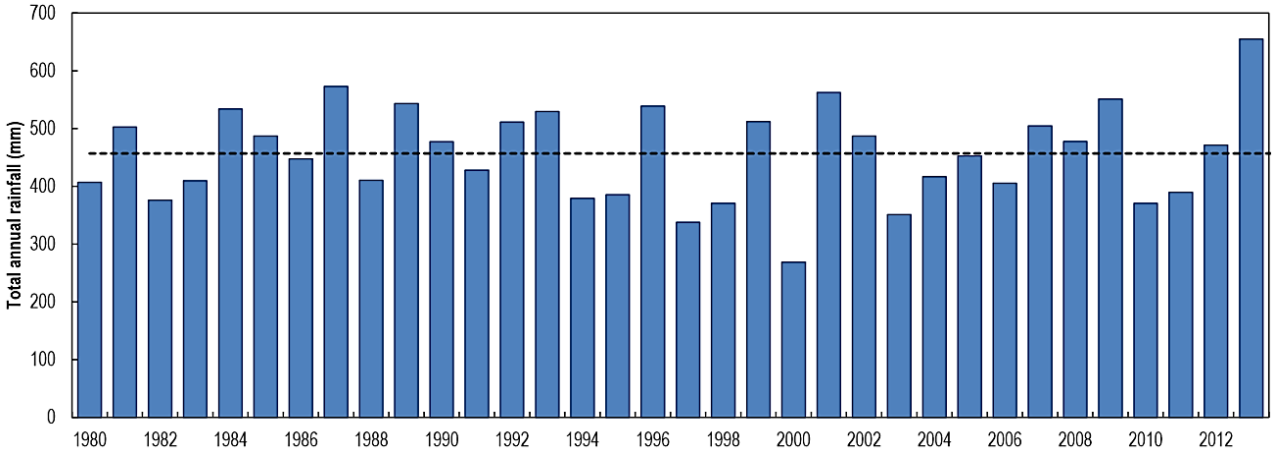

Figure 3.3: Average (- - -) and total annual rainfall (mm) measured from 1980 to 2013 at the Wesfleur Waste Water Treatment Works (WWWTW) in Atlantis (Parsons, 2007). Each intervals occur yearly.

3.3 Geology of the study area

The geological conformation of the Atlantis Primary Coastal Aquifer is characterized by unconsolidated Cenozoic sands of the Sandveld Group distributed from False Bay to Elands Bay along the Atlantic Ocean's border (Tredoux *et al.*, 2009; Jovanovic *et al.*, 2017). Unconsolidated Cenozoic sediments originating from tertiary to quaternary ages overlies the impermeable base of Malmesbury shales. The Malmesbury Group consists of fine to medium-grained greywacke and phyllitic shale and forms the basal unit of the Atlantis aquifer (Roberts, 1999; Jovanovic *et al.*, 2017).

The Witzand Formation unconformably overlies the Springfontyn, Langebaan, and Velddrif formations in the Sandveld Group (Figure 3.4) (Browning and Roberts, 2015). Its lithology is characterized by aeolian deposits consisting of fine- to medium-grained calcareous-rich quartz sands reaching an average thickness of 14 m (Tredoux and Cavé, 2002; Browning and Roberts,

2015). The Witzand formation is identified by its white dunes and unvegetated areas in Atlantis and the Witzand wellfield (Robey, 2014; Browning and Roberts, 2015). In some areas, the surface unit of the Sandveld Group rests unconformably on the Springfontyn formation (Nhleko *et al.*, 2020). The Springfontyn formation comprises of well-sorted quartz aeolian sands made up of fine- to medium-grained calcareous sands with some places containing calcrete lenses (Roberts, 2006; Bugan *et al.*, 2018). Figure 3.5 illustrates the geological map of Atlantis and the study area. Overall, the Witzand formation was identified as the most suitable formation for abstraction as well as injection for ISIR for this study. However, due to its unconformity, some boreholes reach the Springforntein formation, which has also been identified as suitable for ISIR.

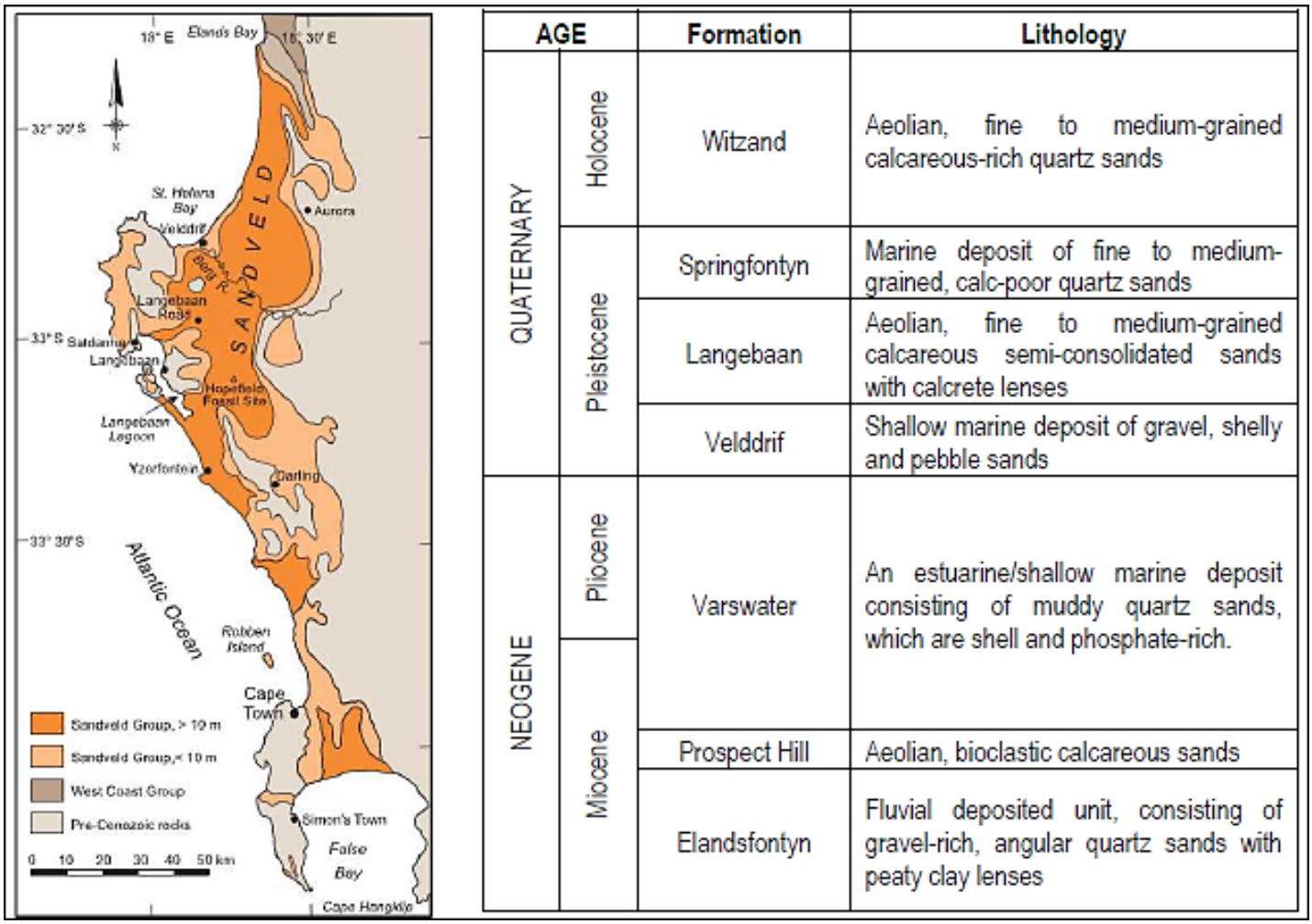

AGE		Formation	Lithology
QUATERNARY	Holocene	Witzand	Aeolian, fine to medium-grained calcareous-rich quartz sands
	Pleistocene	Springfontyn	Marine deposit of fine to medium-grained, calc-poor quartz sands
		Langebaan	Aeolian, fine to medium-grained calcareous semi-consolidated sands with calcrete lenses
		Velddrif	Shallow marine deposit of gravel, shelly and pebble sands
NEOGENE	Pliocene	Varswater	An estuarine/shallow marine deposit consisting of muddy quartz sands, which are shell and phosphate-rich.
	Miocene	Prospect Hill	Aeolian, bioclastic calcareous sands
		Elandsfontyn	Fluvial deposited unit, consisting of gravel-rich, angular quartz sands with peaty clay lenses

Figure 3.4: Exposure and deposition of the Sandveld Group (left), stratigraphy units, formation, and lithology descriptions (right) (Robey, 2014). The stratigraphy units are represented according to Neogene and Quaternary age. The Witzand, Springfontein, Langebaan, Velddrif, Varswater, Prospect Hill, and Elandsfontyn formations are included.

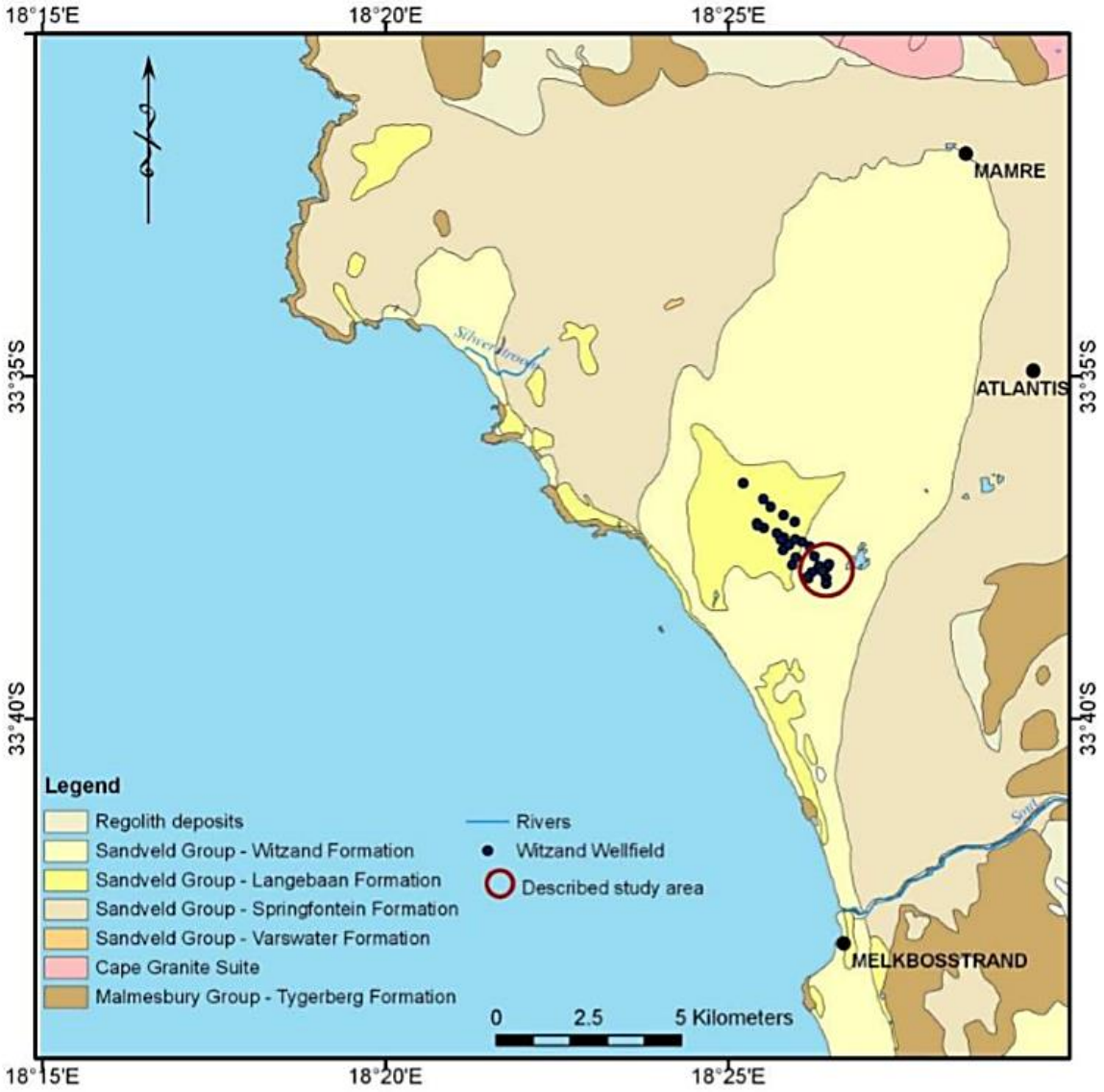

Figure 3.5: Geological map of the West Coast towns (Melkbosstrand, Atlantis, and Mamre). Locations of regolith deposits, formations of the Sandveld Group include the Witzand, Langebaan, Springfontein, Varswater formations. Cape Granite Suite and the Malmesbury Group (Tygerberg) are also included (Robey, 2014). The described study area is located within the Witzand wellfield.

3.4 Hydrology of the study area

The Atlantis Water Resource Management Scheme (AWRMS) is located within the Berg Water Management Area with no major rivers in the area (Robey, 2014). The natural drainage of AWRMS catchment G21B is either towards the Donkergat and Sout Rivers in the south or towards the Silwerstroom in the west (Tredoux *et al.*, 2011). All rivers including Buffels River and streams in the area are non-perennial and are distant from any major arteries of surface water that supply central Cape Town areas (Roberts, 1999). There are two perennial springs at

Silwerstroom, feeding the Buffels River, and Mamre and a minor spring at Groot Springfontein (Tredoux *et al.*, 2011). Precambrian basement topography between 10 and 150 m in elevation around Atlantis has contributed to the distribution of groundwater conduits in the town (Roberts, 1999). Groundwater is most significant for agricultural, industrial, and domestic uses in Atlantis (Roberts, 1999).

3.5 Hydrogeology of the study area

3.5.1 Aquifer types

Atlantis primary coastal aquifer constitutes unconsolidated sediments covering Malmesbury Group bedrock reaching an area coverage of 130 m^2. The thinly sloped sandy aquifer extends from the Atlantic Ocean up until the town of Atlantis in an eastward direction (Tredoux *et al.*, 2011). Sand thickness varies across Atlantis ranging between 25 – 60 m with saturation thickness only reaching a longitudinal maximum of 35 m (Tredoux *et al.*, 2009; Bugan *et al.*, 2016). The Atlantis aquifer system is a heterogeneous anisotropic aquifer overlying an impermeable clay base (Bugan *et al.*, 2018). Two identified aquifer types are within the Witzand Wellfield the primary unconsolidated Atlantis Aquifer and the secondary fractured rock Malmesbury Group Aquifer (Tredoux and Cavé, 2002). Although groundwater is present in the underlying bedrock, weathered bedrock along the upper surface restricts flow between the two aquifers (Tredoux and Cavé, 2002). With no groundwater flow between the two aquifers, bedrock topography has contributed largely to the six hydrogeological sub-units of the Atlantis Aquifer (Figure 3.6) (Tredoux and Cavé, 2002). Topography ranges between 160 and 200 m above sea level, and around 55 m at the study area (MuIIer and Botha, 1986). The Witzand Wellfield is located within the Klein Springfontyn-Witzand sub-unit (Tredoux and Cavé, 2002). Groundwater flow between adjacent sub-units occurs when the water table increases above palaeoridges (Tredoux and Cavé, 2002).

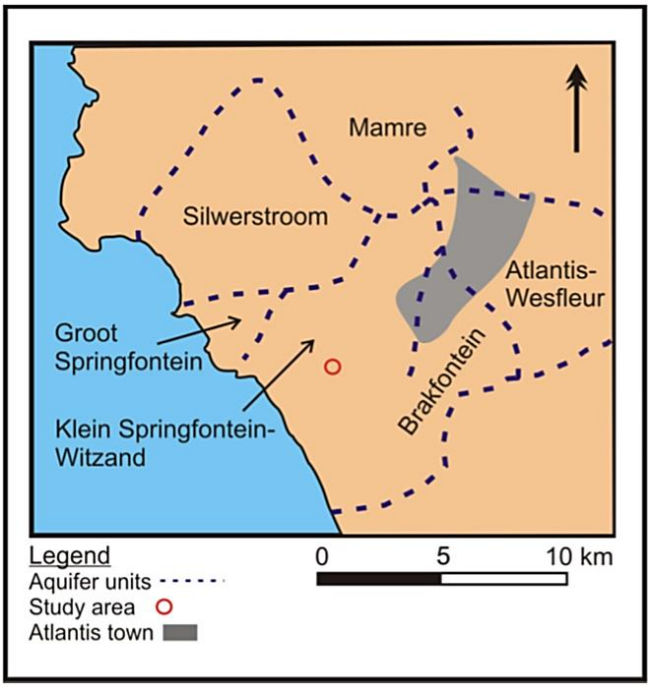

Figure 3.6: Six sub-units of the Atlantis aquifer due to bedrock topography, and the location of the study area and Atlantis town (Robey, 2014). The sub-units include Mamre, Silwerstroom, Brakfontein, Atlantis-Wesfleur, Groot Springfontein, and Klein Springfontein

3.5.2 Groundwater levels and flow direction

Shallow static water levels in the Witzand Wellfield are apparent, as water table records vary between 1 and 6 meters below ground level (mbgl) which is typical of the surface topography (Fleisher, 1990). Groundwater flow direction or groundwater levels at the study site are not significantly affected by seasonal rainfall variation (Visser, 2016). Groundwater levels recorded in December 2010 depicts a steep groundwater elevation decrease from 130 metres above mean sea level (mamsl) down-gradient towards the West Coast (Figure 3.7) (Bugan *et al.*, 2012; Robey, 2014). Regional groundwater flow of the Witzand Wellfield is towards a south-westerly direction from the coastal plain to the Atlantic Ocean coastline, although deviations do exist close to recharge basins (Bugan *et al.*, 2012; Robey, 2014). Although the topography of the study area is fairly flat, two water sinks are apparent in the study area. These sinks occur around the production borehole as a consequence of pumping, and around borehole 11DW due to natural conditions of the study area (Nhleko *et al.*, 2020).

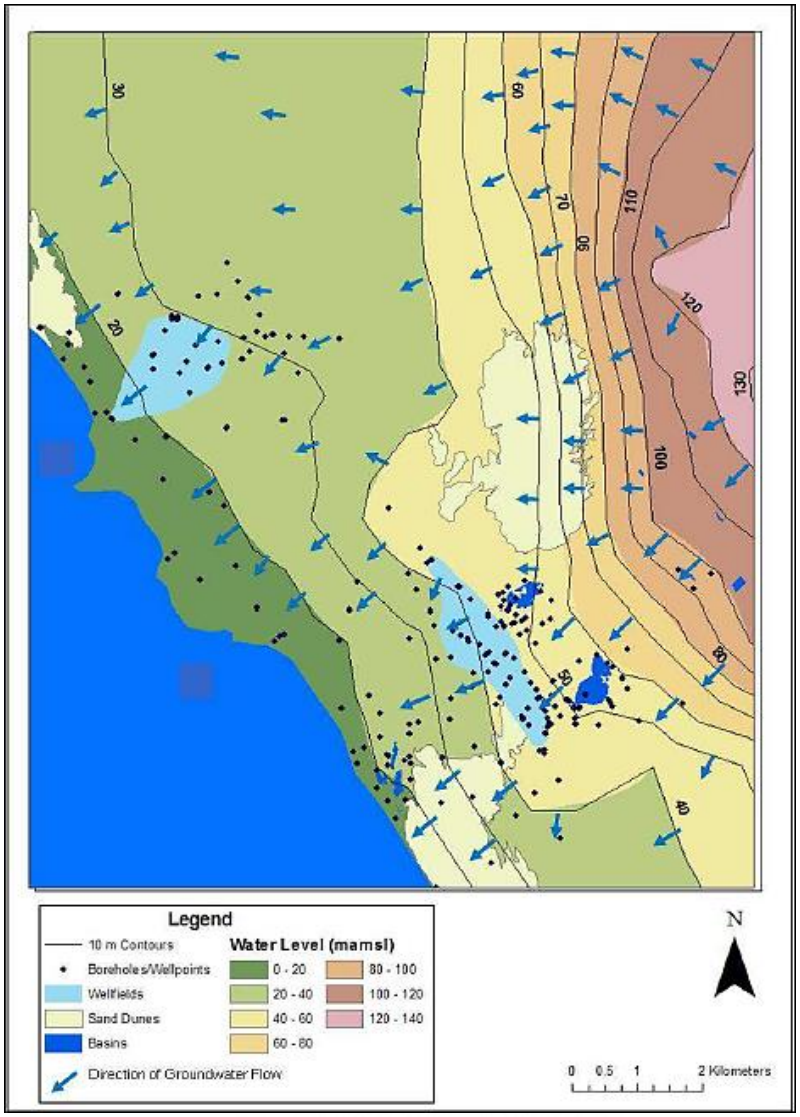

Figure 3.7: Contour map illustrating groundwater level metres above mean sea level (mamsl) in 10 m contours of the Atlantis aquifer, and the general direction of groundwater flow in December 2010 (Bugan et al., 2012). Boreholes and/or well-points, wellfields, sand dunes and basins have also been identified.

3.5.3 Permeability and Recharge

A mixture of clay and sands are present in the Atlantis area with the absence of impermeable layers (Bugan *et al.*, 2018). Sandy soils are medium to coarse-grained in texture, grey in colour, generally alkaline and well leached (Bugan *et al.*, 2018). Soils in the Atlantis region are dominated by homogenous Fernwood and Langebaan soil series (Bugan *et al.*, 2018). These soils lack soil nutrients and high wind erosion susceptibility, limiting agricultural practices (Bugan *et al.*, 2018). However, grain size variations permit high infiltration rates to feed groundwater sources. Almost a third of annual rainfall, between 15 and 35 %, infiltrates its

unvegetated and unconsolidated sandy surfaces which is prone to high infiltration rates (Tredoux *et al.*, 2011; Bugan *et al.*, 2016). Sand thickness varies across the total area, ranging between 25 – 60 m. However, saturation thickness attains a maximum of 35 m longitudinally (Tredoux *et al.*, 2009; Bugan *et al.*, 2016; Bugan *et al.*, 2018).

3.6 Hydraulic properties

Hydraulic properties within the study area are essential for ISIR suitability (Robey, 2014). Aquifer tests performed in the Atlantis aquifer around the mid-1970s have yielded aquifer estimates of porosity, specific yield (Sy), storativity, transmissivity (T), and hydraulic conductivity (K). Aquifer porosity estimate reports (although very few) presented porosity estimates of the Witzand Wellfield at 23% (Fleisher, 1990) and 41% (Parsons, 2007). Specific yield estimates the rate of injection that ISIR can be performed. In an unconfined aquifer such as the Atlantis aquifer, storativity is equivalent to the Sy and has been calculated at 0.04 (4%) and 0.05 (5%) promoting appropriate conditions for injection rates (Visser, 2016).

A diverse range of T-values ranging between 120 and 600 m^2/day has been reported in the Witzand wellfield, characterized by its heterogeneous aquifer type (Fleisher, 1990; Cave, 1997; Robey, 2014). According to ISRRI (2009), high T-values in study areas promote the most effective *in situ* treatments compared to low T-values. However, shallow water table conditions in Atlantis results in injection issues due to limited space available for fluctuating water levels during injection (Robey, 2014). This is explained by the injection rate which is greater when transmissivity is high resulting in faster infiltration rates into the aquifer. Restrictions when T-values are low results in reduced injection volumes or rate of injections due to pressure build-up (ISRRI, 2009; Robey, 2014). Calculated T-values from step-drawdown tests have determined horizontal and vertical K-values (Bugan *et al.*, 2018) for multiple stratigraphic units (Fleisher, 1990).

As a consequence of the Atlantis aquifer possessing a heterogeneous and anisotropic state, K-values differ widely across the aquifer displaying semi-unconfined characteristics (Tredoux and Cavé, 2002). Lower K-values were measured in the higher regions such as the town of Atlantis, with increasing levels closer to the coastline due to the high permeability of soils (Jovanovic *et al.*, 2017). These high K-values are in the area of the Witzand and Silwerstroom wellfields (Jovanovic *et al.*, 2017). The average horizontal K-values calculated for the Witzand

and Springfontyn Formations are 25 m/day and vertical K-values of the Witzand measured at 15 m/day (Fleisher, 1990). A lower K-value between the ranges of 1 and 3.5 m/day has been calculated for the underlying Varswater Formation, due to its high silt content (Fleisher, 1990; Robey, 2014).

3.7 Groundwater quality

Groundwater quality in the Atlantis aquifer has been influenced by surrounding lithology, artificial recharge, vegetation, and groundwater mineralisation along flow paths (Nhleko *et al.,* 2020). Groundwater quality indicates variable spatial differences in soil layers and bedrock conditions (Silveria, 1988). This is apparent in Atlantis due to various Sandveld Group formations that have contributed to the overall hardness in groundwater influenced by calcretes of the Witzand formation, and iron and sulphates from the Springfontein formation (Tredoux and Cáve, 2002). However, groundwater quality variations are not only dependant on geological and hydrological factors, but also subsurface physico-chemical factors and biological activities (Silveria, 1988). Groundwater chemistry studies in Atlantis up until 2010 discovered that northern parts of the Witzand wellfield contain more calcium bicarbonate rich waters, with southern parts containing more sodium chloride type waters due to marine origins from the Varswater marine sands (Tredoux *et al.,* 2002; Bugan *et al.,* 2016). In the Silwerstroom wellfield, lower salinity natural calcium bicarbonate water types were found in this aquifer unit (Bugan *et al.,* 2016). A study by Bugan *et al.* (2018) interpreted hydrochemistry spatial and depth variations of EC, chloride, potassium, ammonium, sulphate, and total organic carbon (TOC) of groundwater around the Atlantis historical landfill.

Electrical conductivity trends in various locations of the Witzand wellfield between 1980 and 2010 ranged between 38 and 110 millisiemens per metre (mS/m), and between 40 and 160 mS/m in the Silwerstroom wellfield (Bugan *et al.,* 2016). According to the Department of Water Affairs and Forestry (DWAF), groundwater quality suitability for EC has been classified between “Suitable” and “Suitable, slightly salty taste” with allocated ranges for domestic use (Meyer, 2001). The range for “Suitable” domestic use was set at EC levels smaller than 70 mS/m, and between 70 – 160 mS/m for the classification of a “Suitable, slightly salty taste” for domestic use (Meyer, 2001). Recent borehole logs performed in October 2017 revealed a rapid increase in EC concentrations in deeper boreholes, ranging between 50 and 250 mS/m in unpolluted and polluted boreholes respectively (Bugan *et al.,* 2018). The maximum EC

concentration recorded is tolerable and marked with a salty taste for domestic use. In 2017, chloride in the study area identified higher concentrations on the southern side in deep monitoring boreholes, and lower on the adjacent side in shallow boreholes. High concentrations of potassium were measured in the deeper boreholes. However, the aquifer is characterized by its organic-rich and silica-rich environment with a minor percentage of clay that can remove potassium through ion exchange. Ammonium generation occurs during the decomposition of nitrogenous organic compounds such as protein under anaerobic conditions. During redox reactions and/or in the presence of bacteria populations, ammonium can be oxidized to nitrate or alternative nitrogen compounds. This explains the decreased concentrations of ammonium at most of the monitoring points surrounding the landfill (Bugan *et al.,* 2018).

Three deep south and south-westerly boreholes to the landfill measured low sulphate concentrations ranging between 2 and 3 mg/L. However, in the south-westerly direction of the landfill, shallow boreholes had a low natural sulphate concentration between 20 and 40 mg/L. Groundwater from deeper boreholes within the aquifer contained low concentrations of hydrogen sulphide (H_2S), measured below 1 mg/L (Bugan *et al.,* 2018). However, the presence of H_2S indicates natural reducing conditions with bacteria-reducing sulphate at strata depths greater than 20 m, and due to the presence of dissolved organic carbon (DOC) that serves as a substrate for the bacteria (Tredoux *et al.,* 2011; Bugan *et al.,* 2018). Dissolved organic carbon of abstracted groundwater in Atlantis has previously been measured up to 4 mg/L (Tredoux *et al.*, 2011). However, DOC tends to fluctuate as natural organic carbon in groundwater tends to increase DOC levels (Tredoux *et al.,* 2011). In June 2008, DOC was measured at 1.9 and 2.6 mg/L in two production boreholes in the Silwerstroom aquifer (Tredoux *et al.*, 2011). Organic carbon is derived from alien vegetation and Fynbos in the area. Natural TOC concentrations in the aquifer calculated carbon between 6 and 7 mg/L (Bugan *et al.,* 2018).

3.8 Study area suitability for *in situ* iron remediation (ISIR) treatment

With studies exposing effects of ozonation, a preference of using either simple aeration or O_3 as a preferred oxidant in the Vyredox method holds promising results in terms of effective iron and manganese removal from groundwater sources (Ebermann *et al*., 2012; Robey, 2014). With variable designs, injection regimes and geological and/or aquifer types, the Vyredox method is mostly utilized based on its efficient iron and manganese removal suitability world-wide. Not only has the Vyredox method been recommended for the past 5 decades as a suitable ISIR technique, but it has also yielded satisfactory results internationally in terms of its reduced iron

and manganese concentrations within country-specific and/or WHO drinking water quality standards (WHO, 2008). Most suitable injection-abstraction regimes have considered suitable injected water volumes in terms of aquifer hydraulic properties and the treatment area (Robey, 2014). Effective iron and manganese removal using aeration or O_3 dosing require meticulous water flow control. Excessive water flow control prevents suitable conditions for iron and manganese oxidation, whereas, insufficient water flow can saturate water sources with DO and corrode the treatment method (MRWA, 2019). To achieve satisfactory results of reduced iron and manganese concentrations in the subsurface, a contact time following the injection phase between 4 to 10 hours allows for subsurface reactions to occur, settling iron and manganese precipitates into the aquifer, before iron-and manganese-free water is abstracted (Hallberg and Martinell, 1976; Braester and Martinell, 1988). Injection-abstraction cycles are site-specific, however, an overall trend amongst ISIR treatments identifies that an increase in the number of cycles increases iron and manganese removal rates (Braester and Martinell, 1988; Dumousseau *et al.*, 1990; Appelo and De Vet, 2003; Van Der Laan, 2008; Van Halem *et al.*, 2010; Ahmad, 2012; Ebermann *et al.*, 2012).

The potential of ISIR treatment suitability in the study area was apparent due to the primary aquifer's high T conditions, which enables easy injection of oxygenated water *in situ* to create a suitable oxidation zone. The mineralogical composition of the Atlantis primary aquifer consists of clean quartz sands. The surface areas are ideal for the adsorption of newly-formed iron oxyhydroxide precipitates to attach to and is appropriate for the ISIR treatment (Sharma, 2001; Robey, 2014). Sediment logs of borehole G30979, located approximately 15 m from production G30966 at the study site confirmed the average grain size in the study area to be fine- to medium-grained quartz sands. The most suitable geology for the ISIR design using ozonated water injection is the Witzand formation, sometimes reaching the Springfontein formation that is composed of fine- to medium-grained sands (Robey, 2014). This study is located within the Witzand formation, and reaches the Springfontein formation in some areas due to unconformity of the Witzand formation. Boreholes are drilled up to 31 meters below ground level (mbgl) and are suitable for ozonation injection since the production, injection, and monitoring boreholes are all screened at depths roughly between 24 to 31 mbgl sections. The absence of structural features, such as faults, or the lack of lithological heterogeneity has the ability to disrupt the flow path of injected water (Appelo *et al.*, 1999).

Successive injections are appropriate in primary aquifer conditions and can increase the extent of oxide coating on the soil grains matrix. This assists in the continuous removal of soluble

iron and manganese ions from the groundwater through adsorption and oxidation processes. A minority of clay and organic matter aquifer sediments result in the expectation of enhanced migration of soluble iron, manganese, and phosphate ions (Robey, 2014). The migration of these ions is based on the presence of carbonate minerals in the aquifer (Tredoux *et al.*, 2002). Groundwater in this study area has high bicarbonate mineral composition. These high compositions provide sufficient buffering capacity to acidify oxidation reactions and maintain pH levels within optimal conditions, that is slightly alkaline, for efficient iron and manganese removal (Tredoux *et al.*, 2002).

Due to the study area's high water table, the injection of ozonated water was into either of the injection boreholes 11DNE, 7DE, or 12DN, instead of directly into the production borehole. In addition to the high-water table, the study area's previous events of clogged boreholes eliminate the stop-start injection approach into the injection boreholes. The high-water table also has the ability of injection to be operated under pressure, which could improve the extent of injections into the aquifer through injection boreholes to increase the volume of oxidant into the aquifer. A distance of 4 m and further was recommended between the injection borehole and production borehole to enable longer contact flow paths for the newly formed iron precipitates and the removal of manganese (Robey, 2014).

3.8.1 Oxidant suitability, equipment design and construction

Based on the study site's suitability for ISIR treatment, ISIR design and application considered the highly concentrated organic compounds and silica-rich groundwater qualities in the study area. As a result, the most suitable oxidant for the ISIR treatment was O_3 gas to remove complex iron and manganese ions effectively. Ozone would also result in higher DO concentrations to enhance DOC and iron and manganese oxidation. Appropriate conditions for using O_3 as the oxidant are favoured by its unharmful by-product formation after treatment and its non-polluting characteristics to the aquifer (Rice, 2002). However, it is impossible to impose a high degree of control over the varied and complex subsurface conditions (both physical and chemical) that affect site-specific design criteria for O_3 injection.

During ISIR application O_3 production is achieved using specialized equipment and designed for site-specific conditions (Plummer *et al.*, 2005). The use of O_3 differs for most oxidation processes as O_3 injection can either occur as a gas or liquid, referred to as ozonated water (Plummer *et al.*, 2005). Critical design considerations that affect O_3 dosages for site-specific

parameters and ISIR applications have previously been outlined. These design considerations include the distribution of O_3 in the contaminated subsurface area, O_3 reactivity with contaminants of concern (COC), regulatory requirements and geological compositions.

Ozone engineers, were selected to manufacture the CD Ozone Generator used in this study (Robey, 2014). The O_3 generator system selected for the study site was compacted onto a 1 m^2 board and placed into a shipping container, protecting the O_3 and oxygen generators from direct sunlight and/or rainfall, and potential vandalism (Robey, 2014). A whirlybird was installed into the shipping container to improve internal airflow. The O_3 generator setup uses an oil-less compressor that consumes ambient air and passes through the oxygen generator (Robey, 2014). A pressure swing adsorption process removes the presence of nitrogen, CO_2, and moisture from the compressed air, forming high purity oxygen gas (> 93% of O_2 at 5 L/min) (Robey, 2014). The high purity gas reaches the CD generator, producing roughly 7 to 8 g/h of O_3 from 4 to 5 L/min of input air (Wassertec, 2012; Robey, 2014). Excess oxygen gas and O_3 are combined and supplied to the venturi in specific doses through the 8 mm Teflon tube (Wassertec, 2012; Robey, 2014).

3.8.2 Borehole suitability and installation

Production borehole G30966 situated in the Witzand Wellfield was selected as the most suitable abstraction/production borehole where the ISIR experiment will be performed (Figure 2.10) (Robey, 2014). Its selection was based on its availability to perform tests without affecting water supply to Atlantis and its location in relation to the Witzand Water Treatment Plant. It is easily accessible and has sufficient security support. The site was most suitable for the project and construction as there were two existing monitoring boreholes in close vicinity to the production borehole G30979 and well-point 63 (WP63). The site had sufficient space requirements to construct the ISIR design and the local geology could facilitate borehole drilling designs for new monitoring and injection boreholes for the study. Since the high water table in the primary aquifer prevented direct injection of ozonated water into the aquifer for ISIR treatment, multiple small-diameter boreholes were drilled within the study area to act as injection or monitoring points during treatment (Robey, 2014).

The quantity and locations of each borehole considered the regional flow path and direction, T rates, distance from the production borehole (G30966), budget constraints and an electrical power supply for the O_3 generator and pumps (Robey, 2014). According to the Vyredox

approach being implemented at the study area, injection boreholes were positioned in a semi-circular configuration around the production borehole and up-gradient to the groundwater flow direction (Hallberg and Martinell, 1976). Well-point screens were placed at the depth similar to the depth of the production borehole screens between 25 and 31 m (Hallberg and Martinell, 1976). Ozone-resistant borehole casing materials stainless steel and schedule PVC were used in this study (Nimmer *et al.*, 2000).

With the exception of the existing boreholes at the study site G30979 and well-point 63 (WP63). An additional eleven small-diameter monitoring boreholes were drilled in January 2013 in the study area within a 16 m radius around G30966 (Robey, 2014). Mud-rotary drilling was used for the study. Mud-rotary drilling uses rotating bits that are attached to the end of the drill rods by a string, transmitting a rotational action from the drill rig to the bit and creating penetration through the formations (Robey, 2014).

Drilling rods in this study were 3 m in length and an outside diameter of 160 mm (Robey, 2014). Nine of the boreholes were drilled to a depth of 31 m and the remaining two at 15 m depths i.e. 6SNE and 7SSW. The deeper boreholes were assigned to function as monitoring points in the Springfontein Formation and the shallower boreholes allocated for monitoring purposes of water quality changes and vertical oxidant transfers in the upper Witzand section of the aquifer during injection (Robey, 2014). In addition to the already existing boreholes G30979 and WP63 and eleven monitoring boreholes, three new injection boreholes (11DNE, 7DE, and 12DN) were installed at the study site. These new larger diameter injection boreholes (2 X 113 mm and 1 X 143 mm) were drilled using the mud-rotary drilling technique between the period of May to June 2019 to allow for injection piping to be fitted. These were drilled at depths of 31 m and perforated between screened sections of 24 – 31 m to mimic the production borehole. Figure 3.8 provides an aerial view of the distribution of boreholes within the study area.

Figure 3.8: Aerial view of the study site in Atlantis representing newly drilled injection boreholes (●), existing monitoring boreholes (●), and the production borehole G30966 (●) (Nhleko et al., 2020). Injection boreholes include 7DE, 11DNE, and 12DN, and existing boreholes include 10DNE, 8DNE, 6SNE, 4DNE, 7SSW, 8DSW, 10DSW, 15DSW, 11DW, WP63, 12DS, 13DN, G3097.

Borehole casing and screen material in these monitoring boreholes were pressure Class 6 PVC pipe with a working pressure of 600 kPa (Robey, 2014). Well-point screening was within the last 6 m of each drilled borehole, i.e. between 25 and 31 m for the deeper boreholes and between 9 and 15 m for the shallower boreholes (Robey, 2014). Multiple perforations were manually constructed into the PVC casings, between 0.5 mm wide and 69 mm in length (Robey, 2014). Each well-point was capped at the base, using a 30 mm PVC end cap and the remainder of the well-point surrounded with a solid PVC casing and secured to the screen using couplers and stainless-steel screws (Robey, 2014). Solid and screened sections of the PVC have outside diameter measurements of 63 mm and a wall thickness of 1.9 mm of the drilled monitoring boreholes (Robey, 2014). A 48.5 mm thick gravel pack of 10/30 grade was used to surround

the screened sections of these boreholes (Robey, 2014). After construction and cleaning of the boreholes, using clean water from the production borehole and flushed for 30 minutes, a steel pipe was fitted over each of the open PVC pipes to provide protection from external factors in the study area such as vandalism (Robey, 2014).

3.8.3 Study area suitability summary

Since the most applicable ISIR technique world-wide and the most recommended choice of ISIR designs has considered the Vyredox principle, its applicability in South African conditions is recommended and has been tested to be feasible (Robey, 2014). It has also been considered internationally as a highly common method to effectively reduce iron and manganese concentrations. These international successes have also used O_3 as a preferred oxidant using the Vyredox principle. The study site selected has the ability to develop the principles design in terms of size, location and access to water supply. High aquifer T allows for easy *in situ* injection regimes to create suitable oxidation zones for iron and manganese oxidation (Robey, 2014). Its ability to perform injection independent from the production borehole considers its suitability for soil and hydraulic properties characterised by primary aquifer conditions. Aquifer suitability for the ISIR treatment is also determined by the Atlantis primary aquifer composition, which is suitable for iron precipitates to settle into (Robey, 2014). The relevance of using O_3 as the selected oxidant instead of aeration in South African conditions is based on South Africa's organic-rich and silica-rich groundwater. These conditions are present at the study site in Atlantis, to yield satisfying iron and manganese removal rates in a primary aquifer. The ISIR treatment design must take into consideration that O_3 decomposes in water both during the contact stage with the recharge water and within water mixing in the aquifer, limiting O_3-based oxidation reactions (EPA, 1999; Robey, 2014). As a result, successive injections using adsorption and oxidation processes are suitable for continuous iron and manganese removal for this study area. This has been identified by Robey (2014).

Chapter 4: Methodology

4. Introduction

Chapter 4 describes the methodologies used for data collection and analysis in this study. Quality control, quality assurance, and study limitations of this study is also identified. The *in situ* iron remediation (ISIR) method used in this study adopted the Vyredox procedure described by Hallberg and Martinell (1976). Treatment functionality and suitable practical processes was implemented to evaluate the effectiveness of this method as follows:

4.1 Study site design and approach

4.1.1. Baseline characteristics of the study site

To evaluate the performance of the production borehole (G30966) and quantify baseline hydraulic characteristics of the Atlantis aquifer under a controlled discharge rate, the step-drawdown was used before ozone (O_3) injection. The test involves increasing the discharge rate from a low constant rate through a series of equal duration pumping intervals of higher constant rates. The step-drawdown test was conducted over 5 hours at the production borehole on the 8th of August 2019. During this test, the period was divided into a pumping and recovery period. Each pumping period was 60 minutes long, and the recovery period approximately 130 minutes long. Due to the study sites unconsolidated soil characteristics, readings were taken 10-minute intervals to monitor the groundwater recovery rate of the subsurface. Depth to water was monitored using a TLC water level metre in the pumping and two monitoring boreholes 10 m away from the pumped borehole (G30966), one upgradient (10DNE) and the other down gradient (10DSW). A total of four pumping periods was performed using a variable gauge, increasing the pumping speed at each period (40.75 Hz, 43.95 Hz, 47.41 Hz, and 49.99 Hz) after every 60 minutes. Although an increase in pumping rates was performed, the sequence of flow rates for each period were inconsistent, respectively (9.94 L/s, 5.95 L/s, 12.8 L/s, and 7.07 L/s). After the pumping period, the pump was switched off allowing the aquifer to recover over 130 minutes.

4.1.2 System design and operation

Groundwater was abstracted from production borehole G30966 at a flow rate of 1.5 L/s (Figure 4.1). This abstracted groundwater served as the water supply into the shipping container where all equipment was stored (Figure 4.2). G30966 was used to fill a 5000 L JoJo tank (Figure 4.3). The 5000 L was separated into 3000 L and 2000 L sections that allow for aerated groundwater to collect in the first 3000 L, and the remaining 2000 L to be used as an area to precipitate solids. This tank, along with all other equipment and pipes were fixed to the walls of the container and stored in the shipping container on-site. A sampling point was positioned at the inlet pipe before entering the storage tank to sample water before treatment. The inlet pipe of the tank was fitted with a 40 mm water meter to control the flow rate into the tank. A venturi is a short tube in the shape of an hourglass that is used to restrict the flow of liquid or gas. This was used to pre-dose groundwater with O_3 from the air to further remove any uncomplexed iron and manganese ions and undesired gases such as hydrogen sulphide (H_2S). The tank was fitted with a mechanical float valve to control the storage levels in the tank. Additional pipework was added to the tank, such as an outlet pipe that is situated to flow out underneath the container. The additional pipework allows for iron and manganese precipitates that have settled in the bottom of the tank to be removed using a washout valve. An overflow pipe was installed to release overflow water out of the container preventing internal flooding.

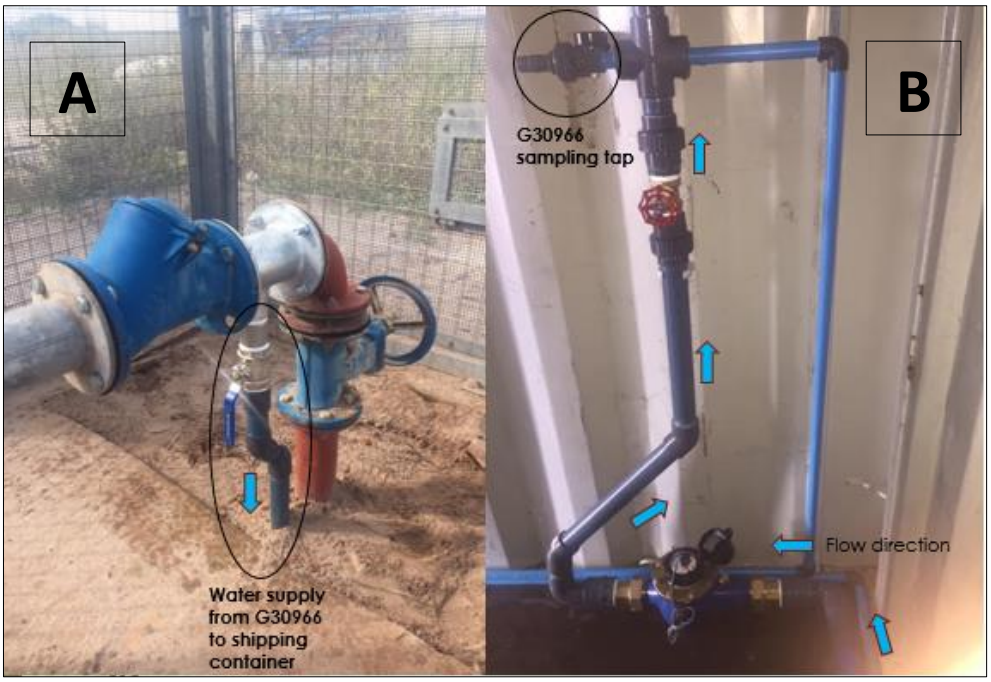

Figure 4.1: ***A****. water supply and direction of the flow of groundwater abstracted from production borehole.* ***B****. flow direction of the groundwater into the shipping container from the production borehole.*

Figure 4.2: The shipping containers position and base design at the study site, used as the groundwater treatment plant, and the production borehole (G30966) enclosed in the perpendicular cage (Nhleko et al., 2020). The base design used gravel and cement for stability.

Figure 4.3: The flow direction of the groundwater extracted from production borehole (G30966) and into the 5000 L JoJo tank before dosed with ozone (O_3) inside the shipping container at the study site, Atlantis.

4.2 Ozone (O_3) injection: *In situ* iron remediation (ISIR)

The stored groundwater in the tank is then diverted to two JA 10 Foras electrical pumps commonly used in domestic swimming pools. Using both pumps, a combined full-flow delivery of 1.5 L/s (0.75 L/s for each pump) forced the water from the tank through reinforced PVC tubing. This water then passed through the parallel venturi's (Venturi 1078 and Venturi 784) connected to the O_3 generator with oxygen generator, mixing equal amounts of O_3 and the aerated groundwater (Figure 4.4). The venturi's are located after the pumps, creating a suction effect when water is pumped through its small orifice (Wassertec, 2012; Robey, 2014). This action creates a vacuum on the suction port as it travels through the O_3 outlet of the CD generator through the 8 mm Teflon tubing, pulling O_3 gas from the O_3 generator to dose the groundwater (Sommerfeld, 1999; Robey, 2014).

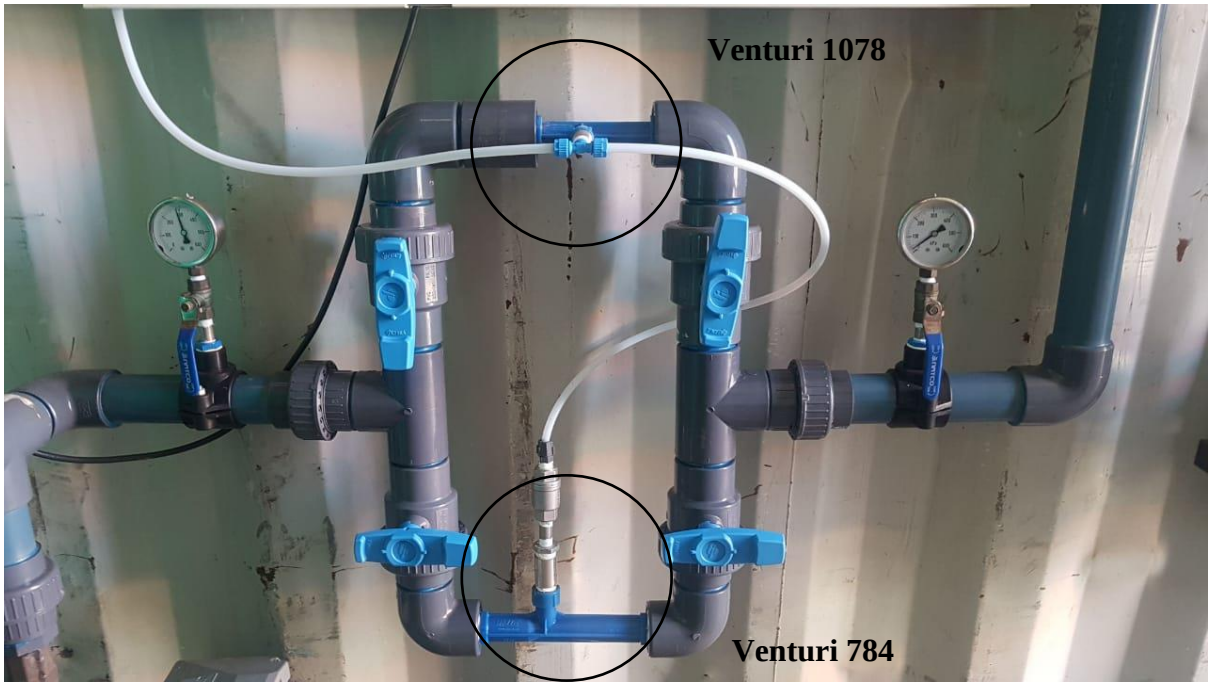

Figure 4.4: Parallel venturi's, Venturi 1078 and Venturi 784, injecting ozone (O_3) into the water source from the JoJo Tank.

Ozone is generated using a CD Aqua Ozone Generator, which is equipped in the shipping container. Once the water is treated with O_3, it passes into a PVC column (1.3 m height x 0.1 m diameter) for O_3 to dissolve in solution and passes the degas valve to remove excess undissolved O_3. Any undissolved O_3 gas, oxygen or by-product carbon dioxide (CO_2), methane, and H_2S was released from the oxygen and O_3-enriched water (hereafter referred to as ozonated water) through a degas valve at the top of the PVC column and led into the tank to prevent any O_3 loss in the system. A sampling tap was positioned after the degas valve to sample water after O_3 treatment before injection. The removal of remaining trapped gas before being introduced into the aquifer prevents the clogging of pore space in the event of gas bubble formation in recharge water, as was experienced in Egypt (Olsthoorn, 2000). The equipment used for the experiment and flow direction of groundwater inside the container is indicated in Figure 4.5.

Figure 4.5: The groundwater treatment set-up (using ozonation) inside the shipping container, displaying: ***A.*** *The 5000 L JoJo tank, power supply, two electrical pumps. The electrical supply was used for both electrical pumps to force water out of the JoJo tank and through venturi's to be dosed with ozone (O_3)* ***B.*** *and O_3 generator, venturi's, degas valve, PVC column and the overall flow direction inside the container.*

The ozonated water then passes through PVC tubing that is separated into three streams, for injection to occur in either of the injection boreholes 11DNE, 7DE, and 12DN. These injection boreholes were fitted with manholes to protect and preserve the data loggers and injection pipework (Figure 4.6). Each set of outlet PVC tubing is equipped with a water meter and globe valve to regulate the injection rates of the ozonated water. The depth of injection is between 24 and 27 meters below ground level (mbgl) and was selected based on the borehole screen depths of the injection boreholes. In addition to the injection selection range, the water column could pressurize the O_3 to remain in solution if injection occurred at depths of less than 6 mbgl (Robey, 2014). The diameter of PVC tubing was selected based on sufficient resistance during injection, in order to retain full ozonated water volumes within the tubing and prevent the introduction of gas bubbles into the injection borehole(s) and subsurface (Olsthoorn, 2000; Robey, 2014). Once the ozonated water is pumped out of the shipping container through the PVC pipe, it is injected into the aquifer via the injection borehole(s), up-gradient to the production borehole (Figure 4.7). Injection occurs up-gradient ± 10 m away from the

production borehole to allow oxide precipitation to form a barrier for attenuation of the soluble iron and manganese ions as groundwater flows past. Furthermore, the injection outlet was placed at 25 m, well within the screened sections of the boreholes, to ensure mixing between ozonated water and groundwater.

Ozone injection began in all three injection boreholes on the 29th October 2019 at 13:15 at the study site. However, the study only closely monitored the response of iron and manganese in 11DNE as the monitoring boreholes positioned at 2 m intervals could assess the response rate of O_3 downgradient more effectively.

Figure 4.6: Boreholes equipped with injection pipework and submerged probes inside the borehole in one of the injection boreholes (10DNE) once the manhole casing was removed at the study site, Atlantis (Nhleko et al., 2020).

Figure 4.7: Ozone (O_3) injection into injection boreholes after groundwater treatment using ozonation inside the shipping container at the study site, and the flow direction from the container into injection boreholes. Injection boreholes include 7DE, 11DNE, and 12DN.

4.3 Injection regime determination

The planned injection regime was to inject O_3 continuously into the central injection borehole (11DNE) using all available O_3 generated from inside the shipping container. The volume of O_3 injection into 11DNE could not have been pre-determined as the volume would be dependent on subsurface conditions such as the water table level. Configuration of the injection volume to ensure no overflowing from the injection borehole, and ultimately the loss of O_3 concentration, was initially suggested. The duration of the injection regime would be determined once subsurface and hydrochemical changes at the production borehole G30966 was proven and monitored as a result of subsurface changes downgradient from 11DNE to G30966. Once injection volumes are configured and durations determined based on the 11DNE injection regime, similar injection regimes, volumes and duration would then be applied and considered for injection boreholes 7DE and 12DN for optimum performance. A timeline of actual injection regimes at the study site was developed to contribute to general understandings of chemical and physical parameters (Table 4.1).

The actual timeline of actions recorded in Table 4.1 differs vastly from the initial planned injection regimes at the study site. Continuous injection took place between 29 October 2019 and 11 March 2020. However, due to constant power outages influenced by city-wide loadshedding, the overall injection regime can be considered to be intermittent. Three injection boreholes were used for the injection of O_3, 11DNE, 7DE, and 12DN. Different ratio volumes of O_3 was injected into each injection borehole, influenced by its subsurface conditions, geological formation and water level. Overflowing was derived by the abundance of O_3 injection directly into the borehole, which was noted in 11DNE on 5 November 2019 (Table 4.1). Overflowing of the borehole is a result of too much ozonated water being injected into the borehole diameter which results in the borehole to overflow as the borehole volume capacity is exceeded. Overflowing results in O_3 being released into the atmosphere, resulting in a loss of O_3 concentration from the initial ozonated water produced. This loss in O_3 over a period of continuous injection ultimately affects hydrochemical data and decreases the opportunity of the ISIR technology to perform optimally to reduce iron and manganese concentrations. A change in injection rates was conducted throughout the period of O_3 injection from 29 October 2019 to 19 February 2020 to determine injection volume suitability and eliminate occurrences of overflow (Table 4.1). Furthermore, testing involved determining optimum injection volumes and regimes which also contributed to injection configurations.

Table 4.1: Recorded timeline of actions at the study site in Atlantis, Western Cape, South Africa. The recorded date of actions, abstraction and injection rates (L/s), and general notes is included (Nhleko et al., 2020). Abstraction occurred in production borehole G30966 and injection of ozone (O_3) occurred in injection boreholes 7DE, 11DNE, and 12DN. The monitoring period was from the 23 May /2019 to 11 March 2020.

Date	Abstraction (L/s)	Injection (L/s)			General Notes
	G30966	7DE	11DNE	12DN	
23 May 2019					Drilling of injection boreholes 7DE, 11DNE, and 12DN
08 August 2019					Step-test pumping of G30966 indicating aquifer characteristics towards 10DNE
21 August 2019					Pumping out of G30979
04 September 2019					Pipework removed and cover plates cut for easy access
26 September 2019					Pumping from all injection boreholes to remove as much drilling mud as possible
01 October 2019					Baseline sampling
16 October 2019	5,37				Start of weeklong pumping of G30966, RWL at 4.55 mbgl
29 October 2019		0,2	1,7	0	Baseline sampling, Ozone injection started at 13:15
01 November 2019	4,7	0,2	1	0,3	Sampling
05 November 2019		0,7	0,5	0,4	11DNE overflowing, new injection rates adjusted
28 November 2019	5,43	0,7	0,5	0,4	G30966 restarted after power cut
02 December 2019		0,7	0,5	0,4	Sampling
17 December 2019		0,7	0,5	0,4	11DNE foam on surface of WL probe (due to injection)
15 January 2020		0,7	0,43	0,4	G30966 off due to power outages
21 January 2020	5,13	0,7	0,43	0,4	11DNE foaming - ozonation resumes - WL reading could not be taken
29 January 2020	5,06	0,7	0,43	0,4	11DNE still foaming - flushed out with water
05 February 2020	4,9	0,44	0,1	0,38	11DNE overflowing - new injection rates adjusted
12 February 2020	4,8	0,27	<0.1	0,46	7DE starts foaming - injection rates adjusted
19 February 2020	4,9	0,27	<0.1	0,46	Ozone generators switched off- injection continues
26 February 2020	5,14	0,27	<0.1	0,46	11DNE overflowing
04 March 2020	5	0,27	<0.1	0,46	Ozone generator is still off
11 March 2020	5,2	0,27	<0.1	0,58	Ozone generator is still off

4.4 Data collection methods

4.4.1 Data collection

During the collection of hydrochemical datasets, samples were collected from the first date of commissioning in October 2019 to March 2020. The following parameters were measured before pumping in monitoring and injection boreholes:

- Static water levels (SWL): Measured before pumping commenced in monitoring and injection boreholes. Once O_3 injection began, SWL was only measured in monitoring boreholes.
- Well diameter: Measured before injection and monitoring boreholes were injected with ozonated water.

- Distances between injection and monitoring boreholes: Measured before injection started, and cross-referenced with the previous datum of boreholes on site
- Borehole locations, depths, and elevations: Records were gathered from existing and newly drilling datum of boreholes on site

4.4.2 Data collection procedure and equipment

Groundwater levels were measured using a dip meter (Figure 4.8) and adopting the procedure from Weaver *et al.,* (2007). Using the sensor of the dip meter, it was lowered down into each borehole until a buzzer went off to notify researchers that the sensor had reached the surface of the water. To read the water level the datum at the top of the borehole casing perimeter was used to measure the distance from the datum to the water level. This measurement was repeated twice before recordings were noted to improve data collection accuracy. Borehole elevations were collected using a GPS, recording locations with less than 5% error margin, and reviewing records from existing datum from Council for Geosciences (CGS). This field measurement involved placing the GPS next to the borehole point and recording elevation values directly from the GPS.

Figure 4.8: Groundwater levels (mbgl) being recorded at 8DSW at the study site in Atlantis using a TLC Water Level Meter.

4.5 Hydrochemical data collection

Before sampling boreholes, purging of boreholes was performed using the procedure adopted by Weaver *et al.* (2007). This method involves purging of groundwater to remove stagnant groundwater that has been in contact with atmospheric conditions and borehole material. Firstly, the resting water levels of boreholes were measured using a TLC Water Level Meter.

Using a submersible pump, the pump was lowered into the borehole within the perforated screen section which was pre-determined using existing borehole drilling data from CGS. Once placed within the perforated borehole screen, the pump was switched on using a car battery, purging water from either monitoring and injection boreholes and into a 25 L bucket, where 3 volumes of 25 L buckets were tossed approximately 10 m from the borehole. The fourth volume using the 25 L plastic bucket was used to measure field parameters, by placing the probes vertically upright into the water-filled bucket and allowing values to stabilize before

they were read and recorded. Once the fourth volume became full, water was diverted into a 10 L bucket, still with probes inserted, to reduce its volume capacity and allowing fresh borehole water to flow into the bucket for continuous field measurements to be recorded.

Measurements of field parameters of the production and monitoring boreholes included: pH, electrical conductivity (EC), temperature, and dissolved oxygen (DO) using a WTW Multi 3420 SET G water quality multi-parameter device (Figures 4.9 and 4.10). Field measurements were recorded once the readings had stabilized. These hydrochemical parameters (pH, EC, DO, and temperature) were determined in the production (G30966) and monitoring boreholes to understand the conditions within the boreholes and surrounding aquifer (Robey, 2014). After the readings had stabilized, a total of 4 or 5 readings were recorded every 2 to 3 minutes apart at each borehole to determine an average of each parameter. However, since DO is slow to stabilize, the last reading was used as the final measurement. During and after ISIR treatment, these parameters were tested repeatedly at least every 1 to 3 weeks to identify any changes as a consequence of the treatment efficiency in the monitoring boreholes and the production boreholes performance (Robey, 2014). After these readings were recorded, water samples were collected from the pumped borehole.

Electrical conductivity, pH, temperature and DO probes of the multi-parameter device were calibrated before each day of testing using appropriate calibration procedures and standard solutions outlined in the WTW manual.

Figure 4.9: Multi-meter equipment, probes, and set-up at the study site measuring field parameters after groundwater extraction using a submersible pump from monitoring borehole 8DNE. Probes include measurements for electrical conductivity (EC), pH, temperature, and dissolved oxygen (DO).

Figure 4.10: Submerged electrical conductivity (EC), pH, temperature, and dissolved oxygen (DO) probes in a 25 L bucket, used to collect field measurements at monitoring boreholes at the study site, Atlantis.

In addition to manual field parameter sampling, an automated GeoTel data collection system (telemetry) for 24/7 continuous data was used (Figure 4.11). Telemetry collects point source data remotely and transmits the data electronically to a cloud-based database which can be viewed continuously in real-time. The telemetry was designed to measure field parameters of DO, water levels, temperature, injection flow rate, and EC. These parameters were allocated in injection and monitoring boreholes using Solinst (F100, M30) and Global Water (WQ-FDO and GL500-7-2) data loggers. These data loggers were lowered to depths of 25 m. Injection boreholes 7DE and 12DN measured continuous water level and temperature parameters. Injection borehole 11DNE and monitoring borehole 4DNE measured continuous water level, EC, and temperature parameters. A DO probe was inserted in monitoring borehole 8DNE to detect DO changes. Two sampling point columns were installed to measure continuous DO of both source water and ozonated injectant water. Continuous measurements of these parameters provide a valuable understanding of the zone of influence and assists in optimizing the ISIR treatment design through responsible logging, viewing, and downloading hydrochemical data.

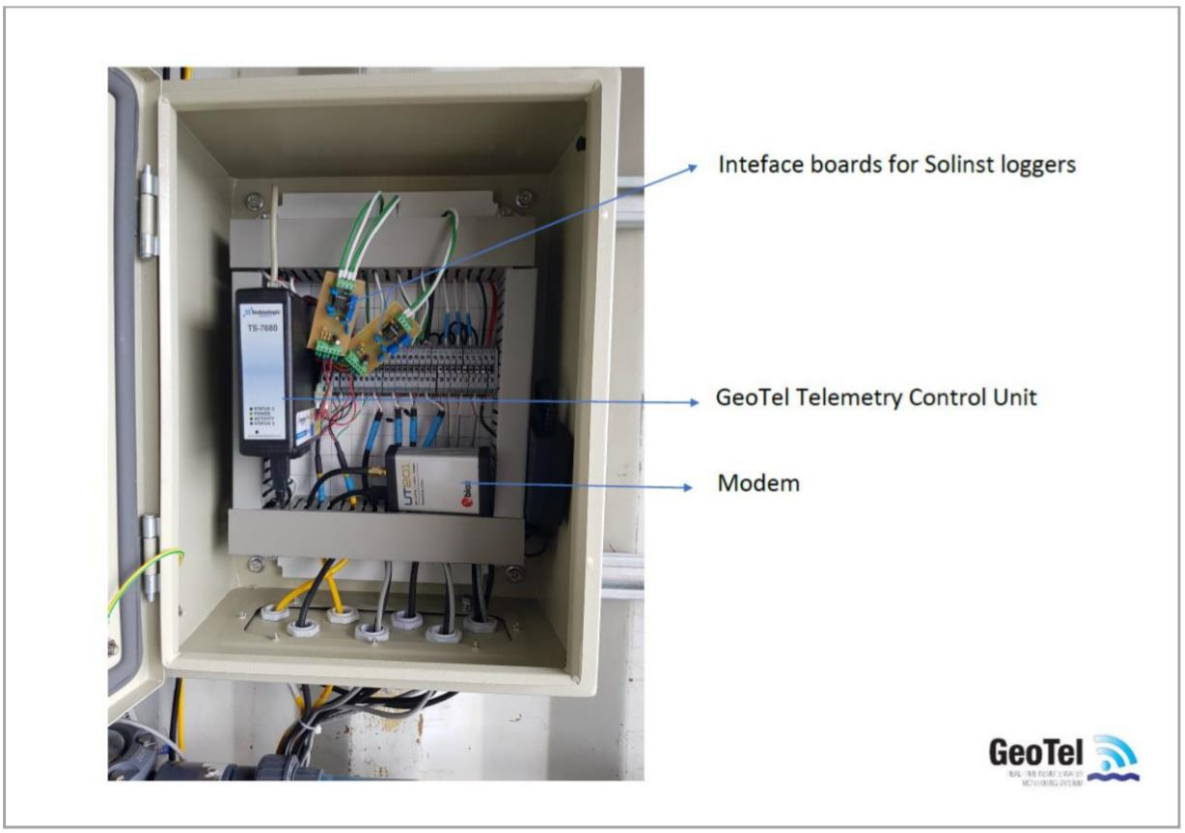

Figure 4.11: Components and set-up of the GeoTel telemetry system inside the shipping container used to collect point source data remotely from the study site in Atlantis (Nhleko et al., 2020).

4.6 Water sampling procedure

The water sampling followed the standard procedure as outlined in Weaver *et al.* (2007). Unfiltered samples were collected using 500 mL plastic bottles which were rinsed thrice with abstracted groundwater, before filling the bottles to the top and closing the fitting caps tightly to prevent further atmospheric conditions to alter the water chemistry of the sample. Additional water samples were collected for future hydrochemical analysis. In this study, the additional samples were either filtered using a 0.45 µm nylon syringe filter and acidified with HCl (0.5 M) or unfiltered and acidified. These additional acidified samples were collected and prepared correctly in either 250 mL or 50 mL plastic bottles (Figure 4.12). Correct labelling, and packaging were considered to prevent spillages, misinterpretations of laboratory results, and/or preserve standard temperatures.

Figure 4.12: Water sampling bottles prepared inside the shipping container at the study site to collect groundwater samples for off-site groundwater chemical analysis

4.7 Sample analyses

4.7.1 Sample analysis method

Chemical analysis of total iron (Fe^{T}), ferrous iron (Fe^{2+}), and dissolved manganese (Mn^{2+}) were performed on-site in the shipping container. As a precaution, latex gloves were used during on-site analysis to prevent contracting unwanted illnesses or chemicals onto the skin and to prevent contamination of the water samples from bare hands, that could affect hydrochemical analyses.

In addition to onsite analysis, selected hydrochemistry samples were sent to BemLab for analysis of TOC, total manganese, and Mn^{2+}. Analyses were performed in a South African National Accreditation System (SANAS) Accredited Testing Laboratory following ISO 17025:2005 for hydrochemical analysis and following the South African National Standards (SANS) hydrochemical analytical procedure.

4.7.2 Sample analysis procedure

4.7.2.1 Ferrous iron (Fe^{2+}) analysis

Using a DR900, the USEPA FerroVer Method was used to analyse for Fe^{2+}. To start the programme the 265 Iron FerroVer Programme was selected for this analysis. Water samples were collected from the pumped borehole and syringed to collect at least 20 mL. To prepare the sample, 10 mL of sample was filtered using a 0.45 µm filter in a sample cell and the FerroVer Iron Reagent Powder Pillow added to the sample cell. The sample cell was swirled with its stopper, mixing all contents sufficiently. The instrument timer was set for a three-minute reaction time, with an orange colour indicating the presence of iron. A blank was prepared by filling a second 10 mL sample cell of sample. In the meantime, the outside of the blank sample cell and prepared sample cell was cleaned using a microfiber cloth and paper towel to eliminate any obscurities during the reading. Once the timer expired, the blank cell was placed upright into the cell holder and the "ZERO" button selected to read the blank sample. Thereafter, the blank sample cell was removed and the prepared sample cell inserted into the cell holder and the "READ" button selected indicating Fe^{2+} results in mg/L.

4.7.2.2 Total iron (Fe^{T}) analysis

Using the same procedure as described in 4.6.2.1 total iron was measured. However, one exception being that the prepared sample of 10 mL was unfiltered when filling the sample cell. This allows for the total iron concentration to be determined in the cell.

4.7.2.3 Manganese (Mn^{2+}) analysis

Using a DR900, the USEPA Periodate Oxidation Method was used to analyse for Mn^{2+}. To start the programme the 295 Manganese, HR Programme was selected for this analysis. Water samples were collected from the pumped borehole and syringed to collect 20 mL. To prepare the sample, 10 mL of sample was filled into a sample cell and the contents of one Buffer Powder, Citrate Type for Manganese Powder Pillow was added to the sample cell. The sample cell was inverted at least ten times until all contents were mixed. Immediately after, the contents of one Sodium Periodate Powder Pillow added to the sample cell and inverted with the stopper on the sample cell to mix all contents. The instrument timer was set for a two-minute reaction time, with a violet colour indicating the presence Mn^{2+}. A blank was prepared by filling a second 10 mL sample cell of sample. In the meantime, the blank sample cell and prepared

sample cell was cleaned using a microfiber cloth and paper towel to eliminate any obscurities during the reading. Once the timer expired, the blank cell was placed upright into the cell holder and the "ZERO" button selected to read the blank sample. Thereafter, the blank sample cell was removed and the prepared sample cell inserted into the cell holder and the "READ" button selected indicating Mn^{2+} results in mg/L.

4.7.2.4 Total organic carbon (TOC) analysis

Hydrochemical samples were sent to BemLab for analysis of TOC. Analyses were performed following the SANS hydrochemical analytical procedure. The temperature of the sample was recorded before and after analyses. The certificate of analysis indicated that sample conditions were received in good quality and that all results were SANAS accredited, unless indicated, which was not the case in the record received.

4.7.2.5 Ozone (O_3) analysis

Using a HACH Ozone Test Kit Model OZ-2, O_3 was analysed on-site according to manufacturer instructions. The test kit measures O_3 concentrations using a comparable colour wheel in terms of colour intensity (Figure 4.13). Provided in the O_3 test kit is the test apparatus which includes two test tubes, calcium carbonate reagent, and two rubber stoppers for each test tube. A blank was prepared by filling one test tube with 5 mL of sample. To prepare the test sample, 5 mL of sample was filled into the second test tube and contents of one DPD Total Chlorine Reagent Powder Pillow was added. A rubber stopper was placed on the second test tube and inverted until all contents of the powder pillow were dissolved. Thereafter, both test tubes were placed in the comparator box with the colour wheel and left to react for roughly 10 min. Using the prepared sample in the plastic holder, the sample colour was compared to the colour wheel to achieve the most suitable concentration measurement (Figure 4.13). This test kit has been identified by HACH as the most accurate visual test kit method that is user-friendly, portable, and cost-effective.

Figure 4.13: HACH Ozone (O_3) Test Kit Model OZ-2 colour wheel measuring O_3 concentration ranges between 0 and 2.2 mg/L in terms of colour intensity.

4.8 Quality assurance and quality control

4.8.1 Validity of results

In this study, measurements were taken to analyse hydrochemical parameters spatial and temporal responses to ozonation and to quantify the efficiency of ISIR using O_3. Measurements and analyses were performed on-site and using a telemetry system to increase the result validity of this study. Apart from direct measurements and analyses, indirect measurements such as the study site hydrology, geology, and hydrogeological factors such as permeability, porosity, hydraulic properties, groundwater quality, aquifer types, etc. contributed to determining the efficiency of ISIR using ozonation.

4.8.2 Reliability of results

To ensure the reliability of the results obtained in this study, calibrations were performed on all equipment used to minimize equipment residuals. Results were also compared with the previous study performed by Robey (2014), which was in the same study area and within similar environmental settings.

4.9 Limitations of the study

The first limitation of the study was the presence of H_2S in the subsurface. This was created during the drilling technique that uses a water-based drilling fluid, known as drilling mud, which infiltrates and is stored in the aquifer after the new boreholes were drilled. Its presence is problematic with the injection of O_3, as O_3 is highly reactive with H_2S, increasing DO concentrations in the subsurface. The study solved this limitation by reducing H_2S concentrations before collecting field measurements and performing analyses, by injecting O_3 *in situ* to decompose H_2S. The removal of H_2S promotes effective ISIR (Filtronics, 1993; Appelo and De Wet, 2003).

Secondly, the choice of drilling methods used for the construction of boreholes compromised the sand profiles of where the injection was occurring. The drilling rods used for drilling purposes were roughly 3 m in length. As a result, soil profiles were only collected at 3 m intervals at each drilling borehole, instead of the recommended 1 m interval for accurate geological formation record. This limitation was overcome through the use of existing sand characteristics, such as grain size, sorting arrangements, and roundness to best describe the logging of geological formations of each drilled well-point.

The third limitation was treatment interruptions at the study site. *In situ* iron remediation (ISIR) treatment interruptions were observed during the pilot study of Robey (2014) due to the study area's shallow groundwater levels. During O_3 injection into the aquifer, overflowing from the injection borehole was noticed as a consequence of the shallow groundwater levels. To avoid similar treatment interruptions in this study, a groundwater level monitoring plan was performed from January 2017 to March 2020 to observe groundwater levels before, during and after O_3 injections to reduce the effects of borehole injection overflowing.

The third limitation of the study was time, which restricted sufficient data to be collected, analysed and observed for longer-term trend development. This restricted the understanding of trend-analysis and -development for this study. The study solved this limitation by interpreting the limited data captured, using both manual and telemetry data to derive sufficient interpretations for the study.

The last limitation of the study was the malfunctioning of the equipment installed on-site. This limitation caused a delay in accessing and collecting suitable periodic data sets to be used for analysis. To overcome this limitation, specialist technicians were assigned and notified of working conditions and equipment failures during site visits. This communication was

important in ensuring that the equipment was in good working conditions. If not, a specialist was allocated to make changes and/or fit suitable equipment or replacement parts to allow continuous data collection during the allocated data collection period.

Chapter 5: Assessing borehole clogging

5. Introduction

Borehole clogging has a large impact on groundwater resource management schemes. Research to mitigate and control the rates of borehole clogging in South Africa has been taking place because of increasing production borehole clogging occurrences (Tredoux *et al.*, 2004; Robey, 2014). This chapter presents and discusses results on assessing borehole clogging effects, thereby addressing the first objective of the study: To assess the effects of clogging on production boreholes using a combination of current and historical data to describe spatial and temporal yield variations in production and monitoring boreholes. The central argument in this chapter is to acknowledge that if borehole clogging effects are identified and understood before *in situ* iron remediation (ISIR) using ozonation, then the successful implementation of ISIR using ozonation could be achieved.

To achieve the first objective, the study collected historical groundwater level datasets, quantitative field measurements during step-drawdown tests from historical and present years, a conceptual model was developed, and historical groundwater quality datasets were gathered. The analysis of line graphs demonstrated the effects of clogging variations on the production and monitoring boreholes.

5.1 Historical groundwater quality

In 1979, production borehole G30966 was drilled using percussion drilling in the Atlantis primary aquifer (Robey, 2014). From 3 April 1979 to 2 December 2019, groundwater chemical analysis has been performed for monitoring purposes of the aquifer. Physical and aesthetic determinants, chemical determinants (macro- and micro-determinants), and organic determinants were monitored, with maximum, minimum, and mean concentrations calculated and compared to the South African Bureau of Standards (expressed as SANS 241:2015) (Table 5.1).

Table 5.1 summarises various chemical determinants monitored before ISIR from April 1979 to December 2019 and emphasizes the concentration standards for drinking water quality with SANS 241:2015. Health- and aesthetic-based guideline values have been provided to determine the overall historical groundwater quality of the study area for G30966. Both iron and manganese mean concentrations exceeded the minimum aesthetic drinking water quality

concentrations of both SANS 241:2015 guidelines. Iron and manganese concentrations in G30966 almost doubled the minimum guideline concentrations given in Table 5.1. This acknowledges the need for in situ iron remediation (ISIR) treatment to mitigate borehole clogging.

A significant physical parameter considered in Table 5.1 is that of pH. The mean pH value recorded as 7.5 is ideal for the rapid oxidation of Fe^{2+} and allows for increased sorption capacity of precipitated iron (Robey, 2014). This mean pH value compares favourably to Walter (1997) who explains that increased pH levels increases the rate of iron precipitation. According to Cavé *et al.* (2004), suitable iron oxidation conditions before oxygenation was noted to have a pH level of around 7. The maximum pH value of 9.5 was most suitable for Mn^{2+} oxidation, and still within both guidelines. This result compares favourably to Homoncik *et al.*(2010) who expressed that manganese oxidation occurs favourably in groundwater environments with pH values greater than 8. Although no aesthetic- or health-based guidelines have been stipulated by SANS 241:2015 the availability of alkalinity in G30966 is ideal for ISIR treatments. Alkalinity determines the suitability for ISIR treatment at the study area since it serves as a buffer to decreasing pH levels as a consequence of Fe^{2+} and Mn^{2+} oxidation in the subsurface.

High total organic carbon (TOC) and DOC levels in the aquifer is usually greater than 5 mg/L. Although the concentrations are well below the standard limits, high DOC and TOC concentrations are problematic for ISIR treatment. These high concentrations affect the rate of oxidation and sorption processes that affect the removal of iron and manganese in the subsurface (Van Der Laan, 2008; Ahmad, 2012; Ezzat *et al.*, 2008). Dissolved organic carbon of abstracted groundwater in Atlantis has previously been measured up to 4 mg/L which is prone to fluctuate as natural organic carbon in groundwater tends to increase DOC levels (Tredoux *et al.*, 2011). Organic carbon is derived from alien vegetation and Fynbos in the area (Bugan *et al.*, 2018). Natural TOC concentrations in the aquifer calculated carbon between 6 and 7 mg/L (Bugan *et al.*, 2018). This result compares favourably to findings of Cromley and O'Connor (1976), Clark (1988), Silvieria (1988), and Sallanko *et al.* (2007) who identified inorganic and organic complexes as inhibiting factors to oxidation reactions of iron and manganese.

Table 5.1: Historical groundwater chemistry data of production borehole G30966 before ISIR treatment from 3 April 1979 to 2 December 2019 (Supplied by City of Cape Town). The number of observations, associated risks, and standard deviation (SD) is included.

Determinant	Unit	Risk	Number of observations (n)	Minimum	Maximum	Mean	Standard deviation (SD)	SANS 241:2015	WHO 2017
Physical and Aesthetic determinants									
pH	pH units	Operational	279	6,7	9,5	7,5	0.29	≥ 5 and ≤ 9.7	
Conductivity	µS/cm	Aesthetic	286	493	1440	960	171.2	≤ 1700	
Total Dissolved Solids	mg/L	Aesthetic	240	330,3	902	606	107.7	≤ 1200	≤ 600
Total Hardness	mg/L	Aesthetic	242	131	788	226,5	78.73	-	
Chemical determinants - Macro-determinants									
Ammonia as N	mg/L	Aesthetic	16	0,04	0,76	0,63	0.08	≤ 1,5	≤ 1,5
Calcium as Ca	mg/L	-	246	40,1	272	76	28.93	-	
Chloride as Cl	mg/L	Aesthetic	265	52	285	160	45.31	≤ 300	
Fluoride as F	mg/L	Chronic Health	61	0,02	0,6	0,29	0.11	≤ 1,5	≤ 1,5
Magnesium as Mg	mg/L	-	245	5	26	10	3.14	-	
Nitrate as N	mg/L	Acute Health	175	0	1,2	0,05	0.1	≤ 11	≤ 11
Potassium as K	mg/L	-	278	0,01	10,7	2,7	2.13	-	≤ 200
Sodium as Na	mg/L	Aesthetic	246	41,5	188	90,5	19.7	≤ 200	≤ 200
Sulphate as SO_4	mg/L	Health	239	2	385,8	47.7	41.45	≤ 500	
		Aesthetic						≤ 250	≤ 250
Total Alkalinity	mg/L	Aesthetic	256	72	261	179,5	29.97	-	
Zinc as Zn	mg/L	Aesthetic	8	0,01	0,12	0,06	0.03	≤ 5	
Chemical determinants - Micro-determinants									
Aluminium as Al	µg/L	Operational	47	1	196	19	42.95	≤ 300	
Cadmium as Cd	µg/L	Health	2	4,4	4,4	4,4	0	≤ 3	

Copper as Cu	µg/L	Chronic Health	36	1	45	7	11.74	≤ 2000	≤ 2000
Total iron as Fe^T	µg/L	Health	217	27	18600	519	2152.74	≤ 2000	
		Aesthetic						≤ 300	≤ 300
Manganese as Mn	µg/L	Health	110	6	827	196	187.96	≤ 400	
		Aesthetic						≤ 100	≤ 100
Chemical determinants - Organic determinants									
Dissolved organic carbon	mg/L	-	41	2,93	10,8	7,8	1.58	-	
Total organic carbon	mg/L	Chronic Health	33	3,7	7,2	5,1	0.79	≤ 10	

: *Mean concentrations exceeding the minimum aesthetic drinking water quality concentrations of the SANS 241:2015 guidelines*

A time-series plot was created to represent the concentrations of chemical macro-determinants of total alkalinity, potassium, sodium, calcium, magnesium, chloride, fluoride, sulphate, nitrate, zinc and ammonia monitored from April 1979 to December 2019 (Figure 5.1). A consistent trend across the macro-determinant's concentrations are apparent in Figure 5.1 with minimal variation from 1979 to 2019. A decreasing trend of chloride's concentration from 1988 to 1999 is identified in Figure 5.1. This trend compares favourably to Walter (1997) and Smith (2007) who mentioned that the oxidation rate of iron increases in the presence of low concentrations of sulphate and chloride through the complexation of free Fe^{2+}. As a result, these reduced concentrations would promote favourable conditions for iron oxidation enhancing the reduction of iron in groundwater concurrently with O_3 injection. The only recorded macro-determinant concentration that exceeded aesthetic SANS 241:2015 and WHO drinking water quality guidelines was recorded for sulphate at 385.8 mg/L (data not visible) on the 7th March 2009. Fluctuating sulphate levels has been apparent in Atlantis due to various Sandveld Group formations that have contributed to the overall hardness in groundwater influenced by calcretes of the Witzand formation, and iron and sulphates from the Springfontein formation (Tredoux and Cáve, 2002). These fluctuating sulphate results in Figure 5.1 compares favourably to the findings of Tredoux and Cáve (2002).

There were inconsistencies in monitoring of the data between the periods of 1997 and 2001, where monitoring interruptions of all macro-determinants concentrations are noted. However, in some instances, there were four concentrations recorded for the same day or up to several concentrations recorded for the same month. No documented explanations for monitored interruptions between 1988 and 2001 has been recorded. This could result in unreliable and inconsistent data that could affect results.

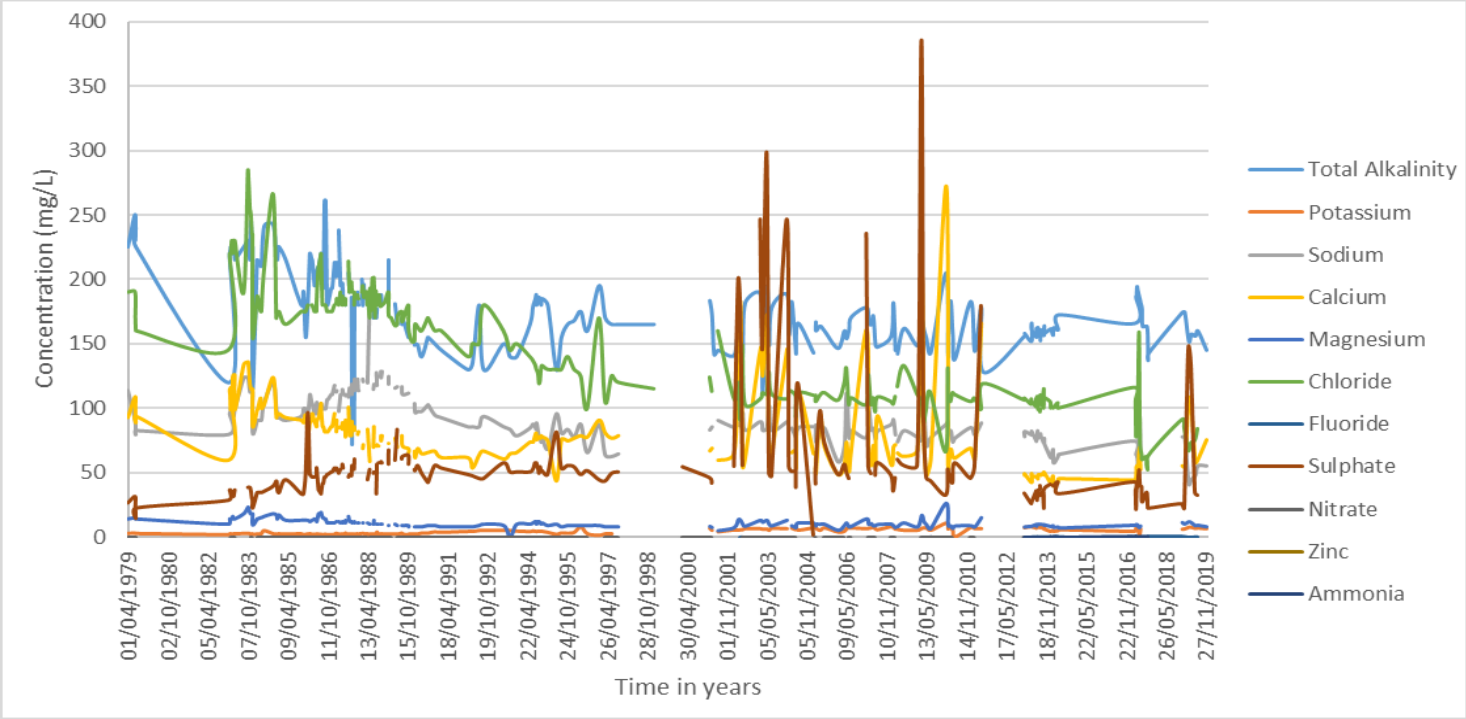

Figure 5.1: Time-series of chemical macro-determinants of production borehole G30966 from April 1979 to December 2019 at the study site in Atlantis (Nhleko et al., 2020). Chemical macro-determinants included total alkalinity, potassium, sodium, calcium, magnesium, chloride, fluoride, sulphate, nitrate, zinc, and ammonia (mg/L).

Both iron (total) and manganese were plotted on separate time-series plot as these are the foremost chemical micro-determinants responsible for borehole clogging in the system (Figure 5.2). The highest recorded value for Fe^{T} was 18 600 µg/L on the 15th August 1983 (Figure 5.2). Similar high iron concentrations was noted in a case study in northern Germany with iron concentrations of 10 000 µg/L (Boochs and Barovic, 1981) which injected oxygen-rich water *in situ* to treat high iron and manganese concentrations in groundwater of coastal areas. This value exceeds the SANS 241:2015 and WHO drinking water aesthetic (≤ 300 µg/L) and health (≤ 2 000 µg/L) standards. This is usually facilitated by geological conditions which affects subsurface iron concentrations, or by incorrectly captured data caused by human error. Except for the highest recorded value and outliers, Fe^{T} concentrations across the analysis period between 1979 and 2019 are generally between the 0 and 4 000 µg/L range (Figure 5.2). It wasn't until 2001 that manganese concentrations were included for analysis as a consequence of iron-related clogging occurrences at the study site (Nhleko *et al.*, 2020). The highest recorded manganese concentration was recorded on 06/02/2010 at 827 µg/L (Figure 5.2). This value greatly exceeds the SANS 241:2015 and WHO drinking water aesthetic (≤ 100 µg/L)

and health (≤ 400 µg/L) standards. Except for the highest recorded value and outliers, manganese concentrations across the analysis period between 2001 and 2019 are generally between the 100 and 600 µg/L range (Figure 5.2). Similar ranges of manganese concentrations before ISIR treatment has been recorded in Kom Hamada by Olsthoorn (2000), western Switzerland by Mettler *et al.* (2001), and Germany by Ebermann *et al.* (2012) which all required treatment as it exceeded either country-specific and WHO guideline standards.

With the exception of maximum and minimum iron and manganese concentration outliers, an overall consistent trend across the micro-determinants concentrations is apparent (Figure 5.2) with minimal variation from 1979 to 2019. Between the periods of 1988 – 1990, 1997 – 2001, 2011 – 2013, and 2017 - 2019 there were monitoring interruptions of iron and/or manganese concentrations. A general trend can be noted between the Fe^{T} and manganese concentrations (Figure 5.2) between 2001 and 2019. It has been noted that both iron and manganese concentrations fluctuate concomitantly. This can be explained by their natural co-existing characteristics such as chemical behaviour and occurrence which are similar to each other (Silveria, 1988; Ahmad, 2012). The majority of simultaneous iron and manganese concentration fluctuations can be noted in Figure 5.2.

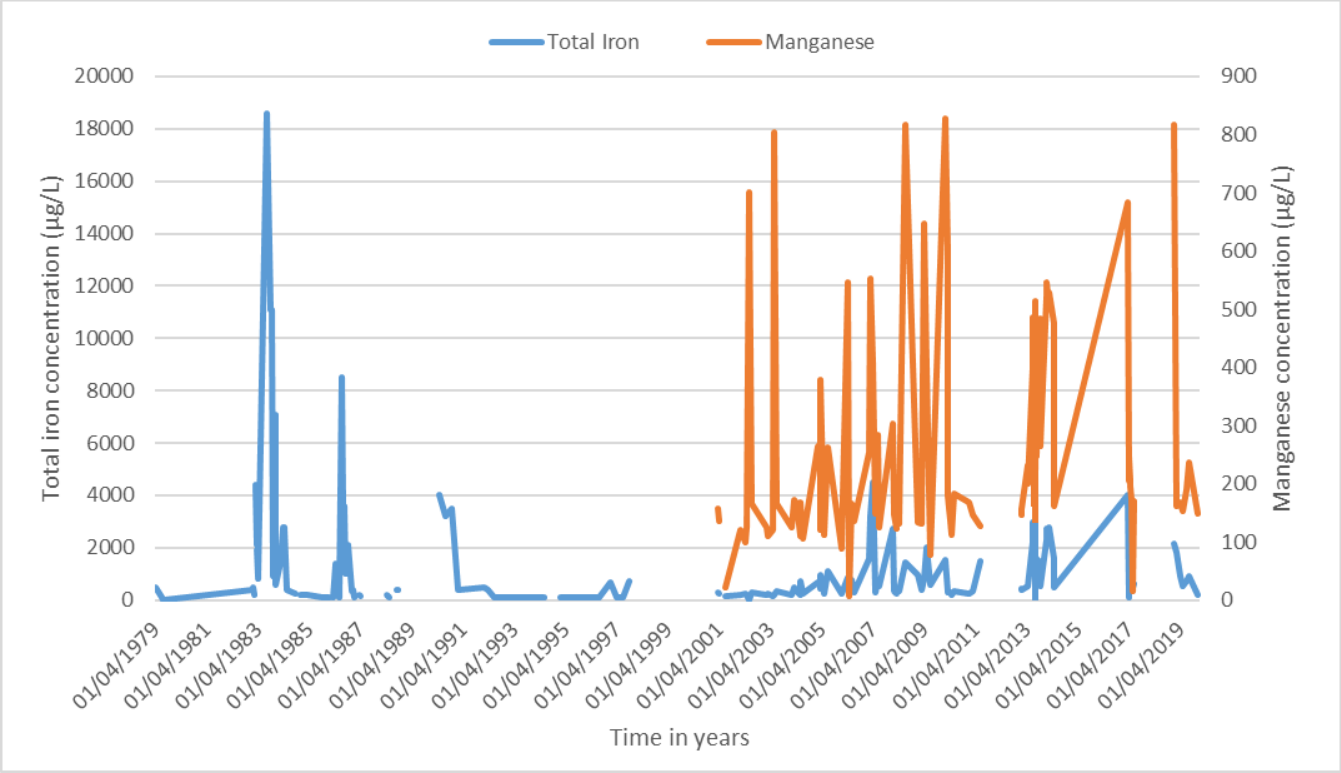

Figure 5.2: Time-series of chemical micro-determinants total iron and manganese concentrations (µg/L) of production borehole G30966 from April 1979 to December 2019 at the study site in Atlantis. Recording interruptions were noted between 1988 – 1990, 1997 – 2001, 2011 – 2013, and 2017 – 2019.

Variability in step duration creates issues when comparing subsequent specific capacity (Sc) values to the initial specific capacity standard value taken after borehole construction in 1979. This is observed in this instance as the step-drawdown test in 1979 was not performed with equal time durations between each step. As a consequence, the initial specific capacity values calculated in 1979 does not suitably serve as a specific capacity standard when compared to step-drawdown tests that followed in preceding years (Driscoll, 1986; Robey, 2014). The results obtained from future step-drawdown tests has, and possibly will not closely match the original specific capacity values (Table 5.2) calculated from the 1979 step-drawdown test (Robey, 2014). The improper construction of G30966 before the step-drawdown test in 1979 could have resulted in the increase in specific capacity values over time (Table 5.2) and/or due to the increase in the groundwater levels that increases the specific capacity over time (Johnson, 2005; Robey, 2014). This increase is influenced by an increase of roughly 2 m in the saturated thickness of the aquifer since the first step-drawdown test in 1979 (Robey, 2014).

The specific capacity of G30966 was determined before O_3 injection (Table 5.2), with the intention of comparing the calculated results before O_3 injection to specific capacity after O_3 injection, and ultimately determining the overall borehole performance and efficiency after ozonation. However, a final pumping test and calculated specific capacity after ozonation was not achieved due to constraints by the international COVID-19 pandemic which prevented access to the site, and could not be resolved within the project timeframe. According to Walter (1997), iron-related bacteria and elevated iron concentrations in groundwater contributes to clogging incidences that decrease well yields and specific capacity. This is supported by a case study in Suffolk Count in Long Island, New York where specific capacity declines in several production boreholes during shut down periods were observed (Walter, 1997). Even though a decrease in specific capacity with increased time is expected, and has been observed in the most recent step-drawdown test in 2019, the inconsistent flow rates affected the specific capacity values. As previously mentioned, although an increase in pumping rates was performed, the flow rates for each period were inconsistent in G30966 that affects the overall accuracy of the data collect. Due to inconsistent flow rate measurements, the calculated specific capacity values fluctuated greatly between each of the four steps in the most recent step-drawdown test data in 2019. As a consequence, the study was unable to derive a suitable understanding and theoretical discussion to explain the conditions of borehole performance and efficiency, due to inaccurate data collected during the pumping test in 2019. Similar inaccuracies in step-drawdown test data and specific capacity calculations have been noted in Robey (2014).

Table 5.2: Step-drawdown tests performed from 1979 to 2019 at production borehole G30966 in Atlantis primary aquifer. Included is flow rates (Q) (L/s), time (minutes), drawdown (Sw) (m), and specific capacity (Sc) (m^3/day/m). Specific capacity (m^3/day/m) = Q (L/s) / drawdown (m)

Step drawdown pumping test No. 1 (08/05/1979)				
Step No.	Q (L/s)	Time (min)	Sw (m)	Sc (m3/day/m) = Q (L/s) / Sw
1	3,02	60	3,81	68,49
2	6,02	180	8,14	63,90
3	7,75	240	10,41	64,32
Step drawdown pumping test No. 2 (22/02/2000)				
Step No.	Q (L/s)	Time (min)	Sw (m)	Sc (m3/day/m) = Q (L/s) / Sw
1	5,00	60	5,14	84,00
2	6,25	120	6,50	83,08
3	10,00	180	8,78	98,41
4	12,50	240	14,55	74,23
Step drawdown pumping test No. 3 (26/02/2000)				
Step No.	Q (L/s)	Time (min)	Sw (m)	Sc (m3/day/m) = Q (L/s) / Sw
1	5,20	60	4,19	91,50
2	6,25	120	5,97	90,45
3	10,00	180	8,07	107,06
4	12,50	240	13,55	79,70
Step drawdown pumping test No. 4 (06/11/2007)				
Step No.	Q (L/s)	Time (min)	Sw (m)	Sc (m3/day/m) = Q (L/s) / Sw
1	0,40	30	0,29	119,17
2	0,90	60	0,77	100,99
3	7,70	90	5,87	113,34
4	14,30	120	11,18	110,51
Step drawdown pumping test No. 5 (09/01/2013)				
Step No.	Q (L/s)	Time (min)	Sw (m)	Sc (m3/day/m) = Q (L/s) / Sw
1	4,79	60	4,68	88,43
2	6,55	120	6,34	89,26
3	11,92	180	11,18	92,12
4	14,04	240	12,89	94,11
Step drawdown pumping test No. 6 (08/08/2019)				
Step No.	Q (L/s)	Time (min)	Sw (m)	Sc (m3/day/m) = Q (L/s) / Sw
1	9,94	60	5,29	162,35
2	5,95	120	11,24	45,74
3	12,80	180	12,04	91,85
4	7,07	240	12,49	48,91

5.2 Groundwater level distribution

Consistent water level recordings (i.e. static groundwater levels) were measured weekly from January 2017 to March 2020 using a dip meter as described in Section 4.3.2. However, unexpected interruptions in the monitoring programme throughout the period can be noted in Figure 5.3 by absent readings. Figure 5.3 shows variable monitored static groundwater levels at the study site between January 2017 and March 2020. Measures of the groundwater levels are presented in Table 5.3. The highest groundwater level was recorded on 2 December 2019 at G30979 of 1.9 mbgl. The lowest recorded groundwater level of 11.71 mbgl was taken at the production borehole G30966 on the 26 February 2020. This is unusually low due to the immediate response of borehole abstraction from G30966 for groundwater treatment inside the shipping container. Based on the overall trend of groundwater levels across the monitoring period, a steady decrease in the curve was observed between January 2017 and June 2018. After June 2018, a slow and natural recovery period was noted. Although a decreasing groundwater level distribution has been noted from January 2017 to March 2020, these conditions are conducive for ozone (O_3) injection in the aquifer. Low groundwater levels allow the aquifer to receive the total injection quantity without oxidant loss during borehole surface overflow, which was experienced in the pilot study by Robey (2014). However, the injection boreholes overflowed during injection and the injection rates were significantly reduced during the operation in this study.

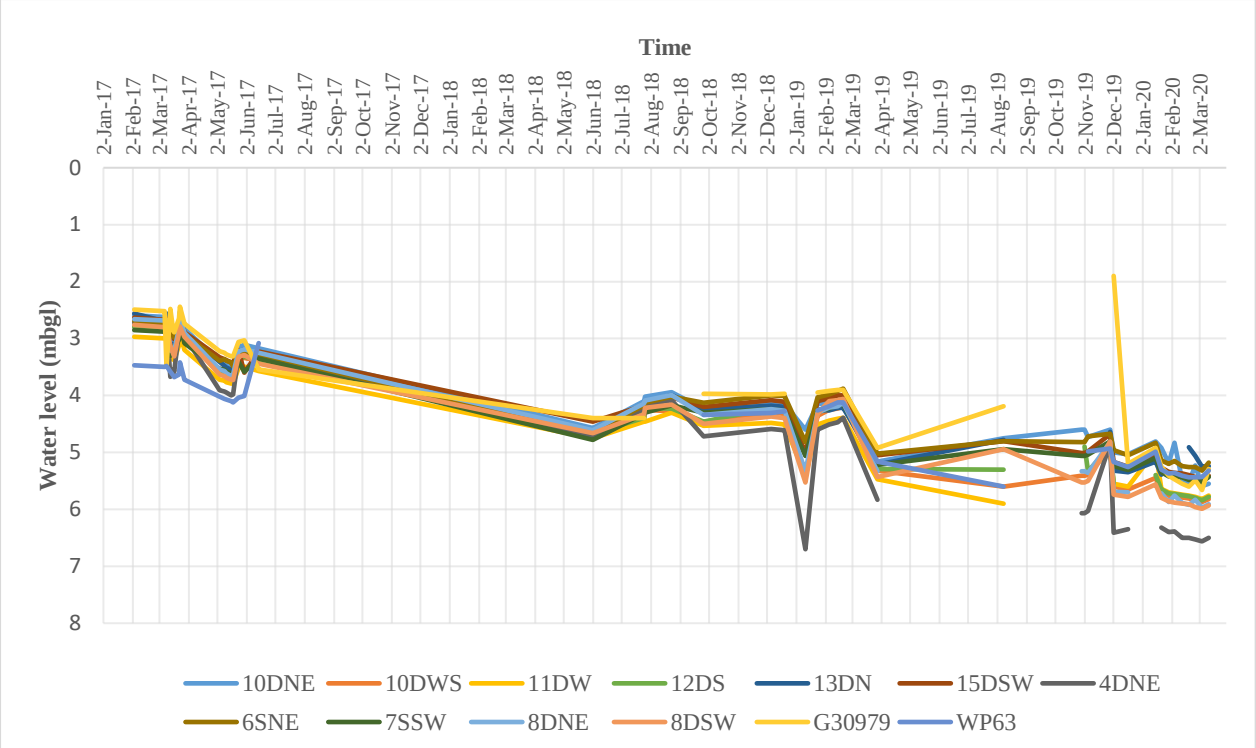

Figure 5.3: Time-series plot from January 2017 to March 2020 indicating groundwater levels in metres below ground level (mbgl) of monitoring boreholes at the study site, Atlantis. Monitoring boreholes include 10DNE, 10DWS, 11DW, 12DS, 13DN, 15DSW, 4DNE, 6SNE, 7SSW, 8DNE, 8DSW, G30979, and WP63. Gaps were discovered due to interuptions that occurred in some monitoring boreholes during August 2019 and February 2020.

According to Visser (2016) and SRK (2014), seasonal rainfall variation does not affect the groundwater levels and groundwater flow direction at the study site. The water table has always had a steady range between 2 and 6 mbgl, which corresponds to the measures calculated in Table 5.3. These measures were used to determine the hydraulic properties or characteristics of the aquifer systems, since the injection boreholes overflowed. In the event of over-injecting, injection boreholes would overflow, losing dissolved O_3 into the atmosphere.

Table 5.3: Measures (minimum, average, and maximum) of calculated groundwater levels in meters below ground level (mbgl) at the study site between January 2017 and March 2020.

Measure:	**Groundwater level (mbgl):**
Maximum	2.65
Average	4.48
Maximum	6.11

5.3 Step-drawdown test and analysis

To determine borehole yield and drawdown data, step-drawdown tests were performed. Figures 5.4 - 5.6 indicate drawdown versus time curves plotted from the step-drawdown test performed in August 2019 at the Atlantis aquifer. Borehole G30966 indicated in Figure 5.4, 10DNE in Figure 5.5, and 10DSW in Figure 5.6.

From all the observed curves, measured drawdown follows a decreasing trend during pumping and increasing trend during the recovery period (Van Tonder *et al.*, 2001). Figure 5.5 shows a lesser precision in the drawdown curve relative to increasing pumping speeds compared to Figures 5.4 and 5.6. The presence of drilling mud in the subsurface suggests that there was an impact of events other than the pumping. This therefore suggests that drilling mud residue left behind after the construction of borehole 11DNE, a meter away from 10DNE, could have affected its overall drawdown curve trend. The drilling mud consisted of a black particulate matter with a sulphuric odour. It was of a high viscosity and in turn affects the overall flow of groundwater in the subsurface (Nhleko *et al.*, 2020). Observed drawdown in all boreholes, G30966 (Figure 5.4), 10DNE (Figure 5.5), and 10DSW (Figure 5.6) appeared to recover close to the original resting water level (RWL). A loss of 0.03 m, 0.04 m, and 0.02 m from their initial RWL was observed in boreholes G30966, 10DNE, and 10DSW respectively (Figures 5.4 - 5.6).

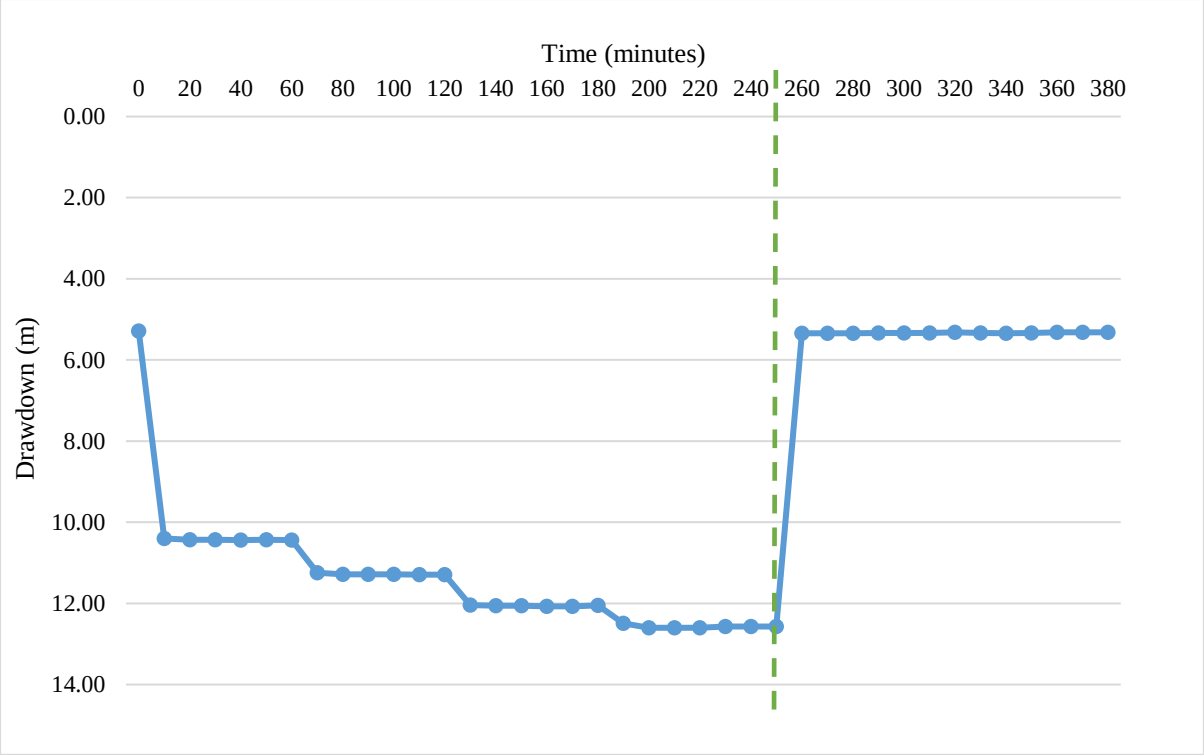

Figure 5.4: Production/pumping borehole (G30966) drawdown (m) versus time graph for the step-drawdown test in Atlantis on the 8th August 2019 indicating measured drawdown taken at 10 minute intervals (•) and separated by the recovery period (- - -). Pumping period was from 0 – 250 min and recovery period from 250 – 380 min.

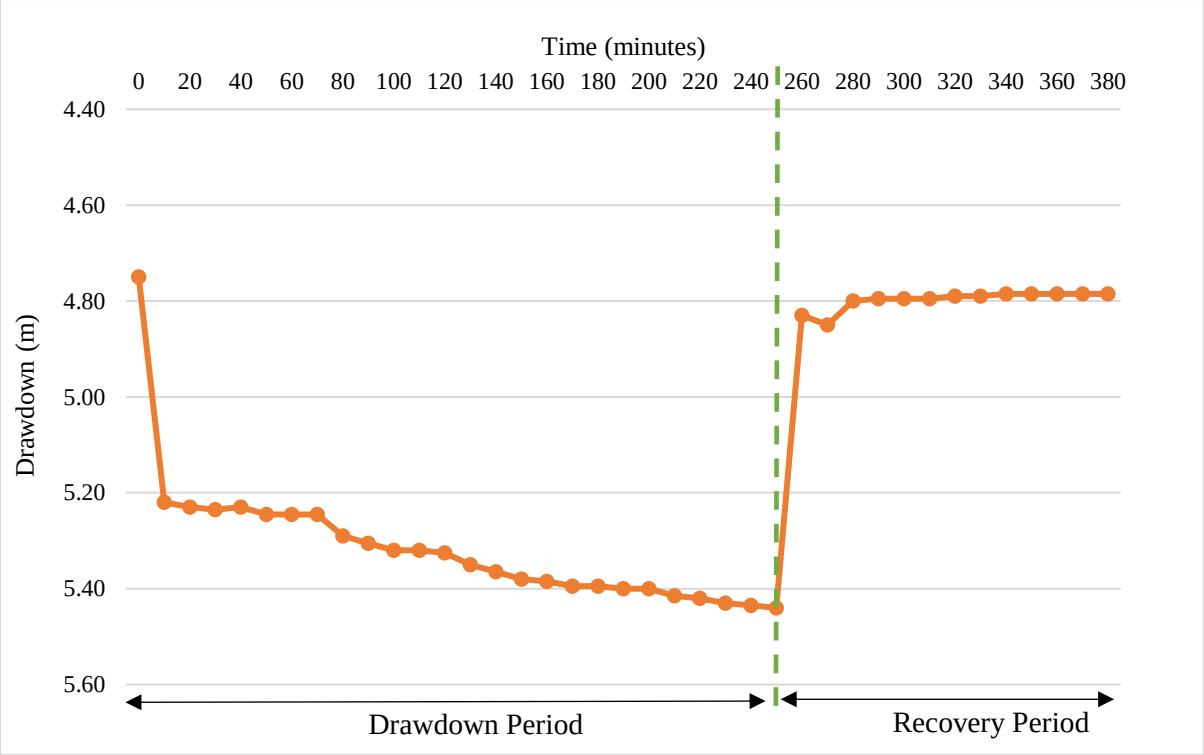

Figure 5.5: Monitoring/observation borehole (10DNE) drawdown (m)versus time graph for the step-drawdown test in Atlantis on the 8th August 2019 indicating measured drawdown taken at 10 minute intervals (•) and separated by the recovery period (- - -). Pumping period was from 0 – 250 min and recovery period from 250 – 380 min.

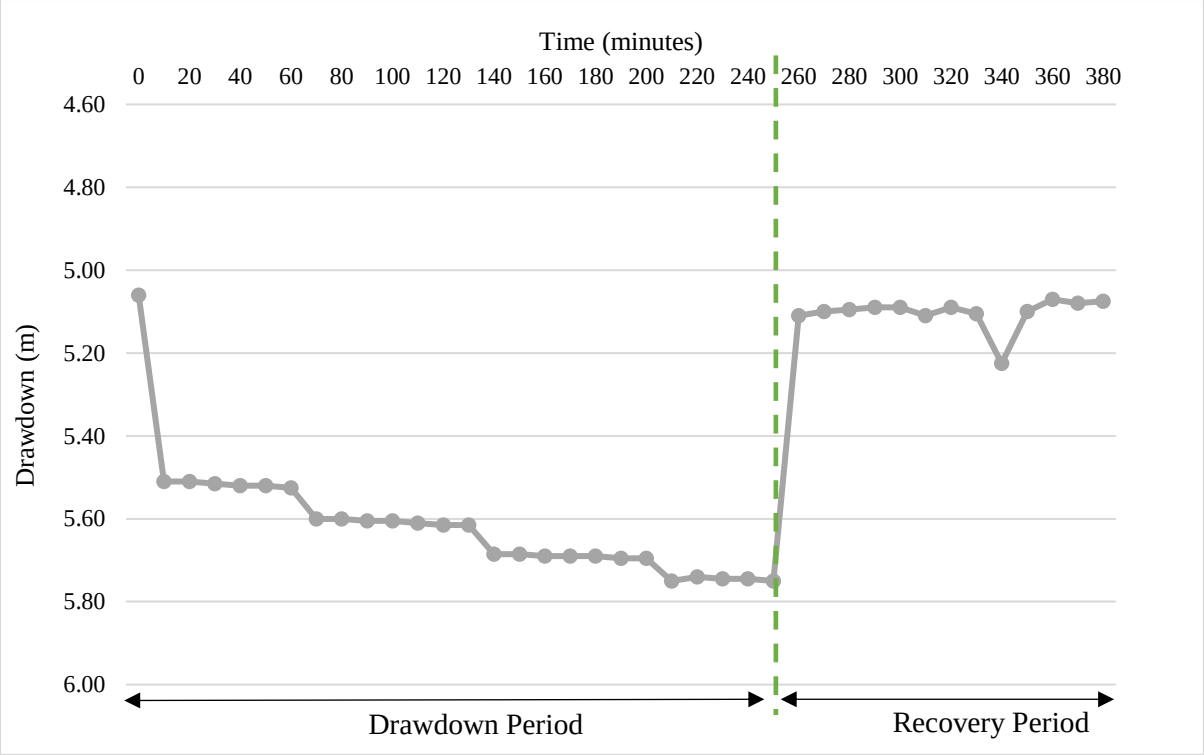

Figure 5.6: Monitoring/observation borehole (10DSW) drawdown (m) versus time graph for the step-drawdown test in Atlantis on the 8th August 2019 indicating measured drawdown taken at 10 minute intervals (•) and separated by the recovery period (- - -). Pumping period was from 0 – 250 min and recovery period from 250 – 380 min.

Historical step-drawdown tests have been performed on production borehole G30966 in 1979, 2000, 2007, 2013, and compared to the most recent step-drawdown test in 2019 demonstrating borehole performance and functionality before the start of O_3 injection. A noted decreasing drawdown with increasing time and abstraction rates was apparent in the most recent step-drawdown test performed on the 8th August 2019. The rapid decreasing trend is a response to borehole pumping, reducing borehole groundwater levels experienced during step-drawdown testing (Figure 5.7) (Driscoll, 1986; Van Tonder *et al.*, 2001). This similar trend was only noted in 1979 after the construction of the borehole which serves as a baseline for comparison for all future step-drawdown test values. The borehole performance in 1979 clearly indicated no signs of borehole clogging, however, the trend in 2019 shows even better borehole performance conditions during increasing pumping rates when compared to 1979 (Figure 5.7). This enhanced borehole performance trend in 2019 can be explained as a result of the abstraction flow rate per step, step duration, and measurement intervals that varies greatly in comparison to the first step-drawdown test in 1979, and the other four historical pump-test data (Table 5.2). Furthermore, the concern over inaccuracies in data collection from all step-drawdown tests

from 1979 to 2019 prevented accurate borehole performance of G30966 to be determined over time.

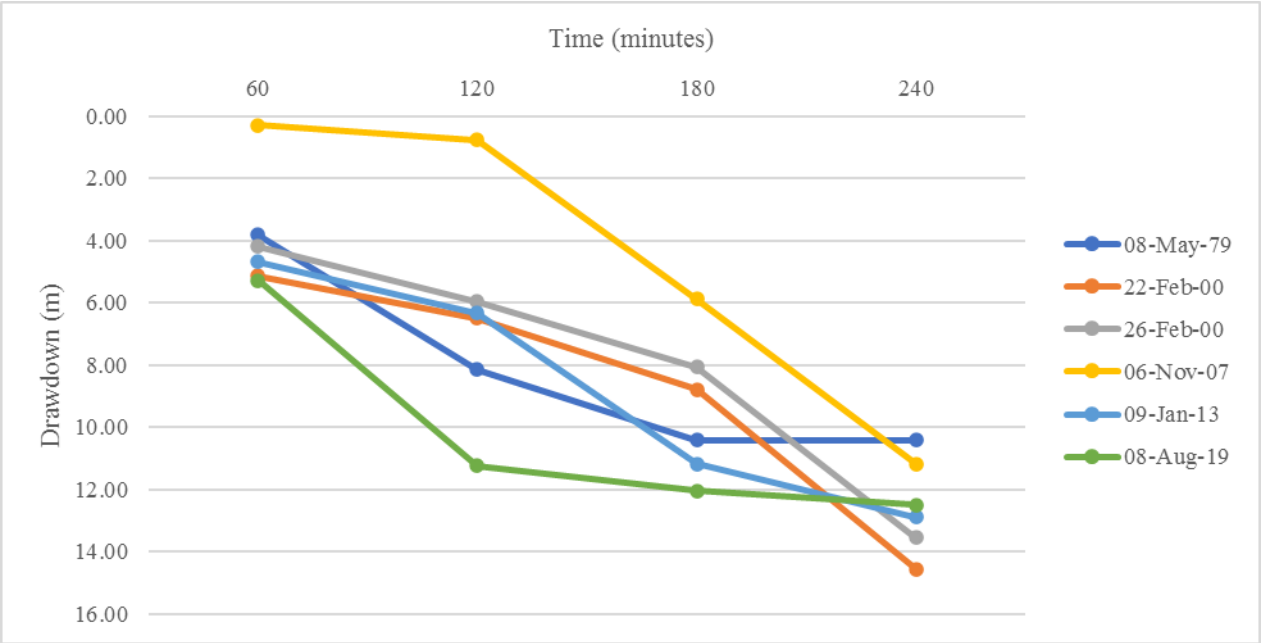

Figure 5.7: Drawdown (m) versus time (minutes) graph for historical and recent step-drawdown tests performed on production borehole G30966 in Atlantis from 1979 to 2019.

Chapter 6: Hydrochemical response to ozonation

6. Introduction

Chapter 6 presents and discusses hydrochemical results obtained before, during and after ozonation using manual field sampling and the telemetry system located at the study site. This chapter addresses the second of the study mentioned in Chapter 1. The second objective focusses on the analysis of hydrochemical parameters spatial and temporal response to ozonation. The intention was to identify when and where hydrochemical changes occurred in the subsurface in response to *in situ* iron remediation (ISIR) technology using ozonation. By identifying the spatial and temporal subsurface hydrochemical changes in response to ozonation, the effectiveness of the ISIR treatment can be determined. The central argument in this chapter is understood by, if favourable spatial and temporal distributions is analysed in the subsurface during ozonation, then ISIR using ozonation could efficiently be implemented.

To achieve the second objective, the collection of baseline (before ozonation) groundwater quality datasets and quantitative field measurements by manual sampling and the telemetry system during and after ozonation was gathered. By analysing the data collected a demonstration on the spatial and temporal effects of ozonation in boreholes can be determined.

6.1 Baseline groundwater quality before ozone (O_3) injection

The production borehole G30966 was not sampled during the first baseline sampling run on the 1st October 2019. However, since the immediate surrounding boreholes to G30966 recorded baseline data, an overall groundwater quality representation for G30966 and the study site can be determined. Field parameters such as pH, electrical conductivity (EC), temperature, dissolved oxygen (DO), and total iron (Fe^T) concentrations collected before the implementation of ISIR treatment are presented in Table 6.1. Baseline manganese data was not measured as suitable reagents for the pre-determined analysis method was not available at the time of baseline monitoring. Implications to unrecorded manganese data includes: The absence of determining and sufficiently concluding manganese-related objections of this study.

Table 6.1: Field parameters of baseline groundwater quality data recorded on the 1st October 2019 in monitoring boreholes (15DSW, 8DSW, 4DNE, 6SNE, 8DNE, and 10DNE), and injection borehole (11DNE) before ozone (O_3) injection. Field parameters measured include sample depths, pH, electrical conductivity (EC), temperature, dissolved oxygen (DO), and total iron (Fe^T) concentrations.

BH ID	15DSW	8DSW	4DNE	6SNE	8DNE	10DNE	11DNE
Date	1 Oct 2019	1 Oct 2019	1 Oct 2019	1 Oct 2019	1 Oct 2019	1 Oct 2019	1 Oct 2019
Sample depth (mbgl)	25	25	22	13	26.5	26	26.5
pH	7.3	7.4	7.3	7.4	7.3	7.2	7.4
EC (µS/cm)	747	688	640	693	651	673	620
Temp (°C)	18.4	18.4	18.7	19.2	18.6	18.7	18.7
DO (mg/L)	0.02	0.01	0.03	0.03	0.03	0.02	0.02
FeT (mg/L)	0.66	0.34	0.54	Bdl	0.78	Bdl	0.42

**Bdl: Below detectable levels*

Drilling mud residue left behind after the construction of borehole 11DNE, a meter away from 10DNE was the initial source affecting groundwater chemistry at the study site. This was determined based on observations at the study site, whereby inaccurate anthropogenic drilling caused chemical behaviour adjustments at the study site. Prior to baseline sampling, monitoring boreholes 10DNE, 8DNE, 6SNE, and 4DNE was pumped to remove as much residual drilling mud, initially observed during groundwater pumping from monitoring borehole 10DNE. A detection of drilling mud in 10DNE initiated further observations and investigations in the downgradient monitoring boreholes 8DNE, 6SNE, 4DNE, and 8DSW to determine the extent of drilling mud interferences at the study site. During the pumping of each monitoring borehole, it was observed that all monitoring boreholes, except 8DSW, possessed variable drilling mud concentrations as noted by the groundwater's distinct colour change ranging from black to grey, and its sulphur odour. In attempt to reduce the existing impacts of drilling mud residue on groundwater chemistry, monitoring boreholes were pumped collaboratively with the injection of highly concentrated doses of ozone (O_3)-rich water using the existing *in situ* iron remediation (ISIR) technology installed at the study site. It is assumed that drilling mud contributed to the increase in organic matter identified as in total organic carbon (TOC).

An increase in TOC concentrations mobilises iron and manganese oxidation rates that causes clogging of production boreholes (Tredoux *et al.,* 2011). A depletion in iron removal efficiencies during a second phase of injection using ozonation has previously been noted by Cromley and O'Connor (1976) in response to organic compound interferences, similarly

identified at the study site due to the presence of drilling mud. The effects of drilling mud on groundwater chemistry has also been identified by Haris *et al.* (2013) who indicates that groundwater contamination by drilling mud seepage occurs during the drilling process and invasion whereby drilling mud enters the underlying porous geological formations. Furthermore, El Araby *et al.* (2009) identified that the presence of carbonate and bicarbonate species reduces the rate of ozone decomposition in water, which affects direct and selective oxidation reactions such as iron and manganese.

Drilling mud is composed of highly in viscous organic compounds, that is expected to interfere with iron and manganese oxidation reactions and groundwater flow in the subsurface (Nhleko *et al.*, 2020). Measures used to remove as much organic material using simultaneous pumping and highly concentrated O_3 injection was deemed successful, as a significant decrease in TOC was observed at the study site (Table 6.2). The pumping of boreholes and injection of O_3-rich water contributed to the oxidation of the drilling mud and partial organic matter in that particular area of the aquifer (Nhleko *et al.*, 2020). The decrease in TOC measurements is supported by comparable previous natural TOC concentrations measured by Bugan *et al.* (2018). The decreasing TOC trend compares favourably to Cromley and O'Connor (1976) who explains that organic compounds are destroyed in the presence of O_3 injection. However, it is suggested that drilling mud residue is still lodged in the aquifer matrix, predominantly above and below the screen depth where groundwater flow is minimal. In light of these suggestions, it is clear that groundwater flow is enhanced at screen depths in monitoring and injection boreholes where the injection of O_3 occurred to remove drilling mud residue.

Table 6.2: Total organic carbon (TOC) (mg/L) spatial concentrations in monitoring boreholes 10DNE, 4DNE, and 8DSW at the Atlantis study site. Total organic carbon concentrations measured in ppm for sampled dates on the 29th October and 1st, and 5th November 2019.

Sample Date:	**10DNE** (mg/L)	**4DNE** (mg/L)	**8DSW** (mg/L)
29/10/2019	15.4	15.7	5.1
01/11/2019	12.5	3	4.9
05/11/2019	6.6	3.4	4.2

Distances of boreholes 10DNE, 4DNE, and 8DSW are 10 m, 4 m, and 8 m respectively apart from the production borehole G30966. 10DNE and 4DNE is upgradient to G30966, and 8DSW downgradient to G30966. Natural TOC concentrations in the aquifer has previously been tested

and measured between 6 and 7 mg/L (Bugan *et al*, 2018). Initial high TOC levels measuring 15.4 and 15.7 mg/L is indicated in boreholes 10DNE and 4DNE, which are the closest boreholes to the drilling mud source. This increase in TOC demonstrates the effect of drilling mud on groundwater chemistry at the study site. High TOC concentrations affects the rate of oxidation and sorption processes that affect the removal of iron and manganese in the subsurface (Robey, 2014). A rapid response in 4DNE was noted from 29/10/2019 to 01/11/2019, decreasing TOC concentrations by 12.7 mg/L in response to O_3 injection and borehole pumping. Thereafter, a consistent decreasing trend continued in 4DNE on the 05/11/2019, which indicates technique success coupled with a prompt response rate to reduce the prolonged presence of drilling mud residue in 4DNE, as noted more apparent in 10DNE. Natural and consistent TOC levels are indicated in 8DSW positioned the furthest and downgradient to the drilling mud source, ultimately indicating the slow response rate of groundwater flow and subsurface organic matter migration.

6.2 Hydrogeochemical conceptual model of the study site

The baseline field parameters served as a simple and easy technique to provide the concept of possible clogging conditions and the suitability of groundwater conditions for ISIR treatment at the study site. A cross-sectional view of the study site was exaggerated to interpret the full effect of all monitoring boreholes, the production borehole, and the injection borehole. This concept is derived from the study of Braester and Martinell (1988), to allow for the redox gradient to expand and distribute iron and manganese concentrations throughout the oxygenated and precipitation zone around the production well. A clear visual effect, the procedure from groundwater extraction to O_3 injection, is represented through Figure 6.1. Figure 6.2 provides a conceptual model based on the cross-sectional view in Figure 6.1. This conceptual model gives an idea of the subsurface site-specific conditions of the Atlantis aquifer during O_3 injection.

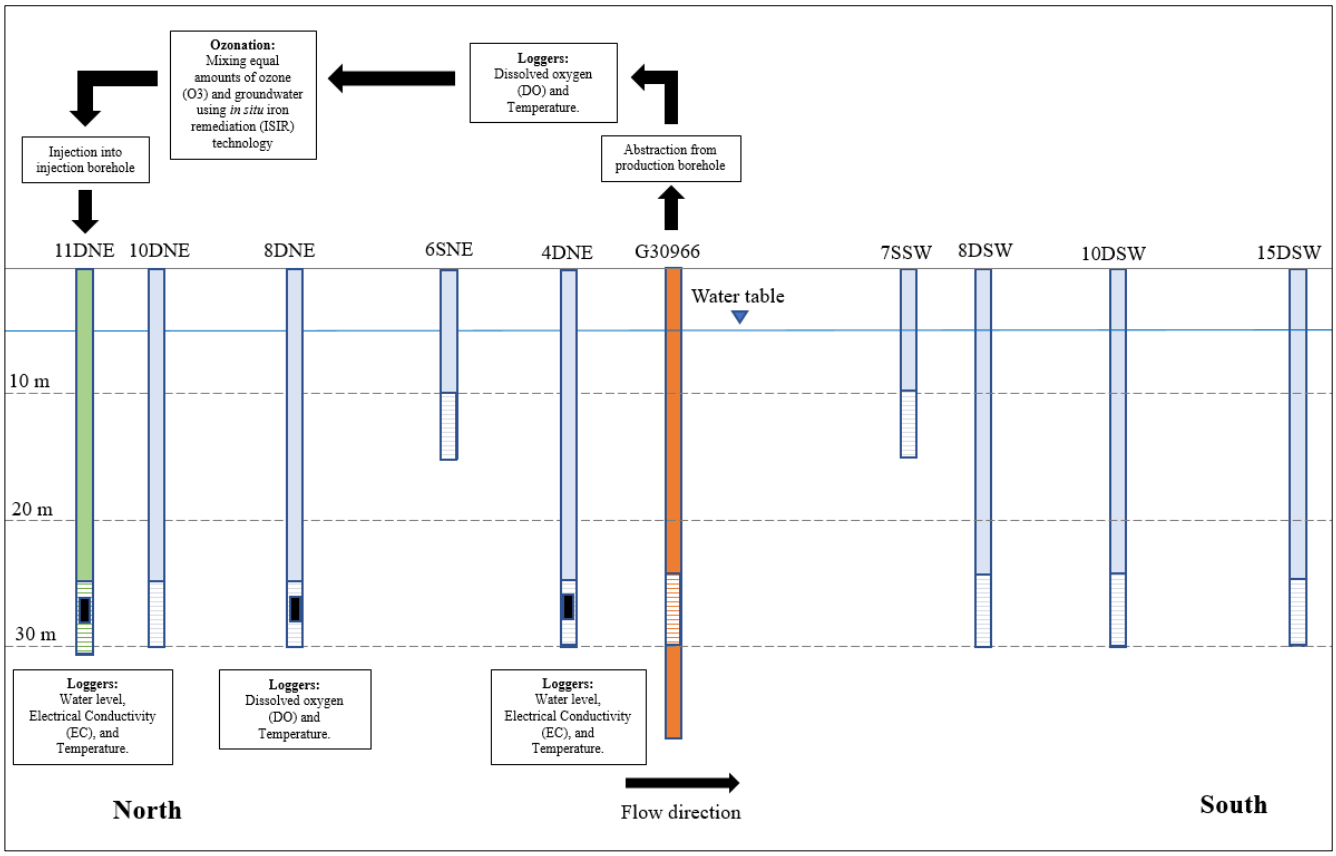

Figure 6.1: Cross-sectional view of production, injection, and monitoring boreholes at the study site in Atlantis. Included are the production (G30966), injection (11DNE) and monitoring boreholes (10DNE, 8DNE, 6SNE, 4DNE, 7SSW, 8DSW, 10DSW and 15DSW), borehole loggers (in 4DNE, 8DNE, and 11DNE), flow direction (from north to south), borehole depths and water table on the 1st October 2019. Treatment at the study site involves water abstraction from G30966, ozonation, detection of dissolved oxygen (DO) and flow (before and after) ozonation, followed by injection of ozonated water into 11DNE.

A conceptual geochemical model was developed to simulate the representation of subsurface chemical reactions and physical processes during O_3 injection. These reactions and processes determines the effects of groundwater chemistry variations likely to occur. This theoretical and physical concept compares favourably to that of Braester and Martinell (1988). The conceptual model reveals that the local groundwater flow follows the surface topographic pattern at the study site, where flow is from high elevated areas to low elevated areas. The conceptual model also indicates that ozonated water reaches the deep monitoring boreholes 10DNE, 8DNE, 4DNE, and the production borehole (G30966) progressively (Figure 6.2).

Ozone as the source oxidant in the aquifer will first oxidize into dissolved oxygen (DO) and hydroxyl radicals (OH^-) consuming most of the energy during this reaction. Hydroxyl radicals enhance oxidation processes, but given their short half-life of microseconds, the higher DO

concentrations can be considered as the dominant oxidation source (Robey, 2014). Organic carbon oxidizes to carbon dioxide (CO_2), alternatively decreasing organic matter, pH, and DO and increasing alkalinity in response to increasing CO_2. Hydrogen sulphide (H_2S) oxidizes to sulphate allowing increased sulphate and ferrous iron (Fe^{2+}) concentrations, and decreasing H_2S and DO levels. Ammonium (NH_4^+) oxidizes to nitrate (NO_3^-), which also decreases DO and increases NO_3^- concentrations in the aquifer. The mobilisation of iron and manganese in groundwater occurs in the absence of sulphide or carbonate ions and under reducing or low pH levels (Nhleko *et al.*, 2020). However, pH levels will increase during O_3 injection.

The injection of ozonated water into injection borehole (11DNE) aims to establish an oxidation zone and redox gradient around the borehole. The increased injection of treated ozonated water from the production borehole into 11DNE initiates chemical reactions and establishes oxidation zones, which are expressed through increasing periods (T1, T2, T3, and T4) in the conceptual model (Figure 6.2). A series of chemical reactions occurs within the oxidizing environment along with subsequent changes in groundwater chemistry. The oxidation zone allows for soluble Fe^{2+} and manganese (Mn^{2+}) to oxidize into its insoluble state of ferric iron (Fe^{3+}) and manganese (Mn^{4+}). As a result, dissolved iron and manganese concentrations in groundwater decreases, and increased iron and manganese precipitates form as ferric hydroxide [$Fe(OH)_3$] and manganese oxide (MnO_2) respectively. This is the initial goal reaction of injecting ozonated water. Decreasing soluble iron and manganese concentrations will prevent the oxidation process of these elements to occur within boreholes, which ultimately facilitates iron- and manganese-related borehole clogging. The DO level decreases in response to the formation of precipitated forms of insoluble iron and manganese. Iron oxidation conditions are decreased during complex formations with silica, phosphate, or dissolved organic carbon (DOC) (Nhleko *et al.*, 2020). Alternatively, higher pH levels or microbial activity will increase manganese conditions (Robey, 2014; Nhleko *et al.*, 2020).

Dissolved oxygen initially reacts with organic carbon present in the aquifer, reducing iron oxidation conditions. The introduction of organic carbon in response to drilling mud lodged within the aquifer will therefore consume majority of DO before other subsurface reactions can occur. However, if the groundwater flow rate within the subsurface is faster than the reaction rate of DO and organic carbon, the downward migration of DO can still effectively contribute to iron oxidation before organic carbon is completely reacted. It is unlikely for iron sulphide (FeS) or H_2S reactions with DO to occur before the removal of the majority of organic carbons. The conceptual model considers the introduction of organics from the drilling mud observed

in the aquifer. The introduction of drilling mud into the aquifer places the system in a highly reduced state during its decomposition process. Its decomposing conditions in the aquifer reduces sulphate to sulphide which precipitates with iron or hydrogen to form FeS or H_2S respectively. This reaction allows for Fe^{2+} concentrations to increase as FeS or H_2S which is oxidized, requiring sufficient DO to initiate the oxidation reaction. Thereafter, decreased Fe^{2+} concentrations will occur as a consequence of oxidation. After the completion of organic carbon, FeS, and H_2S reactions, the principal reaction of iron and manganese oxidation occurs. This reaction takes place within the aquifer zone between the injection and production boreholes, which is demonstrated by T4 in Figure 6.2 and is expressed as the reaction responsible for preventing borehole clogging.

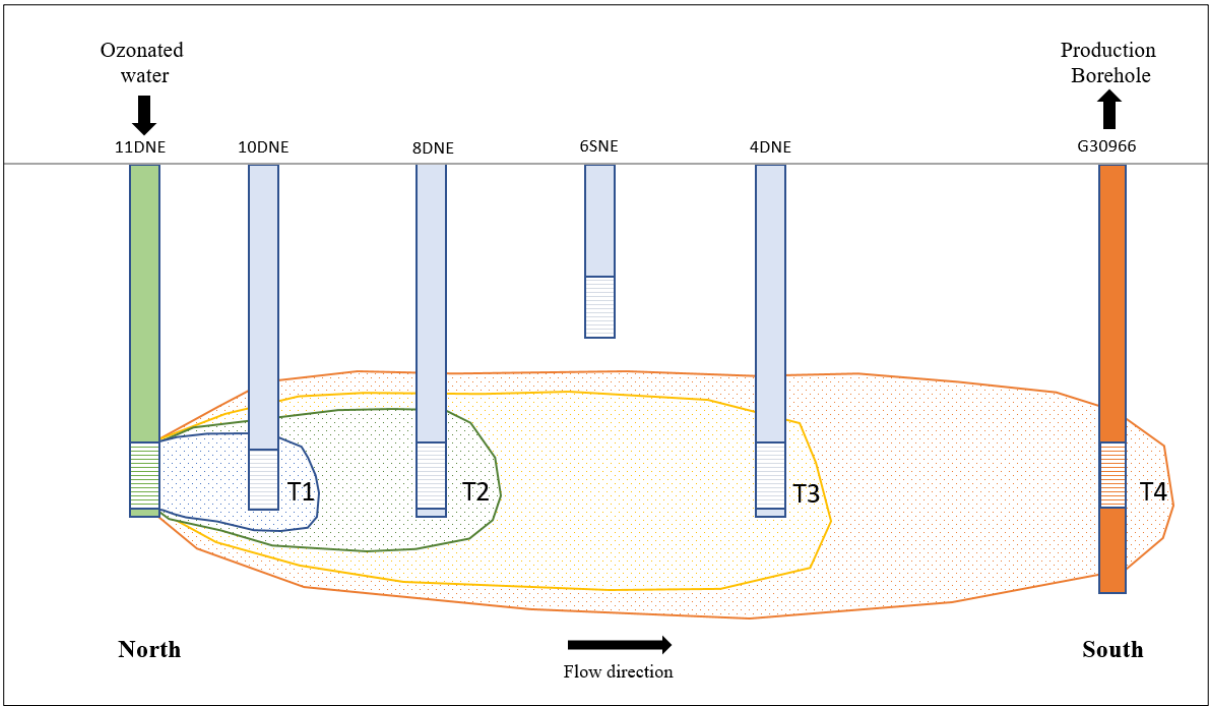

Figure 6.2: Conceptual model of the site-specific conditions between injection (11DNE), production (G30966), and monitoring boreholes (10DNE, 8DNE, 6SNE, and 4DNE) at the Atlantis study site during ozone (O_3) injection following the flow direction from north to south. Reaction and oxidation zones occur progressively between periods (expressed as T1, T2, T3, and T4). The expectation is for reaction and oxidation zones to extend from T1 up until T4.

6.3 Monitoring groundwater quality during ozone (O_3) injection

6.3.1 pH levels during ozone (O_3) injection

pH dependency has been associated with altered oxidation rates of Fe^{2+} (Walter, 1997; Ellis *et al.*, 2000; Lefevre *et al.*, 2016). Favourable groundwater conditions promote the vulnerability of soluble iron and manganese between pH ranges of 5.5 and 8.2 (Ahmad, 2012; Robey, 2014). Ideal monitoring conditions for O_3-based reactions include pH ranges between 7.0 and 8.5 because a pH greater than 10 or high alkalinity promotes the decomposition of O_3 into OH^- ions (EPA, 1999; Nimmer *et al.*, 2000; El Araby *et al*., 2009). The oxidation of Fe^{2+} usually occurs during pH levels greater than 6, within the ranges of 7 and 8, while Mn^{2+} oxidation occurs at pH levels greater than 8 (Robey, 2014). Although Figure 6.3 does not indicate pH levels favourable for Mn^{2+} oxidation, favourable pH levels for Fe^{2+} oxidation is shown in monitoring (10DNE, 8DNE, 6SNE, and 4DNE) and production boreholes (G30966). pH levels generally displayed an increasing response during ISIR with O_3 (Robey, 2014). Findings of the progressive pH monitoring during O_3 injection are presented in Figure 6.3.

There is an overall increasing pH relationship in 10DNE, 8DNE, and 6SNE, which is positioned closest to the injection borehole 11DNE, during O_3 injection. These high pH levels could perhaps contribute to suitable subsurface conditions for iron and manganese oxidation. This idea compares favourably to Walter (1997) and Alıcılar *et al.* (2008) who explains that high pH levels promotes beneficial conditions for iron and manganese oxidation rates. It further supports the study from Robey (2014) who mentions that pH ranges between 7 and 8 are most suitable for iron oxidation (Figure 6.3). The most variable pH levels are noted in 4DNE, which is the furthest monitoring borehole positioned at a 7 m distance from 11DNE. Therefore, pH levels in 4DNE could be indicating subsurface responses due to inconsistent O_3 injection rates more apparently, as a consequence of the 7 m distance from 11DNE. G30966 shows the least variability in pH in response to progressive O_3 injection and could perhaps represent the most natural subsurface pH conditions amongst the monitored boreholes. Consistent natural pH levels in G30966 could possibly suggest inadequate O_3 responses in the subsurface within the injection period from October 2019 to March 2020. In the presence of oxygen and high pH conditions, Fe^{2+} and Mn^{2+} are oxidized to Fe^{3+} and Mn^{4+} respectively (Homoncik *et al.*, 2010). Therefore, DO is a contributing factor to determine the efficient oxidation of Fe^{2+} and Mn^{2+}, which is discussed in Figure 6.4.

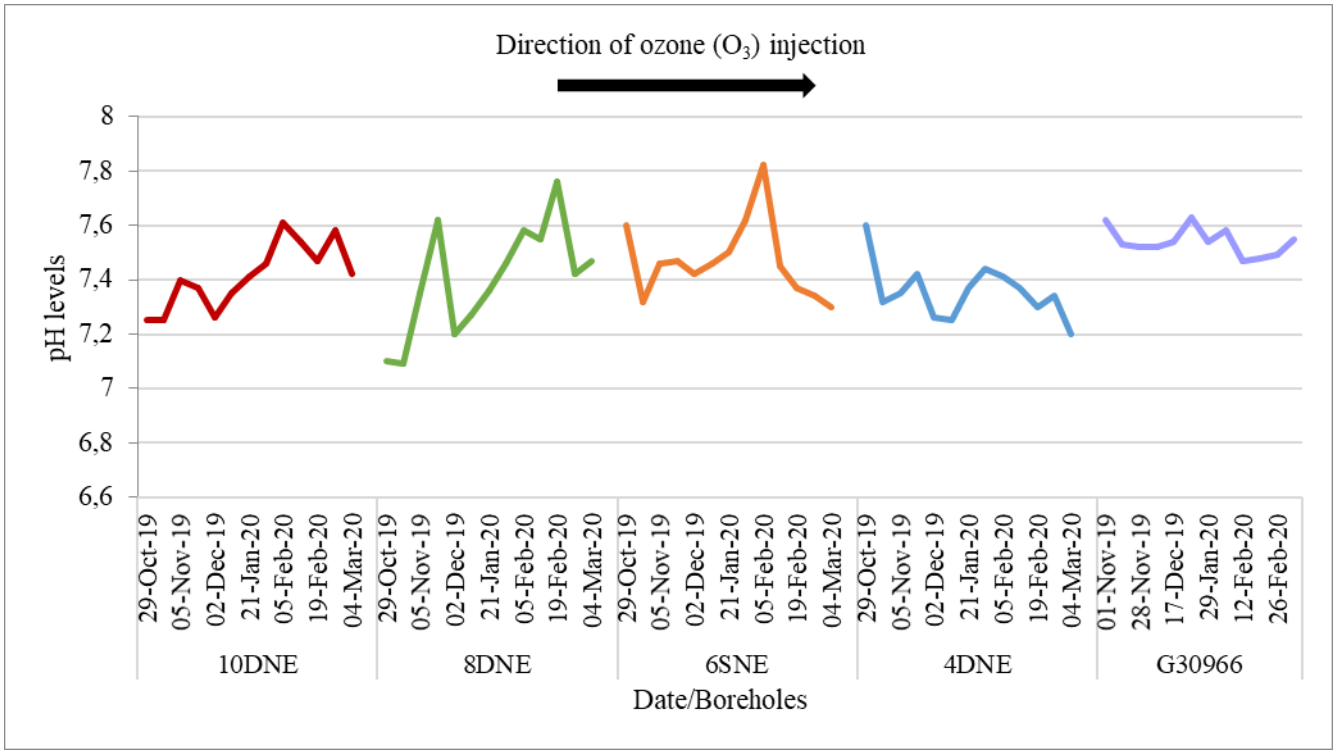

Figure 6.3: Monitored pH levels during ozone (O_3) injection in monitoring (10DNE, 8DNE, 6SNE, and 4DNE) and production borehole (G30966) from October 2019 to March 2020.

6.3.2 Dissolved oxygen (DO) concentrations during ozone (O_3) injection

Oxidation is highly dependent on DO (Braester and Martinel, 1988). Increasing DO concentrations accelerates oxidation reaction times of iron and manganese (Filtronics, 1993; Vance, 1994). Ozone would also result in higher DO concentrations to enhance DOC and iron and manganese oxidation (Rice, 2002). Dissolved oxygen concentrations during oxygen gas dosing have been recorded to yield concentrations at 20 – 30 mg/L (Diliūnas, 2006). ISIR methods are dependent on available DO concentrations in the injected water to promote chemical reactions with dissolved iron and manganese. Groundwater pH in the aquifer is an additional factor that dictates the rates of oxidation and removal efficiency of iron and manganese (Robey, 2014). Using O_3 as a suitable oxidant in ISIR treatment of organic-rich groundwater treatment, suitable DO concentrations between 15 and 30 mg/L should be achieved for successful removal rates (Robey, 2014). The presence of drilling mud is problematic with the injection of O_3, as O_3 is highly reactive with H_2S, increasing DO concentrations in the subsurface. Due to its remaining residue at the study site, the recommended DO concentrations between 15 to 30 mg/L to treat organic-rich groundwater as suggested by Robey (2014) should be considered. Elevated iron levels and low DO

concentrations are associated effects related to iron-related well-screen encrustation (Walter, 1997).

The results show that DO concentrations have fluctuated considerably over time, with a repeated increasing and subsequent decreasing trend in all boreholes. Considering the deepest monitoring boreholes (10DNE, 8DNE, and 4DNE), these boreholes represent the most comparable subsurface conditions relative to DO concentrations during O_3 injection. However, the closest boreholes (10DNE and 8DNE) from injection borehole (11DNE) indicates the highest and an increasing trend in DO concentrations. This reveals the rapid response in DO concentrations relative to O_3 injection, favourable to iron and/or manganese oxidation. However, when compared to 4DNE, lower DO concentrations with a similar increasing trend is apparent (Figure 6.4). The noted decrease in DO concentrations occurred from the 5th November to 28th November 2019, as a consequence of lowered O_3 injection which adjusted the response rates of oxidation reactions of Fe^{2+} and Mn^{2+} (Figure 6.4). After the change in injection rates, a consistent monitoring period with an increasing trend is noted from the 2nd December 2019 to 5th February 2020.

Dissolved oxygen concentrations between 14 and 20 mg/L and possibly higher was achieved in 10DNE and 8DNE, which was suitable conditions for iron and manganese oxidation from the 2nd December 2019 up until after the 5th February 2020. These observed DO concentrations compares favourably to Diliūnas *et al.* (2006) whereby the groundwater dosing of oxygen gas maintained concentrations at 20 – 30 mg/L. Dissolved oxygen concentrations are observed to decrease from 11DNE towards the production borehole G30966. This could possibly mean that iron and manganese oxidation was not prominent enough to use the available DO present in the subsurface. The decreasing DO concentration response to O_3 injection in 4DNE returned to suitable conditions for oxidation only from the 17th December 2019, measuring between 3 and 7 mg/L (Figure 6.4). The DO concentrations in G30966 range between 1.9 and 6.8 mg/L. The DO concentrations measured during manual field sampling was unable to compare to natural subsurface conditions for DO concentrations at the study site generally measured as 0.2 mg/L in untreated groundwater, and compared with data retrieved from Robey (2014). Although DO fluctuations was apparent in G30966 during unstable O_3 injections between October 2019 to March 2020, total iron concentrations (Figure 6.8) indicates little to no effect on iron oxidation rates measured in G30966. Therefore, there is a possibility that DO measurements in G30966 does not demonstrate sufficient oxidation conditions for iron and manganese. Alternatively, there is a likelihood that O_3 escaped through the borehole casing or

via borehole foaming in the form of effervescing, contributing to the inconsistent DO concentrations before reaching G30966 (Walker and Mallants, 2014). Manual field sampling of DO concentrations indicates that O_3 was unable to reach G30966 to efficiently initiate iron and manganese oxidation. The unstable injection rates in 11DNE best describe the fluctuating DO concentrations measured in the subsurface of monitoring and production boreholes.

Shallow monitoring borehole (6SNE) represents the least variability in DO concentrations relative to O_3 injection. It is noted that 6SNE represents natural subsurface DO concentrations, represented by low concentrations from the 1st October 2019 to the 29th January 2020 during O_3 injection. Higher DO concentrations are noted during minimal or no O_3 injection from 5th February to 4th March 2020, representing a decreasing response to injection in the subsurface (Figure 6.4). A general low DO concentration in 6SNE, between 0.2 and 7.8 mg/L, could possibly suggest that less organic matter was present in the shallow borehole's groundwater. Therefore, this reveals that organic matter from the drilling mud, located in deep monitoring boreholes, was unable to penetrate the shallow borehole at a depth of 15 m. However, the graph of DO shows a general trend observing expected outcomes.

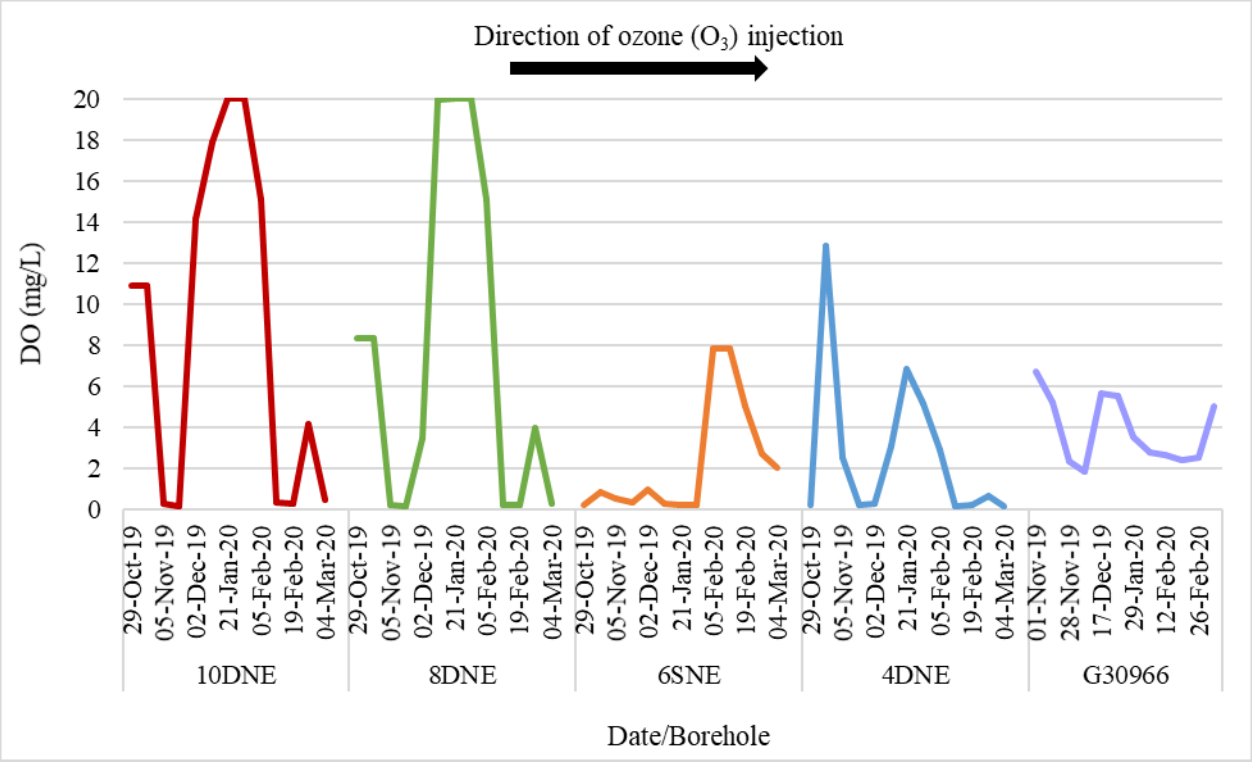

Figure 6.4: Monitored dissolved oxygen (DO) concentrations (mg/L) during ozone (O_3) injection in monitoring (10DNE, 8DNE, 6SNE, and 4DNE) and production borehole (G30966) from October 2019 to March 2020.

6.3.3 Electrical conductivity (EC) during ozone (O_3) injection

Electrical conductivity is regarded as an aesthetic determinant for groundwater quality. According to the Department of Water Affairs and Forestry (DWAF), groundwater quality suitability for EC has been classified as "Suitable" for domestic use set at EC levels smaller than 700 µS/cm, and between 700 – 1600 µS/cm for the classification of a "Suitable, slightly salty taste" for domestic use (Meyer, 2001). Apart from EC's aesthetic determinant it has the ability to pass an electrical current, this provides an understanding of what is dissolved in water (Tutmez *et al.*, 2006). Conductivity in water is affected by the presence of inorganic dissolved solids such as iron, which can conduct electrical current very well, therefore having a high conductivity in water. Conductivity is also affected by temperature, the warmer the water, the higher the conductivity (EPA, 2012).

Electrical conductivity values before O_3 injection were measured in monitoring boreholes under natural subsurface conditions on the 1st October 2019 (Table 6.1). Electrical conductivity values in monitoring boreholes 10DNE, 8DNE, 6SNE, and 4DNE measured 673, 651, 693, and 640 µS/cm respectively (Table 6.1). Electrical conductivity mean values calculated increased slightly by either 20 or 30 µS/cm during O_3 injection (Table 6.4). Mean EC values in 10DNE, 8DNE, 6SNE, and 4DNE were calculated at 700, 687, 710, and 666 µS/cm respectively (Table 6.4).

10DNE and 8DNE closest to injection borehole 11DNE indicated a similar trend in EC values in response to O_3 injection conditions (Figure 6.5). Both 10DNE and 8DNE trend lines displayed slightly increasing initial EC values by roughly 30 µS/cm during O_3 injection. Similarly, the trend in 4DNE with lower EC values indicates a delayed response as a consequence of its 7 m distance from 11DNE (Figure 6.5). The distance between 11DNE and 4DNE provides clarity on the overall delayed response due to subsurface migration in primary aquifer conditions during O_3 injection (Figure 6.5). The lower EC values in 4DNE shows that more subsurface EC reactions occur closer to 11DNE, and is prompted by marginally higher values measured in 10DNE and 8DNE. The slight increase in EC values corresponds to higher temperatures (Figure 6.6) recorded in these boreholes. This result compares favourably to EPA (2012) that mentioned conductivity increases at higher temperatures, stimulating electrical current through groundwater. Although a slight indication of increased EC values was noted, this results compares favourably to the studies of Bhatta *et al.* (2015) and Abbasi *et al.* (2020) who indicated that EC values did not significantly change after the introduction of O_3.

The most variability in EC values are observed in 6SNE and could therefore be due to its shallow borehole characteristics. This could be influenced by atmospheric conditions and inorganic dissolved solids which would much easily influence electrical current and salinity concentrations. However, G30966 shows the least variability in EC values which is positioned the furthest from 11DNE (Figure 6.5). Although these EC concentrations do not reveal natural subsurface conditions, it could suggest that the effects of O_3 was unable to reach G30966 in response to unstable injection rates throughout the injection period from October 2019 to March 2020.

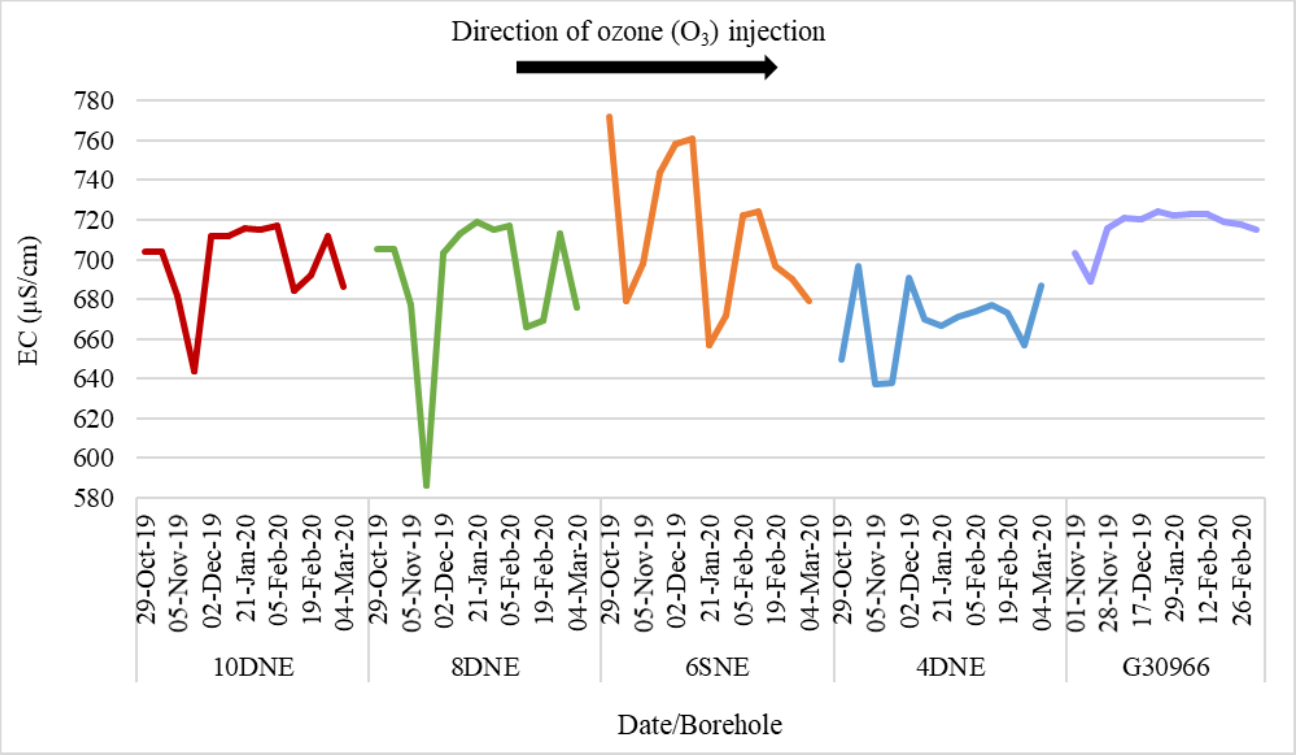

Figure 6.5: Monitored electrical conductivity (EC) (µS/cm) during ozone (O_3) injection in monitoring (10DNE, 8DNE, 6SNE, and 4DNE) and production borehole (G30966) from October 2019 to March 2020.

6.3.4 Temperature during ozone (O_3) injection

The rate of iron oxidation presents effects between temperatures of 5 to 35 °C (Walter, 1997; Smith, 2006). Iron and manganese oxidation rates accelerate at higher water temperatures and decelerate at lower water temperatures (Filtronics, 1993; Vance, 1994).

An overall increasing and subsequent decreasing trend in temperature during O_3 injection was observed in monitoring boreholes 10DNE, 8DNE, and 4DNE (Figure 6.6). This can be explained by O_3 injections rates that affect temperatures as an indication of oxidation reactions in the subsurface. The increasing trend illustrates the rate of subsurface change in response to O_3 injection and oxidation reactions. On the contrary, the decreasing trend illustrates the return to natural subsurface conditions in response to less or no O_3 injection and insufficient oxidation reactions to change the water temperature. 6SNE represents an increasing fluctuation in temperatures (Figure 6.6). This trend in subsurface temperatures is best explained by daily temperature responses experienced closer to the surface. An overall increasing trend and subsequent decreasing trend is observed in G30966 of monitored temperatures during O_3 injection (Figure 6.6). The overall mean temperature of 19.18 °C during O_3 injection (Table 6.6) remains consistent throughout the O_3 injection period (Figure 6.6). This result has also been observed in the studies of EPA (1999), Nimmer *et al.* (2000), and El Araby *et al.* (2009) who mentions that ideal O_3-based reactions are dependent on water temperatures between 15 and 20 °C to promote the decomposition of O_3, stimulating suitable iron oxidation rates. This reveals that G30966 received the least or no effects during O_3 injection. This stable temperature therefore suggests that oxidation reactions in response to O_3 injection were unable to reach G30966 within the injection period from October 2019 to March 2020. Furthermore, the subsurface migration in primary aquifer conditions during O_3 injection is not sufficient to reach G30966 at an 11 m distance from 11DNE within the injection period.

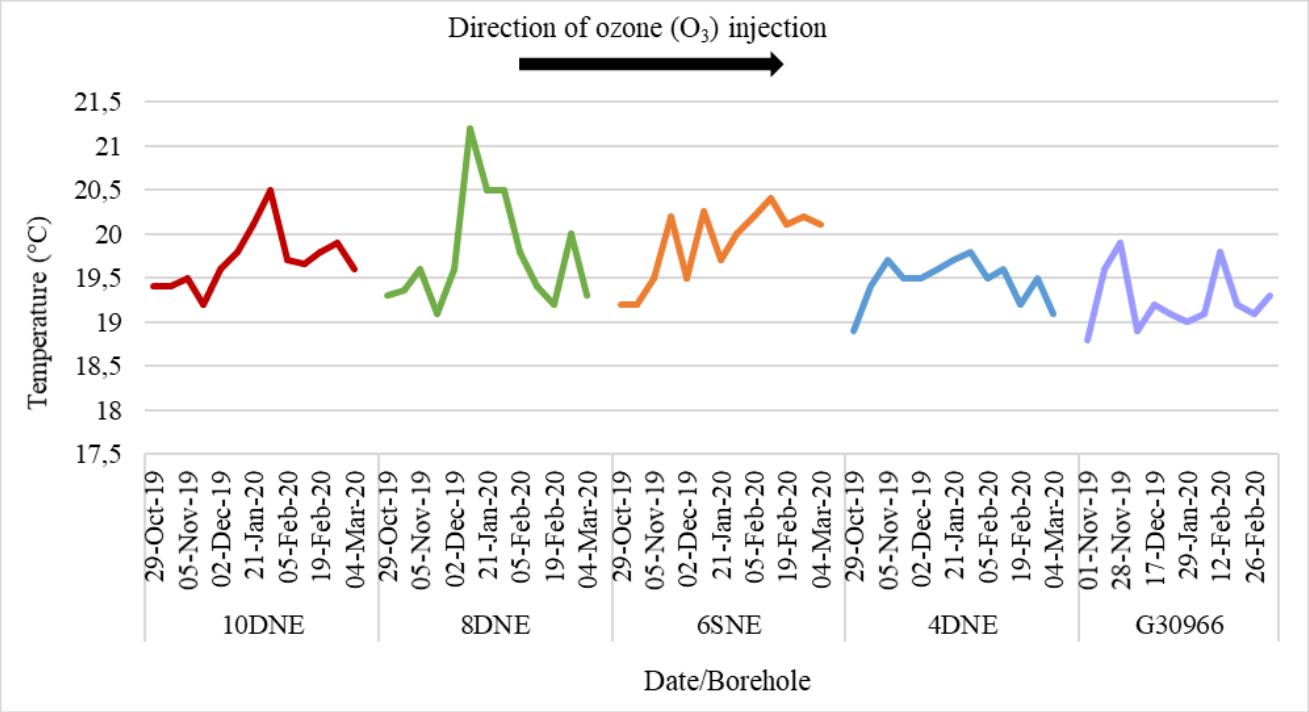

Figure 6.6: Monitored temperature (°C) during ozone (O_3) injection in monitoring (10DNE, 8DNE, 6SNE, and 4DNE) and production borehole (G30966) from October 2019 to March 2020.

6.3.5 Dissolved (Fe^{2+}) and total iron (Fe^{T}) concentrations during ozone (O_3) injection

Monitored field parameters (pH, DO, EC, and temperature) during O_3 injection were collected on-site to provide indications that oxidation zones are present in the subsurface and that iron oxidation would be achievable. Accurate dissolved and total iron concentration determinants require specific analysis approaches since atmospheric exposure affects iron species (Nhleko *et al.*, 2020). The dedicated and most advised approach of iron analysis was considered during this project, involving on-site iron analysis immediately after purging of boreholes, considering the effects of atmospheric exposure (Robey, 2014).

Dissolved iron concentrations in each borehole throughout the injection period indicate great fluctuations. Below detectable limits were observed on several occasions amongst boreholes 10DNE and 8DNE, positioned the closest to injection borehole 11DNE (Figure 6.7) (Nhleko *et al.*, 2020). This could suggest that the oxidation of iron promotes favourable reducing conditions in the presence of O_3 injection. This result supports the theoretical concept derived by Cromley and O'Connor (1976) who mentions that decreasing oxidation of Fe^{2+} concentrations were performed at faster rates and more extensively when using ozonation. They further consider the preference of ozonation which holds promising results in terms of

effective iron removal from groundwater sources. However, concentrations in 4DNE and production borehole G30966 indicated a general increasing trend, that is best explained as a consequence of oxidation of iron sulphides releasing Fe^{2+} (Figure 6.7) (Nhleko *et al.*, 2020). This explanation is supported by Cromley and O'Connor (1976) who further mentions that incomplete organic compound destruction, can result in these compounds to possess aggressive traits during oxidation by forming additional organic compounds, generating additional iron removal interferences in groundwater. Dissolved iron concentrations in 6SNE illustrates the least response to O_3 injection (Figure 6.7), possibly due to its shallow borehole characteristics that reduces the ability of oxidation zones to develop across the shallow subsurface area. This is supported by the hydrogeochemical conceptual model theory (Figure 6.2).

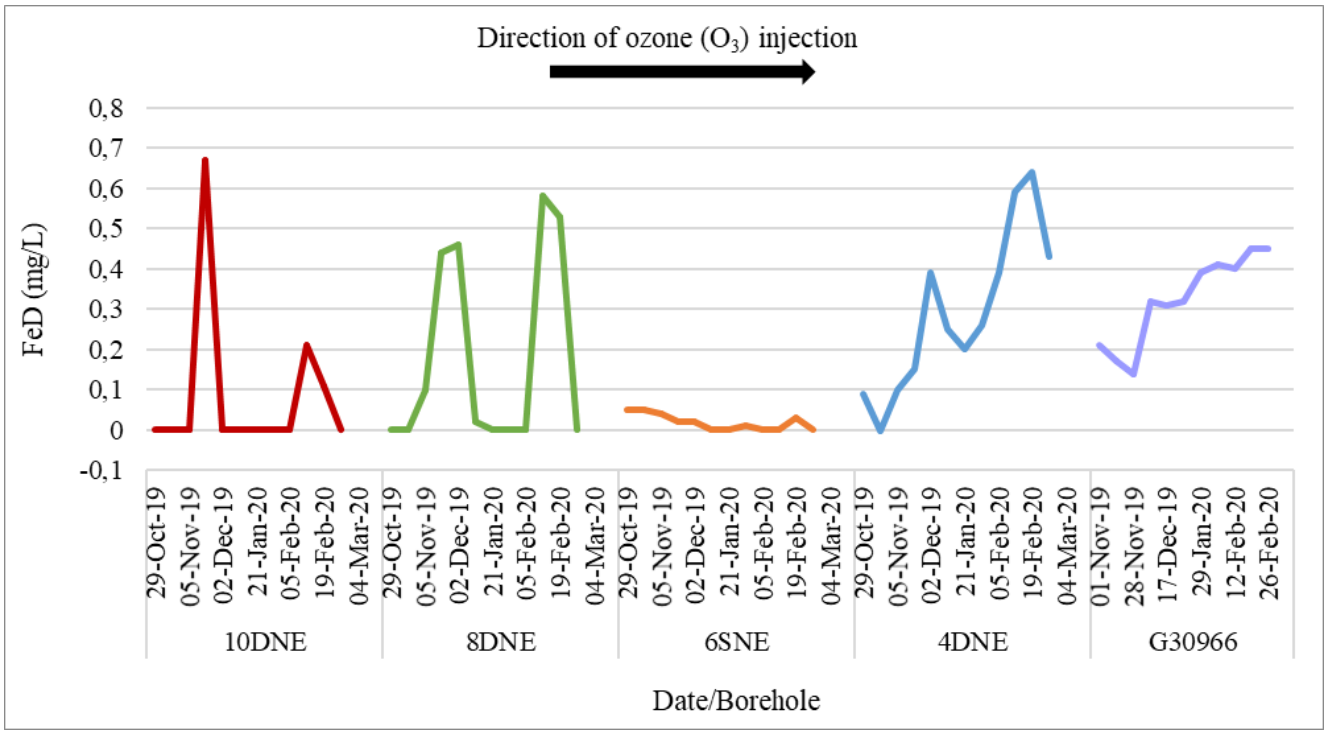

Figure 6.7: Monitored dissolved iron (mg/L) during ozone (O_3) injection in monitoring (10DNE, 8DNE, 6SNE, and 4DNE) and production borehole (G30966) from October 2019 to March 2020.

Total iron concentrations have fluctuated considerably over time. However, from December 2019 onwards Fe^T yielded consistent results, demonstrating less fluctuations. The most significant trend is noted in Fe^T concentrations at G30966 which remained at approximately 0.2 mg/L throughout the injection period. Monitoring borehole 8DSW downgradient to

G30966 demonstrated similar Fe^T concentrations to G30966, measuring < 0.2 mg/L (Figure 6.8, data not visible). This could possibly indicate natural subsurface conditions as comparative concentrations were measured during baseline sampling of these boreholes. Concentrations in 10DNE and 8DNE were much lower in comparison to 4DNE and G30966 (Figure 6.8). Although a lower concentration trend demonstrates direct effects of oxidation reactions in the subsurface, the reliability of the Fe^T concentration is questionable. This is explained by many of the Fe^T concentrations being lower than the dissolved iron concentrations, particularly in 4DNE and G30966 (Figure 6.8) (Nhleko *et al.*, 2020).

It is presumed that an interference removed by filtering of groundwater before dissolved iron analysis resulted in higher dissolved iron concentrations than Fe^T concentrations. This compromises chemical reactions and general trends expressed by probable observations from the hydrogeochemical conceptual model (Figure 6.2). Despite attempts to reduce the risk of exposure to atmospheric conditions, iron analyses were performed with limited laboratory equipment that might have affected the validity of the results. In light of the data accumulated, it is evident that unforeseen circumstances related to power outages at the production borehole, drilling mud residue after borehole drilling of injection boreholes, and complications with injection rates, the site data is difficult to interpret.

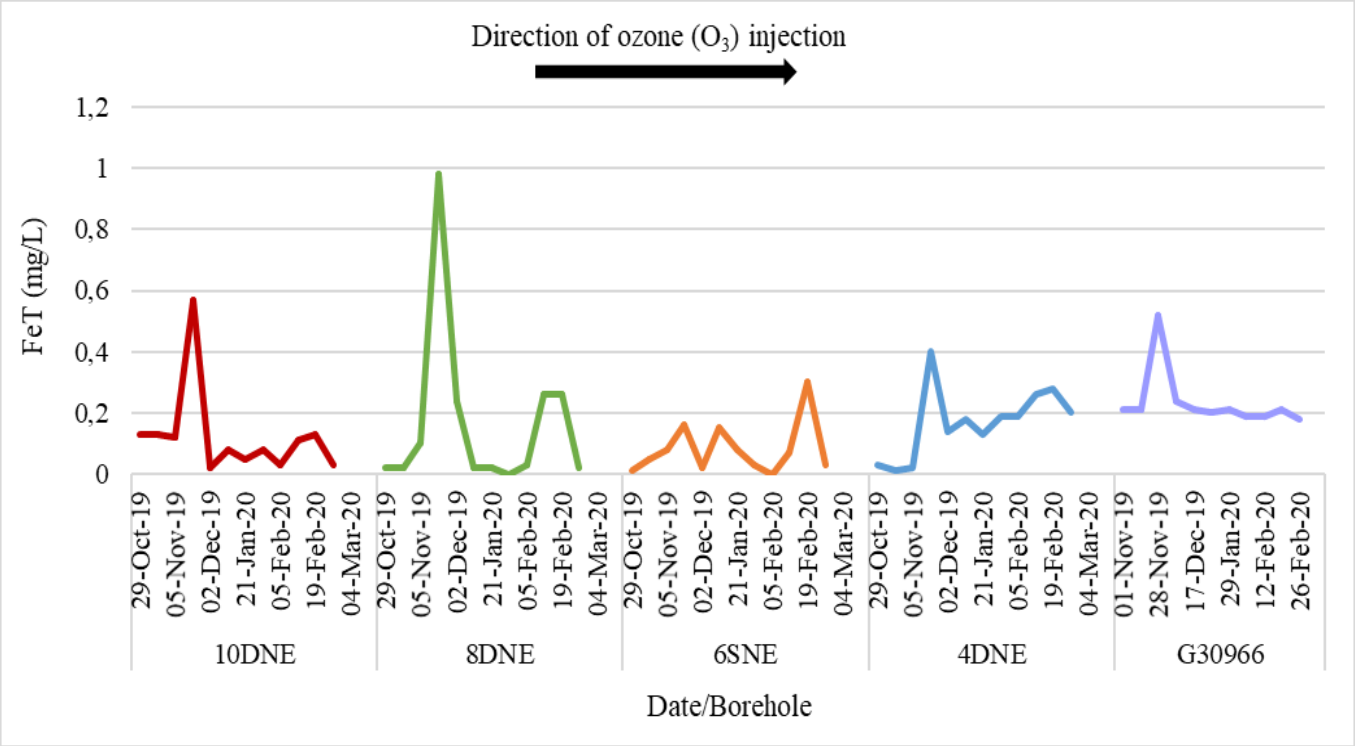

Figure 6.8: Monitored total iron (Fe^T) (mg/L) during ozone (O_3) injection in monitoring (10DNE, 8DNE, 6SNE, and 4DNE) and production borehole (G30966) from October 2019 to March 2020.

6.3.6 Dissolved and total manganese concentrations during ozone (O_3) injection

Dissolved and total manganese data obtained during manual sampling yielded erratic results, making it very difficult to derive justifiable reasons and conclusions. However, two sets of samples were sent for laboratory analysis to determine clear results to draw conclusions from. It is clear that both total and dissolved manganese concentrations were generally similar during the injection period of O_3 from the 1st - 5th November 2019 in monitoring boreholes 10DNE, 4DNE, and 8DSW. Subsurface dissolved and total manganese concentrations at 10DNE and 4DNE, measuring around 0.1 mg/L compares favourably to baseline data of Robey (2014). This is also noted in 8DSW, measuring around 0.2 mg/L for both dissolved and total manganese concentrations. A steady and minor decrease in dissolved and total manganese concentrations is noted for 10DNE and 8DSW, possibly favourable to O_3 injection. According to Braester and Martinell (1988), a decrease in manganese concentrations requires a longer reaction time as opposed to iron. In this study, manganese concentrations decreased only after 2 days of consistent injection, and iron concentrations decreased before the 2 days of injection. A noted

increase in dissolved and total manganese concentrations is observed in 4DNE, which could be explained by the presence of drilling mud residue affecting oxidation rates.

6.3.7 Monitored groundwater quality summary

The four field parameters (pH, DO, EC, and temperature) monitored in Figures 6.3 – 6.6 required using an on-site WTW Multi 3420 SET G water quality multi-parameter device (Table 6.4). Table 6.4 indicates the range of field parameters from October 2019 to March 2020 during on-site monitoring at the study site. An overall consistent trend between mean pH, EC, and temperature values is noted with minor variations between maximum, minimum, and mean values of monitoring (10DNE, 8DNE, 6SNE, 4DNE, 8DSW, G30979) and production borehole (G30966) (Table 6.4). Dissolved oxygen mean values represented the most variation amongst monitoring and production boreholes ranging from 0.11 to 8.18 mg/L. This variation from October 2019 to March 2020 indicates changes in subsurface conditions. High mean DO values could have been affected by drilling mud residue noted in the groundwater after the construction of injection borehole 11DNE, and its migration through the subsurface. Alternatively, high DO values represent the implementation of ISIR treatment as these DO levels accelerate iron and manganese oxidation reactions (Filtronics, 1993; Vance, 1994).

A consistent trend has been noted amongst SD values for pH, EC, DO, and temperatures of monitoring and production boreholes during O_3 injection. The overall trend for SD is represented as small for pH, EC, and temperature values that are concentrated around the mean values for monitoring and production boreholes, indicating low variability. Dissolved oxygen is the exception, where large SD values are noted for monitoring and production boreholes, indicating high variability. This is concerning as the SD values for DO concentrations are not as reliable compared to pH, EC, and temperature. The large SD values for DO concentrations could be due to the drilling mud that influenced the change in subsurface conditions, thereby indicating a change in DO concentrations over the monitoring period during O_3 injection from October 2019 to March 2020.

Drilling of the new larger diameter injection boreholes (11DNE, 7DE, and 12DN) using the mud rotary technique necessitated the establishment of a large drill on site and the digging of large holes for mud circulation (Nhleko *et al.*, 2020). These drilling activities had the greatest chemical and physical impact at the site especially due to the use of the drilling mud and its remaining residue after drilling. As observed in Figures 6.3 – 6.6, the inclusion of monitored

parameters before injection on the 1st October 2019 and 29th October 2019 was included. This data was included to serve as a guideline to distinguish apparent changes from natural to injection subsurface changes to observe a break-through of O_3 response in the subsurface. Furthermore, the inclusion of monitoring parameters continued after O_3 generators were switched off on 19th February 2020 (Table 4.1) to determine the response of subsurface conditions after O_3 injection. Issues with fluctuating injection pressures, power outages at the production borehole and various unforeseen incidents, caused an unsteady injection rate. Although the initial concept was to have continuous injection in all injection boreholes 11DNE, 7DE and, and 12DN, constant power outages influenced by city-wide loadshedding altered the overall injection regime which considered the injection rates to be intermittent, loadshedding dependent.

Monitoring boreholes upgradient (G30979) and downgradient (8DSW) to the study site were considered for monitoring during O_3 injection to determine the extent of changes in subsurface conditions. In the event that rapid fluctuations in these monitoring boreholes were noted, it would serve as an indication that the oxidation zone is compromised and should be re-assessed to ensure that the oxidation zone follows the concept derived from the conceptual model.

Table 6.3: Monitored field parameters of pH, electrical conductivity (EC), dissolved oxygen (DO), and temperature in monitoring and production borehole G30966 during ozone (O_3) injection from October 2019 to March 2020. Included monitoring boreholes are 10DNE, 8DNE, 6SNE, 4DNE, G30979, and 8DSW. The number of observations (n), minimum, maximum, mean, and standard deviation (SD) values is also included.

Monitoring Boreholes					
Field parameter	**Number of observations (n)**	**Minimum**	**Maximum**	**Mean**	**Standard deviation (σ)**
10DNE					
pH	15	7,23	7,61	7,41	0,35
EC (µS/cm)	15	644	739	700	47,07
DO (mg/L)	14	0,02	20	8,18	5,61
Temperature (°C)	15	17,7	20,5	19,5	0,65
8DNE					
pH	14	7,09	7,76	7,39	0,35
EC (µS/cm)	14	586	719	687	43,63
DO (mg/L)	14	0,03	20	7,15	5,69
Temperature (°C)	14	18,6	21,2	19,9	0,55
6SNE					
pH	14	7,3	7,82	7,47	0,35
EC (µS/cm)	14	657	772	710	43,43
DO (mg/L)	14	0,03	7,83	2,06	5,67
Temperature (°C)	14	19,2	20,4	19,84	0,56
4DNE					
pH	14	7,2	7,6	7,4	0,35
EC (µS/cm)	14	637	697	666	43,63
DO (mg/L)	14	0,03	12,85	2,5	5,69
Temperature (°C)	14	18,7	19,8	19,41	0,55
8DSW					
pH	14	7,43	7,76	7,61	0,35
EC (µS/cm)	14	631	688	667	43,74
DO (mg/L)	14	0,01	0,6	0,19	5,52
Temperature (°C)	14	18,2	19,1	18,69	0,58
G30979					
pH	9	8,3	8,63	8,48	0,36
EC (µS/cm)	9	558	626	596	44,24
DO (mg/L)	4	0,08	0,19	0,11	5,8
Temperature (°C)	9	18,8	19,2	19,06	0,53
Production Borehole					
Field parameter	**Number of observations (n)**	**Minimum**	**Maximum**	**Mean**	**Standard deviation (σ)**
G30966					
pH	13	7,47	8,05	7,58	0,34
EC (µS/cm)	13	686	724	714	43,61
DO (mg/L)	12	1,83	6,7	3,84	5,5
Temperature (°C)	13	18,3	19,9	19,18	0,57

6.4 Telemetry data during ozone (O_3) injection

In addition to manual field parameter sampling, an automated GeoTel data collection system (telemetry) was used for continuous data during the injection period from October 2019 to March 2020. Telemetry was used in monitoring boreholes 4DNE and 8DNE, injection boreholes 7DE, 11DNE, and 12DN and production borehole G30966. Telemetry in monitoring boreholes was used for data collection to establish an understanding of the zone of influence at the study site. It also assisted in optimizing the ISIR treatment design through responsible hydrochemical subsurface logging from the point of O_3 injection downgradient towards the production borehole to establish the effect of O_3. Automated monitoring of groundwater treatment at the study site comprised of data loggers Solinst (F100, M30) and Global Water (WQ-FDO and GL500-7-2) which were installed in the injection and monitoring boreholes.

Viewing field parameters of DO, water levels, temperature, injection flow rate, and EC data off-site has also served as a warning detection system during the project timeline to identify vulnerabilities of telemetry. The ability to identify interruptions was noted during the December 2019 holiday season, where a power failure in the area automatically shut-down the telemetry and treatment system for approximately 2 weeks. Most interruptions noted in the telemetry system was the result of a power failure, and has been indicated in telemetry graphs where DO, temperature, and EC data is erratic (Nhleko *et al.*, 2020). It is recommended that manual downloading be considered during telemetry data capturing procedures, and that data loggers have a back-up power supply to operate on either electricity, solar power or a battery source (located inside the logger). Depth limits for telemetry data in injection and monitoring boreholes is represented by red lines, as shown in water level graphs for 4DNE, 7DE, and 12DN (Figures 6.9, 6.10, and 6.11). Boreholes are also screened at depths roughly between 24 and 31 mbgl.

6.4.1 Telemetry data for monitoring borehole 4DNE

The overall pattern of telemetry water levels recorded in 4DNE is generally consistent with historical groundwater levels which never exceeded 7 mbgl (Figure 6.9A). This indicates evidence that the zone of influence as a result of groundwater abstraction in production borehole G30966 showed little to no effect on 4DNE. However, inconsistent rapid decreases in water levels greater than 7 mbgl were recorded throughout the monitoring period which remains questionable in terms of telemetry reliability due to technical difficulties. The trend in

EC values in 4DNE (Figure 6.9B) were similar when compared to manual EC sampling, showing evidence of data accuracy and reliability. The unpredictable and rapid decreasing spikes observed in EC levels is an indication of technical disruptions to the telemetry system. Similar technical interruptions have also been shown in temperature values, indicated by inconsistent increasing temperature spikes (Figure 6.9C). However, the general trend in temperature values recorded in 4DNE by the telemetry system was similarly represented by manual recorded readings (Figure 6.6), which also indicates data accuracy and reliability.

Considering the technical interruptions noted in water levels, EC and temperature values recorded by the telemetry system in 4DNE, reliable and accurate trends have been noted. This is explained by water levels when compared to historical data, and in EC and water temperature when compared to manual sampling.

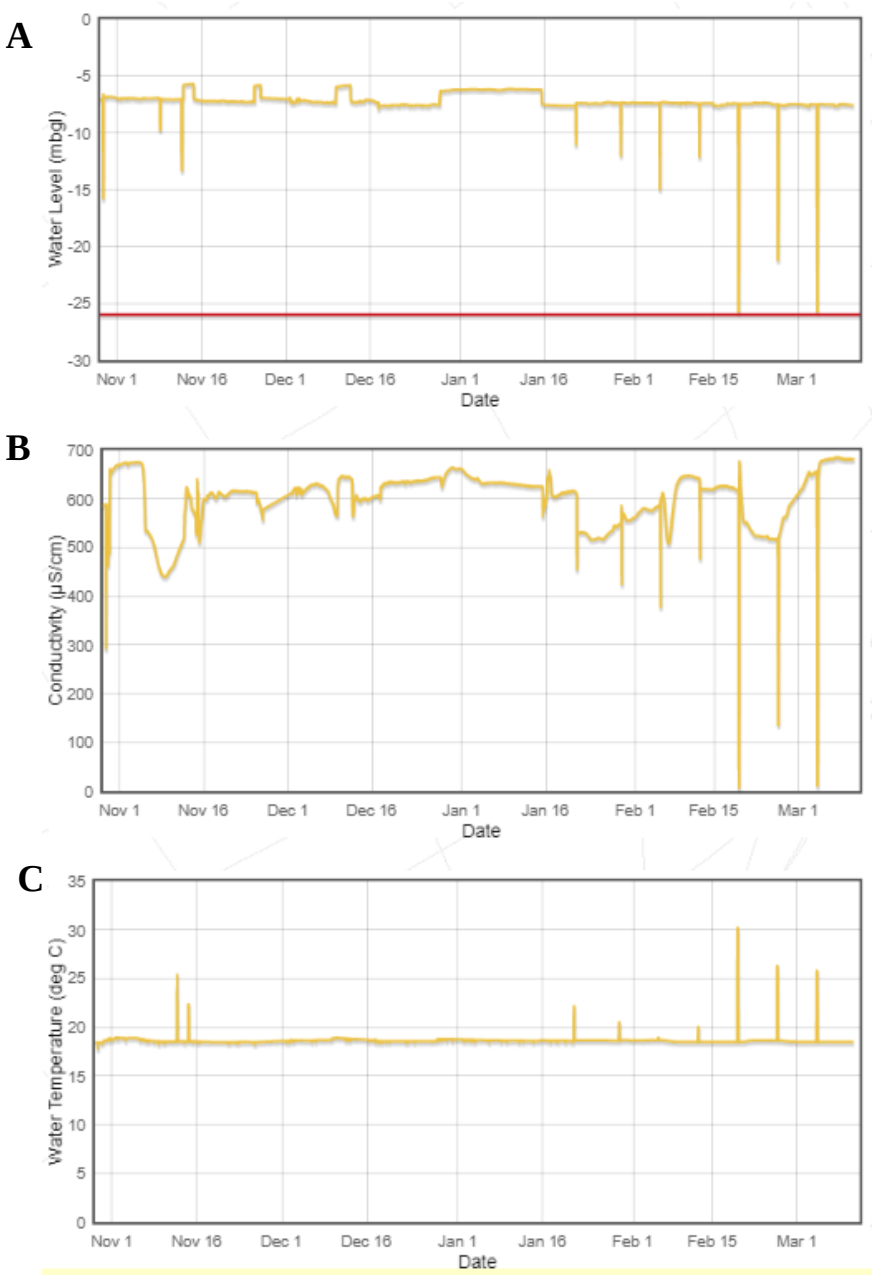

*Figure 6.9: Telemetry data of monitoring borehole 4DNE during ozone (O_3) injection from 29 October 2019 to 11 March 2020. The time series graphs illustrate the dates of monitoring against **(A)** Water level (mbgl), **(B)** Conductivity (µS/cm), and **(C)** Water temperature (°C). Measurements were recorded at hourly intervals during continuous injection. The red line observed in **(A)** indicates the depth limit for telemetry data in the borehole, positioned at 26 mbgl.*

6.4.2 Telemetry data for monitoring borehole 8DNE

The telemetry DO concentrations in 8DNE indicates an increase and subsequent decrease period between the 29th October 2019 to 5th November 2019, which can be explained by the start of O_3 injection followed by the change in injection rates (Table 4.1). Steady and consistent

DO concentrations from the 30th November 2019, despite the rapid decreasing spikes, measured between 18 and 20 mg/L (Figure 6.10A). This steady and consistent DO concentrations can be explained by the response of O_3 in the subsurface relative to injection and favourable for iron and/or manganese oxidation (Smith, 2006). Even during decreasing injection rates and after O_3 generators were switched off on the 19th February 2020 (Table 4.1) DO was still present in the subsurface. These observed DO concentrations compares favourably to Diliūnas *et al.* (2006) whereby groundwater dosing of oxygen gas maintained concentrations around 20 mg/L. This could possibly mean that iron and manganese oxidation was not prominent enough to use the available DO present in the subsurface. Similar DO concentrations were measured during manual sampling (Figure 6.4) which indicates evidence of data accuracy and reliability. There is little variation in temperature despite the spikes as it is generally between 17 and 20 °C (Figure 6.10B). This is similar to the manual sampling (Figure 6.6), showing evidence of data accuracy and reliability. The rapid and inconsistent spikes in DO and temperature is an indication of interruptions recorded by the telemetry system.

Regardless of the rapid spikes in DO and water temperature data, reliable and accurate trends have been noted. This is explained by similarities in DO and water temperature values when compared to manual sampling.

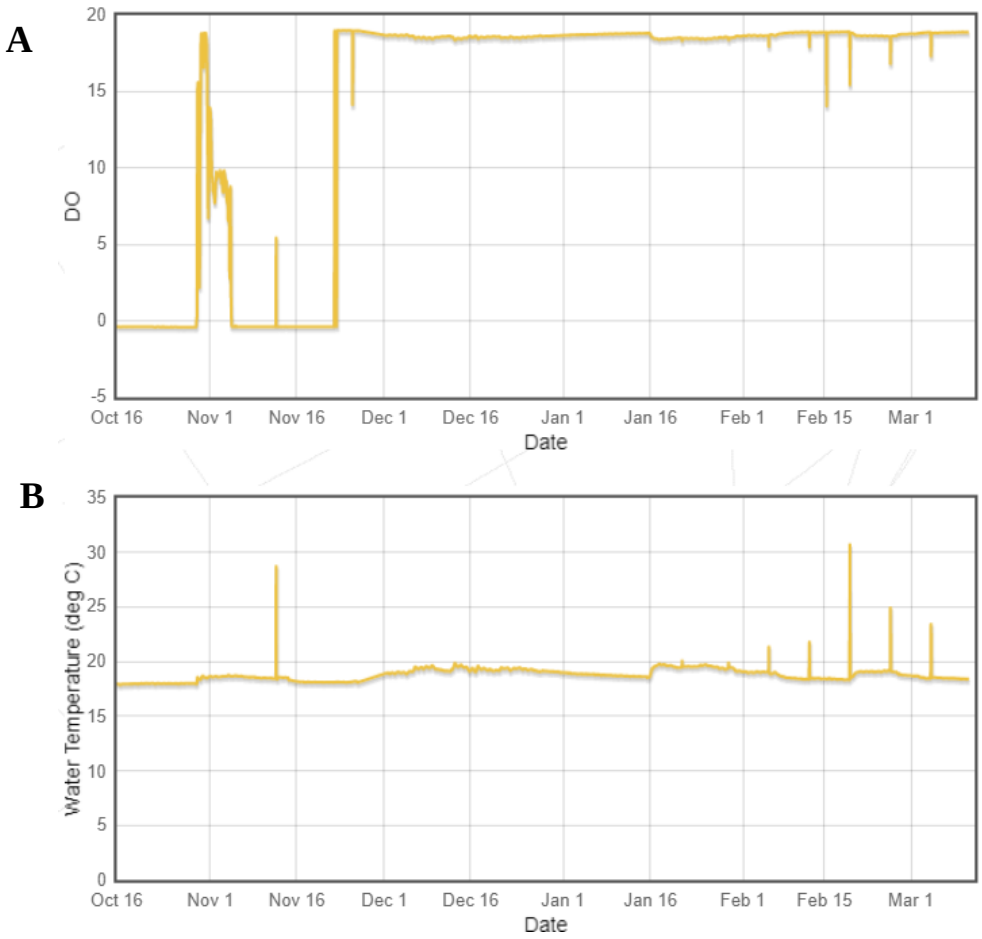

Figure 6.10: Telemetry data of monitoring borehole 8DNE during ozone (O_3) injection from 29 October 2019 to 11 March 2020. The time series graphs illustrate the dates of monitoring against ***(A)*** *Dissolved oxygen concentrations (mg/L) and* ***(B)*** *Water temperature (°C). Measurements were recorded at hourly intervals during continuous injection.*

6.4.3 Telemetry data for injection borehole 7DE

Although no manual sampling or historical data comparisons of water level and temperature can be considered for 7DE as it was newly drilled in 2019, the general trend of both parameters showed little to no interruptions in the telemetry data recorded (Figure 6.11A and 6.11B). The overall trend of water levels was coherently consistent with sampled boreholes surrounding 7DE with recorded values between 0 - 6 mbgl. Similar water level values have been noted in close proximity injection boreholes 11DNE and 12DN, as well as in monitoring borehole 8DNE. Water level values in 4DNE (Figure 6.9A) could not be compared to 7DE as this is the furthest monitored telemetry borehole from 7DE, closest to production borehole G30966. As a result, water levels in 7DE shows little to no variability compared to closer boreholes at the study site, possibly indicating reliability in the telemetry data recorded in 7DE in comparison to the surrounding monitoring boreholes data. High water levels displayed between 0 - 2 mbgl

(Figure 6.11A) can be explained by the injection of ozonated water directly into injection borehole 7DE. This can be compared to Snyder (2008) who indicates that water table depth increases are influenced by increased groundwater storage when the rate of recharge exceeds the rate of discharge. Similar to the current study, Snyder (2008) mentions that human-induced modifications can also result in water table increase or fluctuations. Changes in injection rates and overflowing in injection boreholes have also been reported (Table 4.1), which could have contributed to the high water levels. The increase in water level compares favourably to subsurface conditions obtained during the study of Robey (2014), where borehole overflowing was noticed as a consequence of injection activities in the borehole.

Water temperature was recorded between 17 – 21 °C. Although the general temperature in injection and monitoring boreholes were between this range, all three injection boreholes (7DE, 11DNE, and 12DN) indicated higher water temperatures more frequently, as indicated by the values closer to or higher than 21 °C (Figure 6.11B). This was between 5th February 2020 and 11 March 2020 with similar conditions noted in injection boreholes 11DNE (Figure 6.12C) and 12DN (Figure 6.13B). The increase in water temperature can be due to effects of surface warming such as global warming. This relationship is expressed in the study by Saito *et al*. (2016), whereby subsurface temperatures increased from 0.7 up to 8 °C. In addition, February is considered one of the hottest months in Cape Town, which corresponds to the findings of Saito *et al*. (2016), indicating that surface heat contributes to *in situ* subsurface heating. These findings are also expressed in a later study by Jesußek *et al*. (2013). Furthermore, similarities in water temperature values shown in all three injection boreholes indicates evidence of reliable and accurate trends that have been observed.

A

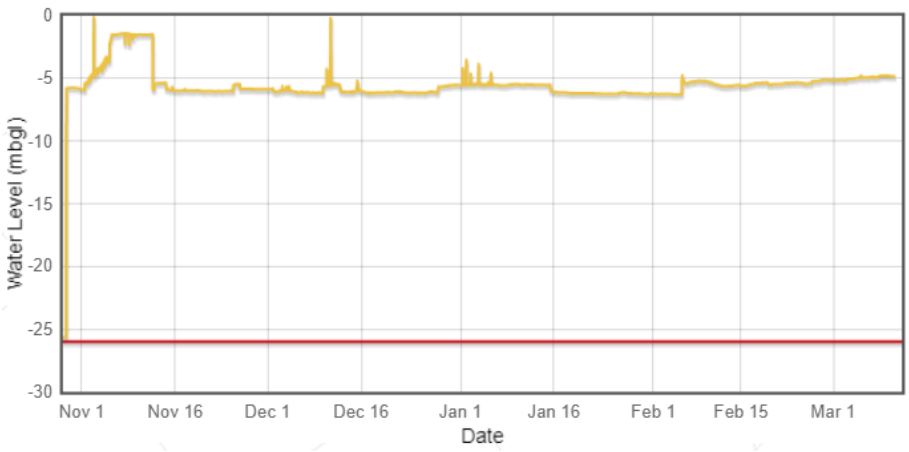

B

*Figure 6.11: Telemetry data of injection borehole 7DE during ozone (O_3) injection from 29 October 2019 to 11 March 2020. The time series graphs illustrate the dates of monitoring against **(A)** Water level (mbgl) and **(B)** Water temperature (°C). Measurements were recorded at hourly intervals during continuous injection. The red line observed in **(A)** indicates the depth limit for telemetry data in the borehole, positioned at 26 mbgl.*

6.4.4 Telemetry data for monitoring borehole 11DNE

Water level values recorded in 11DNE was within the range of 1 – 6 mbgl (Figure 6.12A), similar to that of other injection boreholes 7DE (Figure 6.11A) and 12DN (Figure 6.13A). Prolonged higher water levels recorded by the telemetry system is best explained by the injection of ozonated water into injection borehole 11DNE. As similarly experienced by Robey (2014), Snyder (2008) mentions that water table depth increases are influenced by increased groundwater storage when the rate of recharge exceeds the rate of discharge during human-induced modifications within the subsurface system. The main injection borehole, 11DNE, was mostly used for longer duration injections of ozonated water. It was positioned up gradient to all of the monitoring boreholes to be the source of establishing the zone of oxidation and redox gradient between 11DNE down gradient towards G30966 for iron and manganese oxidation to occur. Evidence of most frequent ozonated injection periods are noted by high prolonged water levels compared to all other telemetry monitoring and injection boreholes.

The absence of historical and manual EC values in 11DNE considers comparisons from the surrounding boreholes as the most suitable representation for accuracy and reliability. Electrical conductivity values in 11DNE was between 650 – 810 µS/cm (Figure 6.12B). Although the only other telemetry borehole which measured EC was 4DNE, which had an EC variability between 510 - 690 µS/cm, the overall consistent trend in EC values in 11DNE was 620 µS/cm (Figure 6.12B) which existed within the range of 4DNE. This value also aligns with

EC values measured by manual sampling before O_3 injection in monitoring boreholes 10DNE, 8DNE, 6SNE, and 4DNE in Section 6.3.3. It was only during 1st January 2020 – 15th January 2020 where EC exceeded 620 µS/cm, which was still well within the mean range of EC values at the study site from historical groundwater data from G30966 (Table 5.2). An increase in EC values usually shows the presence of oxidation reactions during O_3 injection which is prominent in 11DNE as it is an injection borehole with faster reaction times during direct O_3 contact (Meyer, 2001). As a result, reliable and accurate telemetry EC trends have been noted based on historical study area similarities and when compared to manual sampling.

Water temperatures recorded in 11DNE was generally between 18 – 23 °C. This range of water temperature has been noted in all monitoring and injection boreholes which were generally within the range of 17 – 21 °C. However, slightly higher water temperatures recorded between the 5th February 2020 and 11 March 2020 in 11DNE (Figure 6.12C) most likely displays the direct effect of oxidation reactions as a result of longer and more concentrated ozonated injection. Studies by Saito *et al*. (2016) and Jesußek *et al*. (2013) mentions that surface heat contributes to *in situ* subsurface heating, which affects temperatures between 0.7 and 8 °C. Similar conditions were noted in both injection boreholes 7DE (Figure 6.11B) and 12DN (Figure 6.13B). The change in injection rates in 12DN, could represent suitable O_3 concentrations for oxidation reactions to have occurred. Ideal conditions for O_3-based reactions generally require water temperatures between 15 and 20 °C (EPA, 1999; Nimmer *et al.*, 2000; El Araby *et al*., 2009). Furthermore, both iron and manganese oxidation rates are accelerated at higher water temperatures (Filtronics, 1993; Vance, 1994). Based on these previous studies which supports oxidation reactions increasing water temperatures, it indicates reliability and accuracy in the telemetry data recorded.

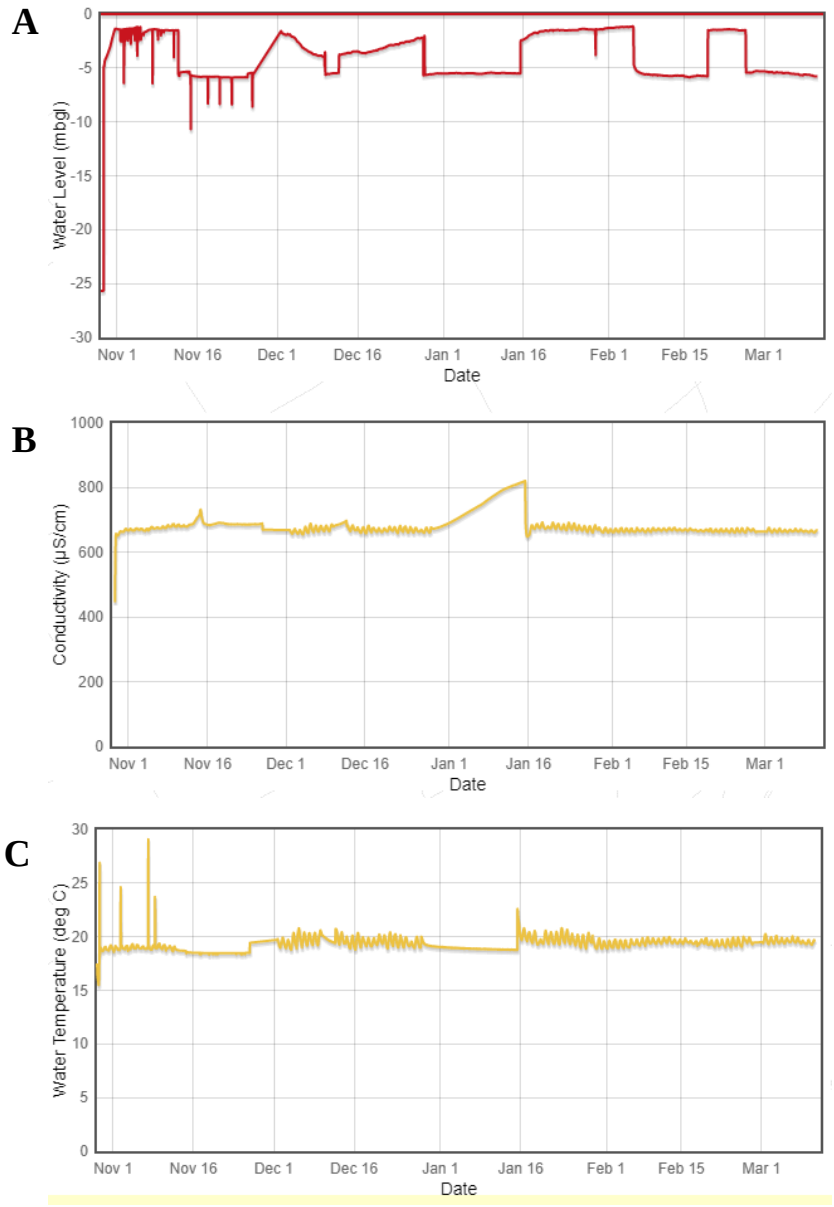

*Figure 6.12: Telemetry data of injection borehole 11DNE during ozone (O_3) injection from 29 October 2019 to 11 March 2020. The time series graphs illustrate the dates of monitoring against **(A)** Water level (mbgl), **(B)** Electrical conductivity (µS/cm), and **(C)** Water temperature (°C). Measurements were recorded at hourly intervals during continuous injection.*

6.4.5 Telemetry data for monitoring borehole 12DN

Water levels remained fairly stable between 2 – 7 mbgl throughout the monitoring period from 29th October 2019 to 11th March 2020. The noted water level increases between the 5th – 13th November 2019, and between the 5th February and 11th March 2020 can be explained by the adjustment of O_3 injection rates (Table 4.1). Increasing water levels in injection boreholes were also visible in telemetry recorded injection boreholes 7DE (Figure 6.11A) and 11DNE (Figure 6.12A). Similar conditions have been noted in Robey (2014) during the introduction of

ozonated water as it increases the volume of water within the borehole. The increase in water level also compares favourably to the theoretical concept of Snyder (2008) who mentions that water table depth increases are influenced by increased groundwater storage during human-induced modifications within the subsurface system. As similarly noticed in 7DE, no manual sampling or historical data comparisons of water level and temperature was possible for 12DN as it was newly drilled in 2019.

Water temperature was recorded between 16 – 21 °C. Similar telemetry temperature ranges in both injection and monitoring boreholes have been noted (Figure 6.9C, Figure 6.10B, Figure 6.11B, and Figure 6.12C). Although the general temperature in injection and monitoring boreholes were between 16 – 21 °C, injection boreholes indicated more frequent higher water temperatures, as indicated by the values closer to 21 °C between the period of the 5th February and 11th March 2020 (Figure 6.13B). This was also noted in injection boreholes 7DE (Figure 6.11B) and 11DNE (Figure 6.12C) and could be a result of the change in injection rates that took place on 5th February 2020 (Table 4.1). Similar results from Saito *et al*. (2016) and Jesußek *et al*. (2013) supports the effects of surface heat on *in situ* subsurface heating, which affected temperatures during their studies between 0.7 and 8 °C. The change in injection rates in 12DN, could represent suitable O_3 concentrations for oxidation reactions to have occurred.

Both parameters indicated a change over the same period between the 5th February and 11th March 2020. This similar trend is only noted in injection borehole 7DE. Telemetry in both boreholes records only water level and temperature parameters. Although there is consistency in injection rates in both boreholes as recorded in Table 4.1, the simultaneous changes in both parameters was evidently influenced by atmospheric temperature (weather parameter considering February as the hottest month in Cape Town) and human-induced modifications. Similarities in water temperature results is mentioned by Saito *et al*. (2016) and Jesußek *et al*. (2013), who explains that surface heating affects subsurface heating of groundwater *in situ*. The similarities in water level results compares favourably to the theoretical concept of Snyder (2008) who describes increasing water table levels increases during human-induced modifications such as *in situ* injection. The general trend of both water level and temperature indicates little to no interruptions in the telemetry data (Figure 6.13A and 6.13B). Furthermore, telemetry water level and temperatures recorded in 12DN was fairly similar when compared to the immediately adjacent boreholes (11DNE, 7DE, 8DNE, and 4DNE), providing a representation of reliable and accurate data.

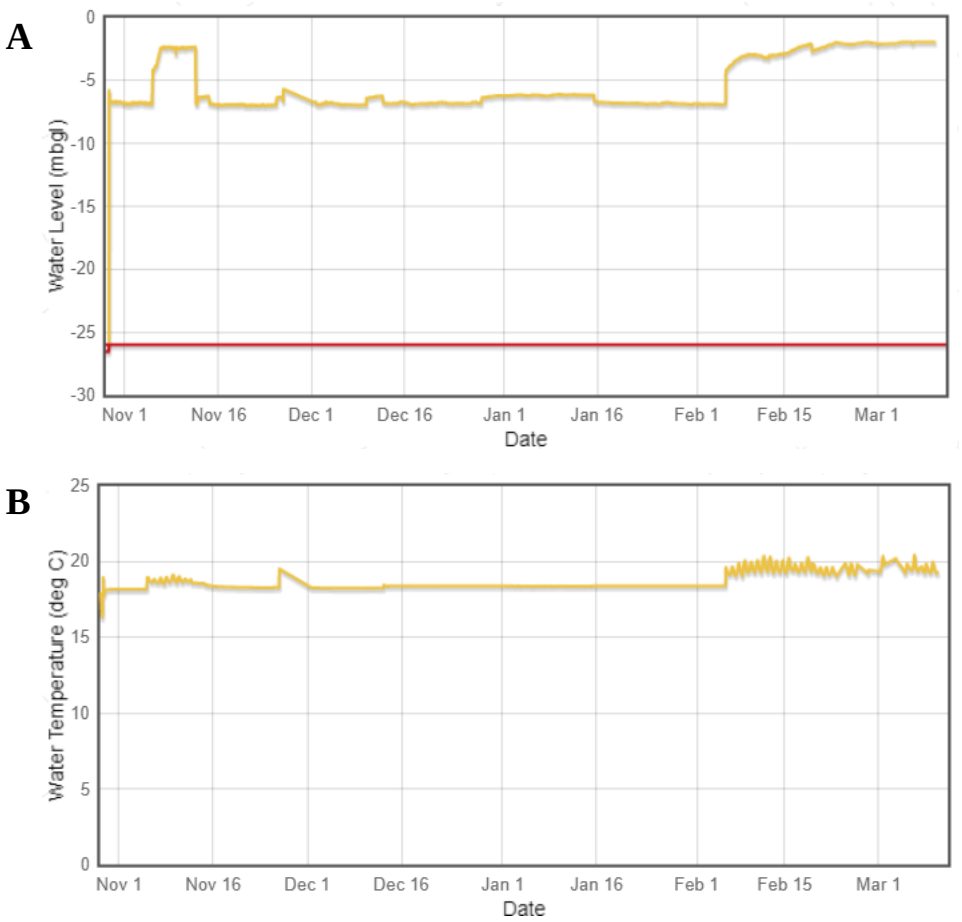

*Figure 6.13: Telemetry data of injection borehole 12DN during ozone (O_3) injection from 29 October 2019 to 11 March 2020. The time series graphs illustrate the dates of monitoring against **(A)** Water level (mbgl) and **(B)** Water temperature (°C). Measurements were recorded at hourly intervals during continuous injection. The red line observed in **(A)** indicates the depth limit for telemetry data in the borehole, positioned at 26 mbgl.*

6.4.6 Telemetry data of raw water at G30966

The DO concentrations measured by the telemetry system of the raw water at G30966 showed minimal response to O_3 injection downgradient from the injection boreholes (7DE, 11DNE, and 12DN). Although an increase in DO concentrations from 0 mg/L to 2.5 mg/L was noted during the initial phase of the injection period between the 1st – 5th November 2019, the remaining period remained absent which measured around 0 mg/L (Figure 6.14A). These consistent low DO concentrations compares differently to DO concentrations in monitoring borehole 8DNE positioned 8 m from G30966 (Figure 6.10A). It could be understood that G30966 distance from injection boreholes 7DE, 11DNE, and 12DN and the rate or duration of injections were only sufficient to reach 8DNE and not G30966. These results would compare favourably to the hydrogeochemical conceptual model (Figure 6.2). This could possibly indicate that the distance from injection boreholes 7DE, 11DNE, and 12DN to G30966 was too far too great to distribute O_3.

In addition, there is a likelihood of the loss or escape of O_3 as an effervescence (Walker and Mallants, 2014). An effervescing gas is whereby gas from an aqueous solution, in this instance O_3 gas, in the form of foaming or fizzing is released from a borehole which was experienced between January and February 2020 in both 11DNE and 7DE (Table 4.1) (Walker and Mallants, 2014). Effervescing and overflowing of injection boreholes was experienced, which could have contributed to low DO concentrations in G30966 due to the loss of O_3. Furthermore, the rate and duration of O_3 injections between October 2019 and February 2020 were also inconsistent, which could have affected the ability of O_3 to extend to G30966. This corresponds to the intended reaction generated by the hydrogeochemical conceptual model (Figure 6.2), which demonstrates that majority of subsurface chemical reactions should occur within the oxidation zone before reaching G30966. As a result, the intended reaction and oxidation zone initially derived from the hydrogeochemical conceptual model (period T4 in Figure 6.2) could have possibly been fulfilled as minimal DO response is noted in G30966 (Figure 6.14).

The injected ozonated water was possibly only able to precipitate out the iron and manganese before reaching G30966. This could possibly mean that O_3 was consumed during iron and manganese oxidation in monitoring boreholes 10DNE, 8DNE, 6SNE, and moderately in 4DNE, before it reached G30966. This is supported by low total iron concentrations measured in 10DNE, 8DNE, 6SNE, moderately in 4DNE, and highest concentrations in G30966 (Figure 7.3). It has also been noted that the changes in O_3 injection rates and malfunctioning of the system (Table 4.1) did not correspond coherently with the telemetry results obtained.

Furthermore, the low DO concentrations recorded by telemetry is inconsistent when compared to the manual sampling (Figure 6.4) which indicates more variability in measured DO concentrations. Although little to no interruptions is noted in the telemetry data of raw water at G30966, the reliability of the DO concentrations when compared to manual sampling has probable cause to support its low DO concentrations. However, DO measurements during both manual field sampling (Figure 6.4) and the telemetry system (Figure 6.14) demonstrate similar conditions, indicating O_3 was unable to reach G30966 to efficiently initiate iron and manganese oxidation. Dissolved oxygen is a volatile measurement that changes rapidly in response to its sensitivity with atmospheric and external environmental factors. It has a short time period to measure accurate and a true reflection of DO concentrations in the subsurface, but a long waiting period to stabilize readings using manual equipment. Therefore, it is suspected that the telemetry data of DO concentrations are more reliable and accurate compared to the manually recorded DO.

Water temperature showed the most fluctuations when compared to the other monitoring boreholes, ranging between 10 – 37 °C (Figure 6.14B). Although steady temperatures were noted between the injection period from the 29th October 2019 to 11th March 2020 at 17 °C, three fluctuating periods remained questionable. These fluctuating increasing and subsequent decreasing temperature periods were between 12th – 26th November 2019, 9th – 12th December 2019, and 26th December 2019 -16th January 2020 (Figure 6.14B). These results are best described by the influence of atmospheric temperature on subsurface temperatures, which is supported by the studies of Saito *et al*. (2016) and Jesußek *et al*. (2013). In both studies, it is explained that surface atmospheric temperatures have the ability to affect subsurface heating of groundwater *in situ.* However, increased temperatures during these months are considered less likely as the hottest months are generally between February and March in Cape Town. Manual water temperatures recorded (Table 6.6) indicated little to no variation which ultimately deems the reliability and accuracy of the telemetry water temperature questionable when compared to manual sampling. Little to no variability in water temperature would seem more appropriate when considering both theoretical concepts and atmospheric conditions at the study site. Therefore, the questionable telemetry water temperatures recorded in G30966 makes it very difficult to derive accurate and reliable data correlations, instead, manual water temperatures are deemed more reliable and accurate in this instance.

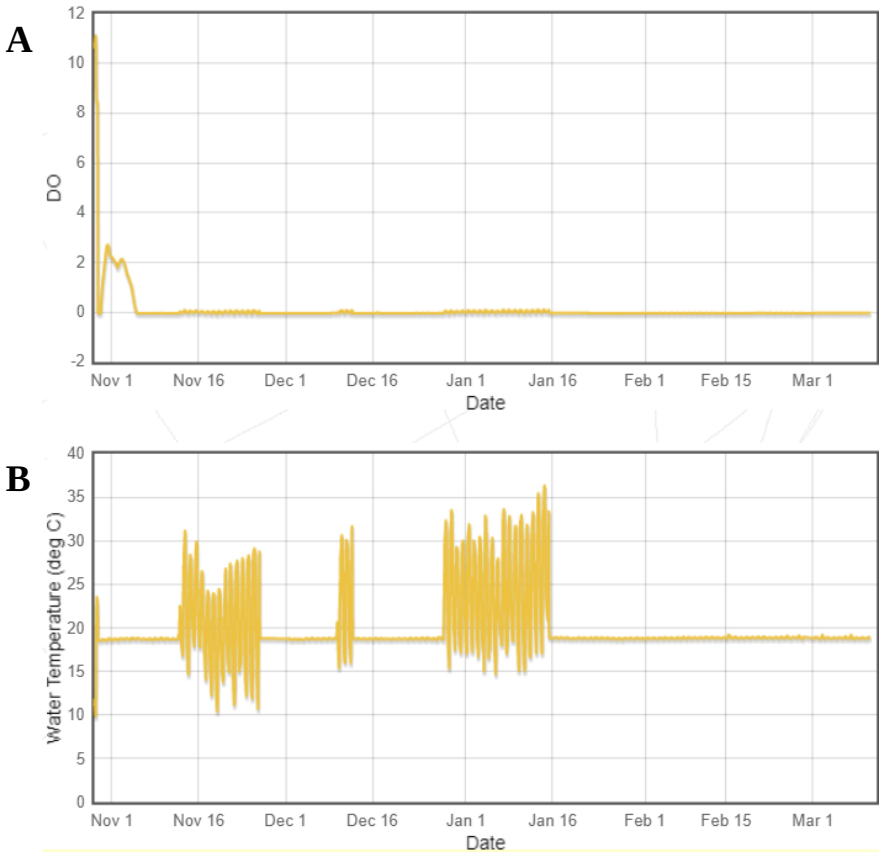

Figure 6.14: Telemetry data of production borehole G30966 during ozone (O_3) injection from 29 October 2019 to 11 March 2020. The time series graphs illustrate the dates of monitoring against ***(A)*** *Dissolved oxygen concentrations (mg/L) and* ***(B)*** *Water temperature (°C). Measurements were recorded at hourly intervals during continuous injection.*

Chapter 7: Efficiency of ISIR using ozonation

7. Introduction

Despite some inconsistencies, both manual sampling and telemetry system has been deemed to work well enough to derive reasonable accurate conclusions, with minor questions which remain unanswered in terms of the results obtained. This is highlighted in section 6.1, indicating implications of the study due to the absence of recording manganese data. In light of the data collected, overall patterns in the results have been observes with favourable descriptions correlating existing theoretical concepts, technology, comparable treatments and considering the malfunctions and power outages to derive suitable conclusions. Both favourable and opposing comparisons has been observed and recognised in Chapter 6 for manual recordings in Section 6.3 and telemetry data in Section 6.4.

7.1 Manual and telemetry interpretation

The relationship between dissolved and total iron concentrations, and manual sampling and telemetry DO concentrations relative to O_3 injection rates demonstrates promising results (Figure 7.1). Decreased iron concentrations (Figures 6.7 and 6.8) corresponds suitably with increased DO concentrations (Figures 6.4 and 6.11) (Robey, 2014). Subsequently, slightly increased iron concentrations respond favourably with decreased DO concentrations (Figure 7.1). Furthermore, increased O_3 injection in 11DNE (Figure 6.13) contributes to increased DO concentrations during manual sampling (Figure 6.4) and telemetry data (Figure 6.11), that possibly initiates oxidation reactions in the subsurface (Rice, 2002). Subsequently, decreasing O_3 injection (Figure 6.13) displays decreasing DO concentrations during manual sampling (Figure 6.4) and telemetry data (Figure 6.11) and compares to studies from Rice (2002) and Robey (2014). Although an overall trend is noted, the exact times and DO concentrations are not identical when compared between manual sampling and telemetry, which is expected considering the surface and subsurface sampling technique differences. It has also been noted that DO concentrations recorded from the telemetry system indicates a continuation of high DO levels even after O_3 injection stopped, which brings into question the reliability of the telemetry DO levels. Increasing and subsequent decreasing total and dissolved iron concentration patterns supports the response of O_3 injection rates which have also been supported by studies from Rice (2002) and Robey (2014).

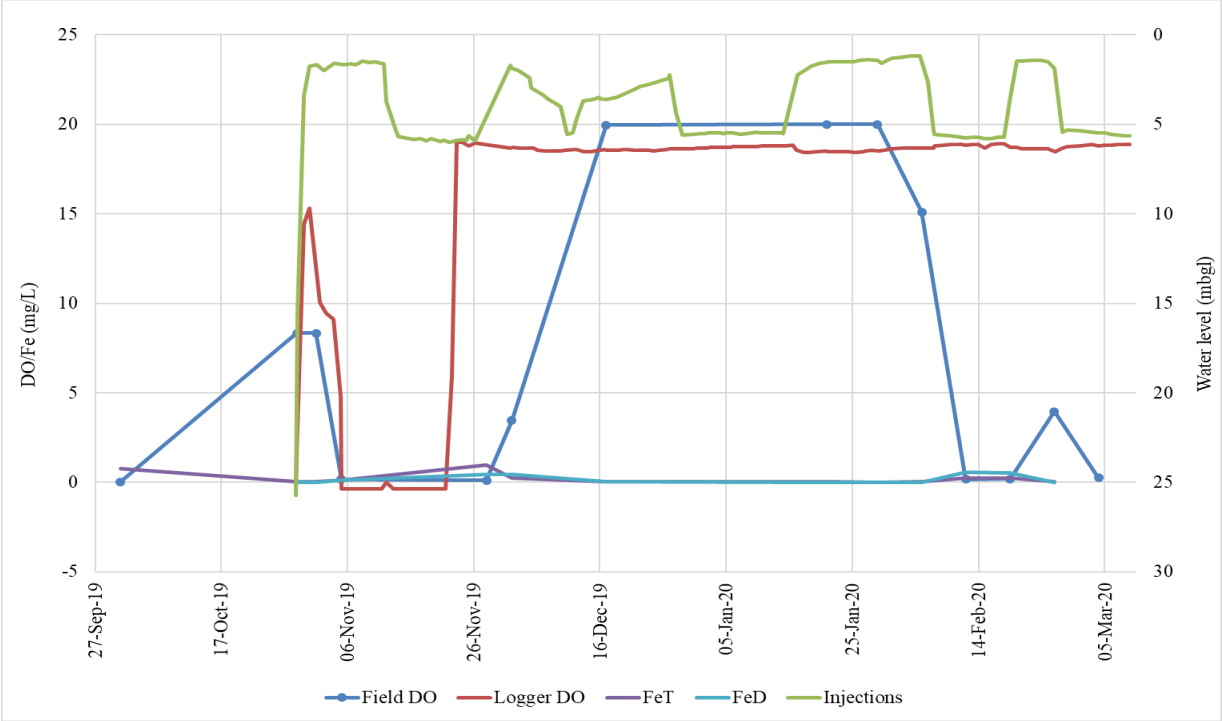

Figure 7.1: The relationship between iron concentrations, dissolved oxygen (DO) concentrations, injection rates and water levels in monitoring borehole 8DNE during ozonation at the study site. Dissolved oxygen concentrations (mg/L) are plotted from manual sampling (Field DO) and the telemetry system (Logger DO). Dissolved (FeD) and total (FeT) iron concentrations (mg/L), with corresponding water levels (mbgl) and injection rates (L/s) in 11DNE (Injections). Concentrations were measured during the injection period from 29 October 2019 to 11 March 2020.

The relationship between dissolved and total iron concentrations, and manual sampling and telemetry DO concentrations relative to injection rates demonstrates promising results (Figure 7.2). This is expressed by the lowered iron concentrations (Figures 6.7 and 6.8) that corresponds suitably with increasing DO concentrations (Figure 6.4) only in monitoring boreholes 10DNE, 8DNE, 6SNE, and moderately in 4DNE (Robey, 2014). Increased O_3 injections in 11DNE (Figure 6.13) displays subsequent increased manual sampling DO concentrations (Figure 6.4), that should have initiated suitable subsurface oxidation reactions for iron and manganese (Rice, 2002). However, the increase in manual sampling DO concentrations (Figure 6.4) indicates that the effect of O_3 injection sufficiently reached 10DNE, 8DNE, 6SNE, moderately 4DNE, and even though indications of fluctuating DO concentrations was noted in G30966 (Figure 6.4), it was not sufficient to promote suitable iron and manganese oxidation reactions.

Telemetry measured DO concentrations (Figure 6.13) represents G30966 more suitably based on probable causes. These probable causes recognises that that the distance from injection boreholes 7DE, 11DNE, and 12DN to G30966 was too far to distribute O_3 efficiently. In addition, the lowered iron concentrations corresponding to increasing DO concentrations in monitoring boreholes 10DNE, 8DNE, 6SNE, and moderately in 4DNE indicates that O_3 was consumed during iron and manganese oxidation in monitoring boreholes before reaching G30966. Alternatively, the foaming observed in injection boreholes 11DNE and 7DE, suggests the loss or escape of O_3 be means of effervescing, which could have largely contributed to low DO concentrations downgradient to G30966 (Walker and Mallants, 2014). This is also supported by DO concentrations factors which is prone to change due to its volatile response to atmospheric and external environmental influences. Although unstable injection rates throughout the injection period between October 2019 and March 2020 was observed, suitable conditions for iron and manganese oxidation resembling the hydrogeochemical conceptual model (Figure 6.2) was derived. This supports the demonstration that the majority of subsurface chemical reactions including DO should occur within the oxidation zone in monitoring boreholes 10DNE, 8DNE, 6SNE, and 4DNE, before reaching G30966.

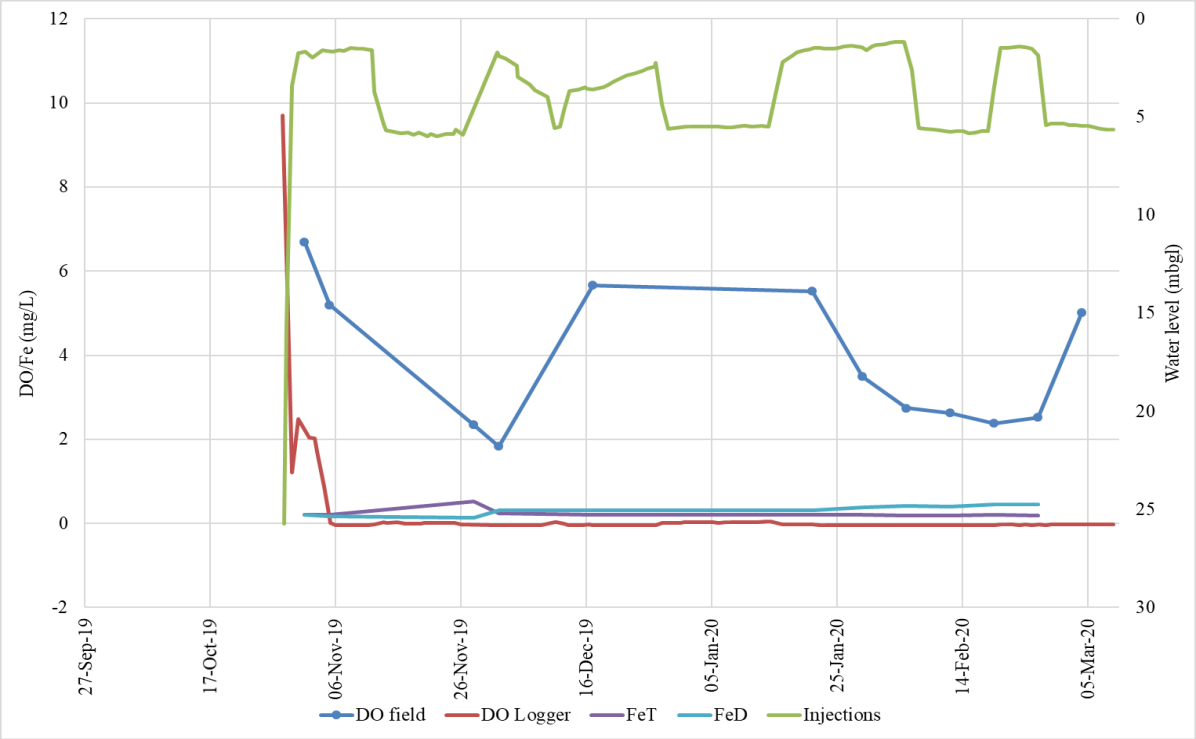

Figure 7.2: The relationship between iron concentrations, dissolved oxygen (DO) concentrations, injection rates and water levels in production borehole G30966 during ozonation at the study site. Dissolved oxygen concentrations (mg/L) are plotted from manual

sampling (DO Field) and the telemetry system (DO Logger). Dissolved (FeD) and total (FeT) iron concentrations (mg/L), with corresponding water levels (mbgl) and injection rates (L/s) in 11DNE (Injections). Concentrations were measured during the injection period from 29 October 2019 to 11 March 2020.

7.2 Total iron (Fe^T) concentration interpretation

During O_3 injection in 11DNE from October 2019 to March 2020, Fe^T concentrations were monitored in the production and several other monitoring boreholes downgradient to 11DNE (Figure 7.3). The Fe^T analysis in these boreholes in response to ozonation to determine borehole clogging was understood. As indicated in Figure 7.3, an overall decreasing Fe^T concentration trend is observed in the production and monitoring boreholes with inconsistent, however, favourable O_3 injection rates. Subsequently, slow and steady increased Fe^T concentrations have been noted after O_3 generators were discontinued after the 19th February 2020 (Figure 7.3). The overall increasing trend observed after O_3 injection was discontinued compares favourably to the study of Braester and Martinell (1988). Braester and Martinell (1988) mentions that increased pumping activities from the production borehole during the absence of injected oxygenated water *in situ* reduces the oxidation zone and redox gradient initially developed during oxygen injection in the injection borehole. With increased abstraction from the production borehole, the iron and manganese (Figure 6.7) precipitation zones typically occur closer to the injection borehole 11DNE, increasing iron and manganese concentrations yet again (Braester and Martinell, 1988). The re-commissioning of injected ozonated water possibly allows the redox gradient to expand downgradient from 11DNE, to monitoring boreholes as a consequence of pumping from G30966, distributing iron and manganese concentrations across the oxygenated, oxidation and precipitated zone.

A concerning trend is noted between November and December 2019, where rapid increases in Fe^T concentrations (i.e. decreased the rate of iron oxidation) in all monitoring and production boreholes is the result of decreased O_3 injection rates and/or a significant reduction in injection rates as a consequence of 11DNE overflowing (Table 4.1). The increased Fe^T concentrations caused by the lower injection rates introduced less O_3 into 11DNE, which, in turn, decreased the rate of iron oxidation (Rice, 2002). Consequently, increasing Fe^T concentrations and considering the fact that G30966 was switched off due to power failure (Table 4.1). The contributed effect of the power failure at G30966 could have suggested that the oxidation zone and redox gradient downgradient was slowed down, increasing Fe^T concentrations yet again. According to Van Halem *et al*. (2010), oxidation zones are dependent on oxidant concentration,

injection rate, injection volume, and the hydraulic properties of the aquifer. Van Halem *et al*. (2010) further explains that over time the oxidation zone is depleted in the absence of consistent oxidant injection such as O_3 gas.

The relationship between inconsistent injection rates results in increased iron and manganese concentrations in downgradient monitoring boreholes as the existing oxidation zone that was initially formed during O_3 injection becomes depleted. Once oxidant injection commences with an abstraction phase to follow, it regenerates the subsurface oxidation zone (Van Halem *et al.*, 2010; Robey, 2014). This was noted once G30966 was restarted on the 28th November 2019, a noted decrease in Fe^T concentrations occurred very soon after (Van Halem *et al.*, 2010; Robey, 2014). The immediate response in Figure 7.3 best explains the effect that the pumping activity at G30966 has on subsurface conditions relative to the oxidation zone, redox gradient, and possibly the precipitated zone at the study site. During the period that G30966 was shut off due to power failure, injection at injection boreholes were also shut off. This demonstrates that simultaneous pumping from G30966 and continuous O_3 injection has the most success in reduced Fe^T concentrations.

It has also been noted that the first reaction phase of iron removal using ozonation is generally more significant as opposed to the second phase of reinjection. Similar reaction effects during iron removal have also been supported in the study of Cromley and O'Connor (1976). The depletion in iron removal efficiencies in the second phase of injection using ozonation noted by Cromley and O'Connor (1976) was as a consequence of organic compound interferences. The organic compound from the drilling mud interfered with the injected O_3, in turn, affecting the iron concentrations and its removal, which, ultimately, negatively impacted the efficiency of the O_3 injection/remediation. Despite organic compound interferences, ozonation over simple aeration was still demonstrated as the most effective iron remediation method from groundwater sources by Cromley and O'Connor (1976).

Based on the results and interpretations demonstrated by Cromley and O'Connor (1976), Von Gunten (2003), Plummer *et al*. (2005), El Araby *et al.* (2009), and Robey (2014), this study confirmed reduced iron concentrations by ISIR technology using ozonation (Figure 7.3). Monitoring boreholes 10DNE and 8DNE, expressed the most reduced total iron concentrations as a result of these boreholes positioned the closest to injection borehole 11DNE, and demonstrating the most reduced states of iron concentrations (Van Halem et al., 2010; Robey, 2014). Further monitoring boreholes from 11DNE indicates lesser reduced states of iron

concentrations. This is best described by the effects of the oxidation zone formed during O_3 injection and the conceptual model (Figure 6.2) which compares favourably to Braester and Martinell (1988). Iron concentrations are well below the SANS 241:2015 and WHO drinking water guidelines of ≤ 0.3 mg/L during and after the O_3 injection period in all monitoring and production boreholes (Figure 7.3). With regards to manganese concentrations, although an overall reduced trend was only observed in 10DNE and 8DSW during the progressive O_3 injection period, insufficient data captured throughout the duration of the project could not identify suitable, consistent, and reliable data to interpret the efficiency of manganese removal using O_3.

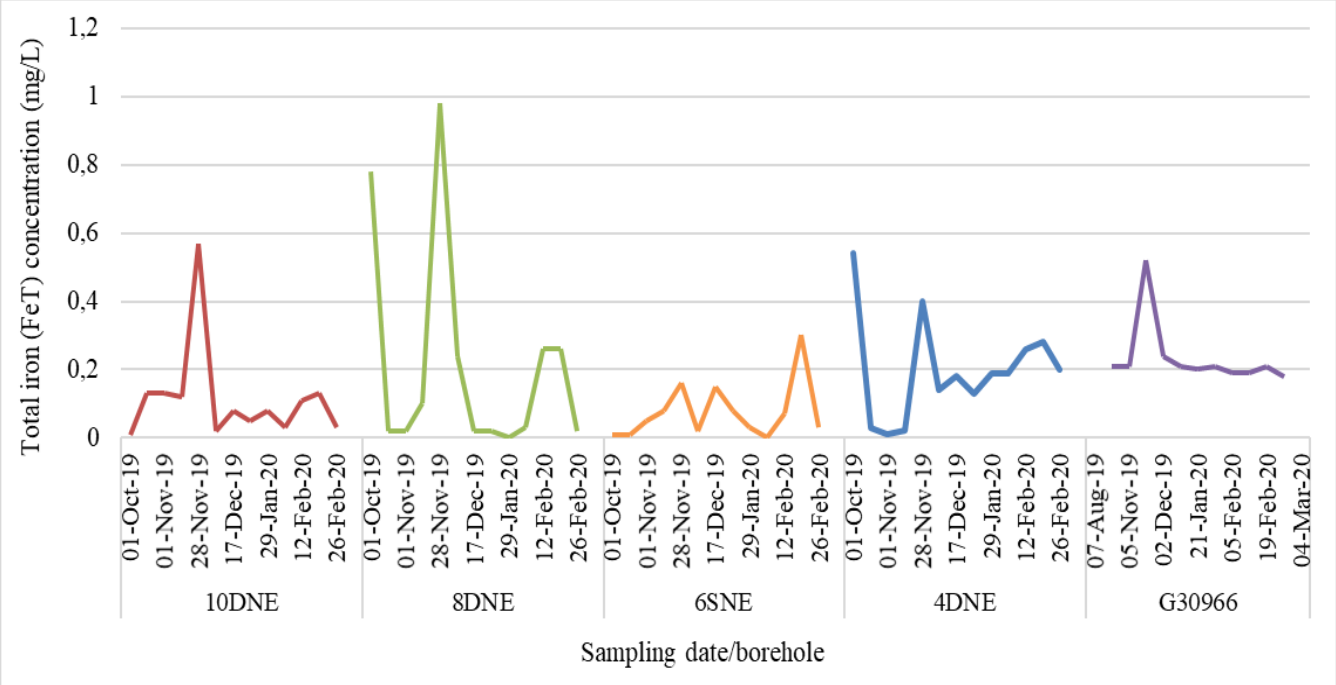

Figure 7.3: Total iron (Fe^T) concentrations (mg/L) monitored in the production (G30966) and monitoring boreholes during the ozone (O_3) injection period from October 2019 to March 2020 in injection borehole 11DNE. Monitoring boreholes downgradient to 11DNE includes 10DNE, 8DNE, 6SNE, 4DNE, and 8DSW.

Chapter 8: Conclusion and recommendations

The main objective of the study was to determine the efficiency of *in situ* iron remediation (ISIR) technology using ozonation on a production borehole. As a consequence, it would provide an explanation to the success of implementing ISIR technology using ozonation in a primary aquifer to prevent production borehole clogging, thereby promoting sustainable borehole abstraction yields. To address the main aim of the study, three specific objectives were formulated.

The first objective focussed on the assessment of borehole clogging on the production borehole. The intention was to determine the current state of the production borehole before the implementation of ISIR technology using ozonation. The second objective focussed on the response of hydrochemical analysis in response to the application of ozonation. The intention for the second objective was to analyse hydrochemical parameters spatial and temporal responses to the implementation of ozonation. Lastly, the third objective focussed on determining the efficiency of ISIR using ozonation at the study site. The intention for the third objective was to quantify the efficiency of ISIR using ozonation, informing whether the efficient use of ozonation as an ISIR technology in a primary aquifer promotes reduced borehole clogging occurrences. Reduced borehole clogging would ultimately maximize production borehole abstraction efficiencies for water supplies to industrial, agricultural, and surrounding towns in the Western Cape.

For the first objective, the results showed an overall decrease in specific capacity (Sc) in the production borehole G30966. Considering the three step-drawdown tests performed in the years 2000, 2013, and 2019, these tests had readings taken every 60 minutes with a total of 4 readings taken per step-drawdown test. Based on the specific capacity averages for each year, a difference (decrease) of 4.91 m^3/day/m in G30966's specific capacity between 2000 and 2019 was observed. This provided an indication that the production borehole's performance declined, possibly due to iron- and manganese-related production borehole clogging. However, due to a combination of inaccurate historical data collected and inconsistent flow rates that affected specific capacity during the recent step-drawdown test in 2019, a suitable understanding and theoretical conclusion to accurately explain the borehole clogging conditions could not be achieved. Based on these findings it is recommended that more frequent and accurate pumping tests be performed with consistent abstraction flow rates per step, step duration, and measurement intervals to gain more conclusive evidence on the effects of

clogging on production boreholes. It is further recommended that borehole clogging effects should be coupled with down-hole camera logging at G30966 after the step-drawdown test for a visible inspection of the condition of the borehole screen.

For the second objective that focussed on hydrochemical analysis in response to the application of ozonation using ISIR technology. The systems design and operation was set up as accurately as possible to promote remote data capturing and data accessibility for convenience. However, during this study, operational issues were not considered during its manufacturing and installation, which ultimately affected data trends derived from the system. It is recommended that back-up power supplies to electricity should be incorporated into the ozone (O_3) generator and telemetry system to promote consistent O_3 injection and reduce the occurrence of inconsistent data capturing. A highly recommended O_3 generator would be a system that relies on alternative power supplies such as a back-up battery source or solar power to promote continuous injection *in situ.* For the telemetry system, manual downloading of data should be possible and data loggers should have a back-up battery supply to operate independently without electricity.

Results derived for the second objective indicated that hydrochemical parameters in response to O_3 injection at variable injection rates (1.7, 1.0, 0.5, 0.43, 0.1, and < 0.1 L/s) were affected. This is explained by the noted favourable responses to groundwater parameters. Hydrochemical analysis included pH, EC, temperature, DO, and iron and manganese concentrations. Variable hydrochemical analysis during the application of ISIR technology at inconsistent O_3 injection rates were favourable enough to indicate reducing iron and manganese (in some instances) concentrations. Based on these findings, the study concluded that these variable injection rates of O_3 significantly influences spatial and temporal groundwater hydrochemical data favourable to iron and manganese concentrations. This can be explained by ozone's *in situ* chemical oxidation compound (ISCO) characteristic to adjust hydrochemical data, even at low injection rates, suitable for iron and manganese oxidation. It is also concluded that subsurface chemical reactions, interactions and the influence of drilling mud contributed to subsurface chemical interferences. The presence of this organic compound species reduces the rate of O_3 decomposition in water, which affects direct and selective oxidation reactions such as iron and manganese. After further observations and investigations, it is further concluded that drilling mud residue was the greatest contributor affecting the groundwater chemistry (Section 6.1), the influence of O_3 injection and the overall removal efficiency of iron and manganese at the study site.

It is recommended that well-defined and consistent O_3 injection rates are needed to improve the response of hydrochemical parameters and derive suitable and consistent spatial and temporal trends for the removal efficiency of iron and manganese concentrations. A range between 0.43 mg and 0.87 mg should be used to remove atleast 1 mg of iron and manganese (Table 2.1). It is also recommended that on-site analysis continues to be the preferred method to confirm field results, however, same day off-site laboratory analysis of hydrochemical data be used in conjunction to improve inconsistencies and interruptions experienced during data analysis in the field. It is further recommended that study sites free from organic compound interferences, such as drilling mud, is most suitable to derive the most accurate spatial and temporal trends for data analysis and iron and manganese concentration removal efficiency rates.

For the third objective focussing on quantifying the efficiency of ISIR using ozonation, the intention was to use the removal efficiency equation (Equation 5). The equation was unable to substitute the volumetric ratio of the abstracted volume of groundwater with reduced iron (Vgw) over the volume of injected volume (Vinj) values. As a result, the equation could not be used in this study, as these values were not recorded effectively during monitoring purposes. However, the results obtained from monitored and telemetry interpretations were able to determine that the injection of O_3 *in situ* reduced iron and manganese concentrations in the subsurface even during inconsistent O_3 injection rates. Reduced iron and manganese concentrations in this study was comparable to the successful pilot study of Robey (2014) and has been recorded to be within the SANS 241:2015 and World Health Organisation (WHO) drinking water standards after the application of ozonation.

Based on these findings, the study concluded that despite subsurface interferences from drilling mud, atmospheric and external environmental influences, chemical reactions and interactions with O_3, ozonation is considered favourable to reducing iron and manganese concentrations. Furthermore, it was also concluded that hydrochemical monitoring and analysis of iron and manganese concentrations could be performed at the study site to determine the efficiency of ISIR technology using ozonation in the Atlantis primary aquifer, Western Cape, South Africa. It is recommended that a prolonged duration of the study be re-introduced at the study site to collect suitable parameters to derive the removal efficiency of ISIR using ozonation using the removal efficiency equation. It is further recommended that more data to be collected for hydrochemical, iron and manganese concentration trend analyses to be performed to gain more conclusive evidence on the nature and extent of removal efficiency.

References

Abbasi, U., Z. A. Bhatti, Q. Mahmood, F. Maqbool and M. T. Hayat, (2020). “Ozone oxidation of wastewater containing trichlorobiphenyl and used transformer oil.” Heliyon **6**(9): e05098.

Ahmad, M. (2012). Iron and manganese removal from groundwater: geochemical modeling of the Vyredox method. Department of Geosciences, University of Oslo. **Geosciences**.

Alıcılar, A., G. Meriç, F. Akkurt and O. Şendil (2008). "Air oxidation of ferrous iron in water." J. Int. Environmental Application & Science **3**(5): 409-414.

Albrechtsen, H. and T. H. Christensen (1994). "Evidence for microbial iron reduction in a landfill leachare-polluted aquifer (Vejen, Denmark)." Applied and Environmental Microbiology **60**(11): 3920-3925.

American Water Works Association, A. (1984). "Removing Iron and Manganese From Groundwater." Journal of American Water Works Association **76**(11): 67-68.

Anderson, T., T. Cauchi, F. Ibrahimi, B. Llewellyn, M. Mozina and E. Ray (2010). "Groundwater Bore Deterioration: Schemes to Alleviate Rehabilitation Costs.". Retrieved 13 August 2020, from http://archive.nwc.gov.au/__data/assets/pdf_file/0018/10962/32_Groundwater.pdf.

Appelo, C. and W. De Vet (2003). Modeling in situ iron removal from groundwater with trace elements such as As. Arsenic in Ground Water, Springer**:** 381-401.

Appelo, C., B. Drijver, R. Hekkenberg and M. De Jonge (1999). "Modeling in situ iron removal from ground water." Groundwater **37**(6): 811-817.

Appelo, C. and D. Postma (2005). "Geochemistry, groundwater and pollution. 2nd." Ed. Balkema, Rotterdam.

Aral, M. M. and S. W. Taylor (2011). Groundwater quantity and quality management, American Society of Civil Engineers.

Bhatta, R., R. Kayastha, D. P. Subedi, R. Joshi (2015). " Treatment of Wastewater by Ozone Produced in Dielectric Barrier Discharge." Journal of Chemistry: 2015.

Bishop, R. (2006). "Management strategies to mitigate clogging and biofouling in production boreholes." Groundwater Pollution in Africa: 325-328.

Boochs, P. and G. Barovic (1981). "Numerical model describing groundwater treatment by recharge of oxygenated water." Water Resources Research **17**(1): 49-56.

Bouchard, M., F. Laforest, L. Vandelac, D. Bellinger and D. Mergler (2007). "Hair manganese and hyperactive behaviors: pilot study of school-age children exposed through tap water." Environmental health perspectives **115**(1): 122-127.

Braester, C. and R. Martinell (1988). "The Vyredox and Nitredox methods of in situ treatment of groundwater." Water Science and Technology **20**(3): 149-163.

Brown, D. A., T. J. Beveridge, C. W. Keevil and B. L. Sherriff (1998). "Evaluation of microscopic techniques to observe iron precipitation in a natural microbial biofilm." FEMS Microbiology Ecology **26**(4): 297-310.

Browning, C. and D. Roberts (2015). "LITHOSTRATIGRAPHY OF THE WITZAND FORMATION (SANDVELD GROUP), SOUTH AFRICA." South African Journal of Geology **118**(3): 317-322.

Bruckner, M. Z. (2016). "Measuing Dissolved and Particulate Organic Carbon (DOC and POC)." Retrieved 12 November 2019, from https://serc.carleton.edu/microbelife/research_methods/biogeochemical/organic_carbon.html.

Bugan, R., G. Tredoux, N. Jovanovic and S. Israel (2018). "Pollution plume development in the primary aquifer at the atlantis historical solid waste disposal site, South Africa." Geosciences **8**(7): 231.

Bugan, R. D., N. Jovanovic, S. Israel, G. Tredoux, B. Genthe, M. Steyn, D. Allpass, R. Bishop and V. Marinus (2016). "Four decades of water recycling in Atlantis (Western Cape, South Africa): Past, present and future." Water SA **42**(4): 577-594.

Bugan, R. D., N. Z. Jovanovic and W. P. De Clercq (2012). "The water balance of a seasonal stream in the semi-arid Western Cape (South Africa)." Water SA **38**(2): 201-212.

Cave, L. (1997). "Inventory of Atlantis production boreholes." Report No. ENV-SC **97134**.

Cavé, L. C., S. Clarke and J. F. P. Engelbrecht (2004). Review of iron bioclogging and strategies for management. Unpublished CSIR report, CSIR, Stellenbosch.

Clark, L. (1988). field guide to water boreholes and boreholes, Open University Press.

Cromley, J. T. and J. T. O'Connor (1976). "Effect of ozonation on the removal of iron from a ground water." Journal-American Water Works Association **68**(6): 315-319.

Cullimore, D. R. (2007). Practical manual of groundwater microbiology, CRC Press.

DEP, N. J. (2017). "In Situ Remediation: Design Considerations and Performance Monitoring Technical Guidance Document"

Department Water Affairs and Forestry, D. (2009). "Does Cape Town have enough water?", DWAF.

Department of Water and Sanitation (DWS) (2016). "National groundwater strategy: Draft 4".

Diliūnas, J., K. Jonaitis, A. Jurevičius and E. Rinkevičienė (2006). "Intensified elimination of iron and other thindispersed compounds from groundwater in situ by magnetic activation." Geologija **56**: 60-66.

Driscoll, F. (1986). "Groundwater and boreholes second edition." Published by Johnson Screens, St Paul, Minnesota **55112**.

Dumousseau, B., P. Jaudon, C. Massiani, E. Vacelet and Y. Claire (1990). "Origin of manganese in the water table of Beaucaire(Gard, France). An attempt of demanganization in situ(Vyredox method)." Revue Des Sciences De L'Eau/Journal of Water Science **3**(1): 21-36.

Ebermann, J. P., D. Eichhorn, W. Macheleidt, J. Ahrns and T. Grischek (2012). "Field tests for subsurface iron removal at a dairy farm in Saxony, Germany." Groundwater Quality Sustainability. Selected Papers on Hydrogeology **17**.

Edition, F. (2011). "Guidelines for drinking-water quality." WHO chronicle **38**(4): 104-108.

El Araby, R., S. Hawash and G. El Diwani (2009). "Treatment of iron and manganese in simulated groundwater via ozone technology." Desalination **249**(3): 1345-1349.

Ellis, D., C. Bouchard and G. Lantagne (2000). "Removal of iron and manganese from groundwater by oxidation and microfiltration." Desalination **130**(3): 255-264.

Engelbrecht, J. (1998). Groundwater pollution from cemeteries. The Water Institute of Southern Africa, Biennal Conference and Exhibition.

Environment, N. S. (2008). "Iron and manganese." Retrieved 1 June 2019, from http://www.gov.ns.ca/nse/water/docs/droponwaterFAQ_IronManganese.pdf

Ezzat, B., H. Fouad, A. Abo-Elmagd and A. Bakry (2016). Utilization of Rice Straw in Removing Iron & Manganese from Groundwater.

Famiglietti, J. S. (2014). "The global groundwater crisis." Nature Climate Change **4**(11): 945-948.

Filtronics (1993). "Iron and manganese Filtration Systems. A Technical Discussion." Retrieved 14 September 2019, from http://www.filtronics.com/pdf/EM-1TechDisc.pdf

Fleisher, J. (1990). Atlantis Groundwater Management Programme–the Geohydrology of the Witzand Wellfield, Report.

Flower, P. and R. Bishop (2003). "Atlantis Water Supply Scheme: A Case Study on Borehole Clogging and Biofouling Management Initiatives." Bulk Water, Water Department of City of Cape Town, Cape Town.

Giordano, M. (2009). "Global groundwater? Issues and solutions." Annual review of Environment and Resources **34**: 153-178.

Gorelick, S. M. and C. Zheng (2015). "Global change and the groundwater management challenge." Water Resources Research **51**(5): 3031-3051.

Hallberg, R. O. and R. Martinell (1976). "Vyredox—in situ purification of ground water." Groundwater **14**(2): 88-93.

Haris, M., M. K. Zahoor, M. S. Khan, M. Z. A. Bakar, M. M. Iqbal and Y. Majeed (2013). "Underground water contamination by drilling mud." Pakistan Journal of Nutrition **12**(1): 101.

Homoncik, S. C., A. M. MacDonald, K. V. Heal, B. É. Ó. Dochartaigh and B. T. Ngwenya (2010). "Manganese concentrations in Scottish groundwater." Science of the total environment **408**(12): 2467-2473.

IDEM (2005, 6 July 2016). "In-Situ Chemical Oxidation." Retrieved 23 February 2020, from https://www.in.gov/idem/cleanups/files/remediation_tech_guidance_in-situ.pdf.

Islam, A. T., M. Rakib, M. S. Islam, K. Jahan and M. A. Patwary (2015). "Assessment of health hazard of metal concentration in groundwater of Bangladesh." Chemical Science International Journal: 41-49.

ISRRI (2009). Technical Report: Subsurface Injection of In Situ Remedial Reagents (ISRRs) Within the Los Angeles Regional Water Quality Control Board Jurisdiction, In Situ Remediation Reagents Injection Working Group.

Ityel, D. (2011). "Ground water: Dealing with iron contamination." Filtration & Separation **48**(1): 26-28.

Jesußek, A., S. Grandel and A. Dahmke (2013). “Impacts of subsurface heat storage on aquifer hydrogeochemistry.” Environmental Earth Sciences **69**(6): 1999-2012.

Johnson, T. (2005). "Specific Capacity – A Measure of Well Performance, Well Problems and Aquifer Transmissivity: Part 1 of 2." Technical Bulletin Volume 2. Retrieved 20 August 2020, from www.wrd.org/engineering/specific-capacity-well-1.php.

Jolly, J. (2002). "Sustainable use of the TMG aquifer and problems of scheme failure, In (Petersen K and Parsons R eds.): A Synthesis of the hydrogeology of the TMG Formation of a research strategy, WRC Report No." TT **158**(01): 108-117.

Jovanovic, N., R. D. Bugan, G. Tredoux, S. Israel, R. Bishop and V. Marinus (2017). "Hydrogeological modelling of the Atlantis aquifer for management support to the Atlantis Water Supply Scheme." Water SA **43**(1): 122-138.

Karakish, A. (2005). Subsurface removal of iron and manganese from groundwater-case study. Ninth International Water Technology Conference, IWTC9, Citeseer.

Katsoyiannis, A. and C. Samara (2007). "The fate of dissolved organic carbon (DOC) in the wastewater treatment process and its importance in the removal of wastewater contaminants." Environmental Science and Pollution Research-International **14**(5): 284-292.

Kinsbergen, K. (2019). "Ultrasonic device provides permanent solution to borehole clogging " Borehole Water Journal of Southern Africa **118**: 1-8.

Kruseman, G. P., N. A. De Ridder and J. M. Verweij (1970). Analysis and evaluation of pumping test data, International institute for land reclamation and improvement The Netherlands.

Lefevre, E., N. Bossa, M. R. Wiesner and C. K. Gunsch (2016). "A review of the environmental implications of in situ remediation by nanoscale zero valent iron (nZVI): behavior, transport and impacts on microbial communities." Science of the total environment **565**: 889-901.

Lo, W., Y. M. Nelson, L. W. Lion, M. L. Shuler and W. C. Ghiorse (1996). "Determination of iron colloid size distribution in the presence of suspended cells: Application to iron deposition onto a biofilm surface." Water research **30**(10): 2413-2423.

Mettler, S., M. Abdelmoula, E. Hoehn, R. Schoenenberger, P. Weidler and U. Von Gunten (2001). "Characterization of iron and manganese precipitates from an in situ ground water treatment plant." Groundwater **39**(6): 921-930.

Misstear, B. D., D. Banks and L. Clark (2006). Water boreholes and boreholes, Wiley Online Library.

Morris, B. L., A. R. Lawrence, P. Chilton, B. Adams, R. C. Calow and B. A. Klinck (2003). Groundwater and its susceptibility to degradation: a global assessment of the problem and options for management, United Nations Environment Programme.

MRWA (2019). "Minnesota Water Works Manual, Chapter 14: Iron and Manganese." Retrieved 17 June 2020, from https://www.mrwa.com/WaterWorksMnl/Chapter%2014%20Iron%20and%20Manganese.pdf

MuIIer, J. L. and J. F. Botha (1986). "A preliminary investigation of modelling the Atlantis Aquifer."

Murray, R. and J. Harris (2010). Water Banking – A Practical Guide to Using Artificial Groundwater Recharge. Strategy and Guideline Development for National Groundwater Planning Requirements.

Nhleko, L., G. Tredoux, M. Mills, R. Rehman, A. Steyn, P. Ravenscroft and N. Jovanovic (2020). LONGER-TERM FEASIBILITY STUDY OF IN-SITU IRON AND MANGANESE REMOVAL BY OZONATION: A NOVEL APPROACH TO PROTECTING GROUNDWATER SUPPLY SCHEMES Water Resource Commision**:** 76.

Nimmer, M. A., B. D. Wayner and A. Allen Morr (2000). "In-situ ozonation of contaminated groundwater." Environmental progress **19**(3): 183-196.

Olsthoorn, T. (2000). "Background of subsurface iron and manganese removal." Amsterdam Water Supply Research and Development, Hydrology Department **9**.

Parsons, P. R. (2007). Extension and Upgrading of the Wastewater Treatment Works and Associated Infrastructure Serving the Blaauwberg Area: Specialist Groundwater Assessment.

Piwoni, M. and J. Keeley (1990). Basic concepts of contaminant sorption at hazardous waste sites (ground-water issue), Environmental Protection Agency, Ada, OK (United States). Robert S. Kerr ….

Plummer, C., M. Luckett, S. Porter and R. Moncrief (2005). " Ozone Sparge Technology for Groundwater Remediation." Retrieved 23 Januray 2020, from www.westshoreconsulting.com/download/ozone/Plummer2005.pdf.

Rice, R. G. (2002). "Century 21-pregnant with ozone." Ozone: science & engineering **24**(1): 1-15.

Roberts, D. (1999). "The geology of Melkbosstrand and environs." Explanation, Sheet 3318CB (1: 50 000), Council for Geoscience, 36pp.

Roberts, D. (2006). "Lithostratigraphy of the Sandveld Group." S. Afr. Committee Stratigr. Lithostratigraphic Ser **9**: 25-26.

Roberts, D.L., M.D. Bateman, C.V. Murray-Wallace, A.S. Carr, and P.J. Holmes (2009). "West coast dune plumes: Climate driven contrasts in dunefield morphogenesis along the western and southern South African coasts." Palaeogeography, Palaeoclimatology, Palaeoecology **271**(1-2): 24-38.

Robey, K. (2014). A feasibility study of in-situ iron removal in the atlantis primary aquifer, Western Cape province, South Africa, University of the Free State. **Geohydrology**.

Robey, K., G. Tredoux and L. Chevallier (2014). Preventing production borehole clogging by in-situ iron removal in South African aquifer systems, WRC Report.

Rott, U. and B. Lamberth (1993). "Groundwater clean up by in-situ treatment of nitrate, iron and manganese." WATER SUPPLY-OXFORD- **11**: 143-143.

Saito, T., S. Hamamoto, T. Ueki, S. Ohkubo, P. Moldrup, K. Kawamoto and T. Komatsu (2016). "Temperature change affected groundwater quality in a confined marine aquifer during long-term heating and cooling." Water research **94**: 120-127.

Sallanko, J. T., E. J. Lakso and R. L. Kamula (2007). "The effect of ozonation on the size fractions of iron and total organic carbon in groundwater." Journal of Environmental Science and Health, Part A **42**(6): 795-801.

Sharma, S. K. (2001). Adsorptive iron removal from groundwater, CRC Press.

Silveria, L. (1988). "In situ'Groundwater Treatment." Encyclopedia of Life Support Systems (EOLSS). Groundwater III. Accessed September **25**: 2011.

Simonson, B. M., M. Chan and A. Archer (2003). "Origin and evolution of large Precambrian iron formations." Special Papers-Geological Society of America: 231-244.

Smith, M. (2006). Prediction, control and rehabilitation of iron encrustation in water supply boreholes, Western Cape, South Africa: a geochemical approach, University of Cape Town.

Snyder, D. T. (2008). “Estimated depth to ground water and configuration of the water table in the Portland, Oregon area” (No. 2008-5059). Geological Survey (US).

Sommerfeld, E. O. (1999). Iron and manganese removal handbook, American Water Works Association.

SRK Consulting (2014). “Site Safety Report for Duynefontein – Section 5 11 Geohydrology, Draft 4.”

Teunissen, K. (2007). Iron removal at groundwater pumping station Harderbroek, Kiwa Water Holding.

Teutsch, N., U. Von Gunten, D. Porcelli, O. A. Cirpka and A. N. Halliday (2005). "Adsorption as a cause for iron isotope fractionation in reduced groundwater." Geochimica et Cosmochimica Acta **69**(17): 4175-4185.

Tredoux, G. and L. Cavé (2002). "Atlantis aquifer; a status report on 20 years of groundwater management at Atlantis." Report No ENV-SC **69**.

Tredoux, G., L. Cavé and R. Bishop (2002). "Long-term stormwater and wastewater infiltration into a sandy aquifer, South Africa." Management of Aquifer Recharge for Sustainability; Dillon, PJ, Ed.; Balkema Publishers: Exton, PA, USA: 35-40.

Tredoux, G., B. Genthe, M. Steyn, J. Engelbrecht, J. Wilsenach and N. Jovanovic (2009). "An assessment of the Atlantis artificial recharge water supply scheme (Western Cape, South Africa)." WIT Transactions on Ecology and the Environment **127**: 403-413.

Tredoux, G., S. Israel and L. Cavé (2004). "The Feasibility of in situ groundwater remediation as robust low-cost water treatment option." Water Research Commission Report **1325**(1): 04.

Tredoux, G., M. Steyn and J. Germanis (2011). Managed aquifer recharge in Atlantis, South Africa, IWA Publishing.

Tutmez, B., Z. Hatipoglu and U. Kaymak (2006). "Modelling electrical conductivity of groundwater using an adaptive neuro-fuzzy inference system." Computers & geosciences **32**(4): 421-433.

United States Environmental Protection Agency (EPA) (2012). "Water monitoring and assessment. Chapter 5.5 Conductivity" Retrieved 18 June 2021, from https://archive.epa.gov/water/archive/web/html/vms59.html.

Van Beek, C. and H. Vaessen (1979). "In situ iron removal from groundwater." H, O **12**: 15-19.

Van Der Laan, H. (2008). "Modeling subsurface iron removal-application of a geochemical model to describe subsurface aeration at pumping station Schuwacht." Additional MSc thesis, Delft Univ. of Technology, Delft, Netherlands.

Van Halem, D., S. Olivero, W. de Vet, J. Verberk, G. Amy and J. van Dijk (2010). "Subsurface iron and arsenic removal for shallow tube well drinking water supply in rural Bangladesh." Water research **44**(19): 5761-5769.

Van Tonder, G., J. Botha, W.-H. Chiang, H. Kunstmann and Y. Xu (2001). "Estimation of the sustainable yields of boreholes in fractured rock formations." Journal of Hydrology **241**(1-2): 70-90.

Vance, D. (1994). "Iron: The environmental impact of a universal element." Natl. Environ. J. **4**(3): 24-25.

Visser, D (2016). "Specialist Geohydrology Impact Assessment for the Proposed Transient Interim Storage Facility at Koeberg"

Von Gunten, U. (2003). "Ozonation of drinking water: Part I. Oxidation kinetics and product formation." Water research **37**(7): 1443-1467.

Walker, G. R and D. Mallants (2014). "Methodologies for investigating gas in water bores and links to coal seam gas development." Report for the Queensland Department of Natural Resources and Mines.

Walter, D. A. (1997). Geochemistry and microbiology of iron-related well-screen encrustation and aquifer biofouling in Suffolk County, Long Island, New York, US Department of the Interior, US Geological Survey.

Wang, Y., S. Sikora, H. Kim, B. Dubey and T. Townsend (2012). "Mobilization of iron and arsenic from soil by construction and demolition debris landfill leachate." Waste management **32**(5): 925-932.

Wassertec (2012). CD Aqua Manual. C. T. Wassertec Ozone Systems.

Winter, T. C., J. W. Harvey, O. L. Franke and W. M. Alley (1998). Ground water and surface water: a single resource, DIANE Publishing Inc.

Xu, Y. and B. Usher (2006). Groundwater pollution in Africa, UNEP/Earthprint.

Zhang, Z. and A. Furman (2020). "Soil redox dynamics under dynamic hydrologic regimes - A review". Science of The Total Environment: 143026.